IMPROVED TARGETING AND BIOPHARMACEUTICAL PROPERTIES OF PRODRUGS OF ANTI-INFECTIVE AGENTS

by

Kefeng Sun

A dissertation submitted in partial fulfillment
of the requirements for the degree of
Doctor of Philosophy
(Pharmaceutical Sciences)
in the University of Michigan
2013

Doctoral Committee:

Professor Gordon L. Amidon, Co-Chair
Professor Kyung-Dall Lee, Co-Chair
Professor Emeritus John C. Drach
John M. Hilfinger, TSRL Inc.
Associate Professor Duxin Sun

DEDICATION

In loving memory of my father,

SUN Yong

(1956-2007)

ACKNOWLEDGEMENTS

I would like to thank my thesis co-advisors, Dr. Gordon Amidon and Dr. Kyung-Dall Lee, for all the mentorship, support and encouragement they constantly gave me. Their visions and insights for the research projects kept me on the right track throughout my five years of lab work. Their patience with me when things were not working gave me confidence to push forward. They always challenged me to think critically and independently and I obtained the mindset of a scientist because of them. I also want to thank my other thesis committee members, Dr. John Drach, Dr. Duxin Sun and Dr. John Hilfinger, for their help and suggestions on the research projects. I was extremely fortunate to have five distinguished scientists from diverse backgrounds on my committee and there was always an answer for any problem I presented to them.

I want to thank my lab mates, mentors and good friends Dr. Chet Provoda, Dr. Yasuhiro Tsume and Hao Xu for their guidance on research methodologies in biochemistry, cell culture, analytical chemistry and organic synthesis. No matter how busy they might be, they would always answer my questions with patience and the utmost details. I learned most of the experiments from their meticulous hands-on instructions, which proved to be indispensable for my research.

Many other colleagues in the Amidon / Lee lab including, but not limited to, Stefanie Goodell and Drs. Chasity Andrews, Arik Dahan, Na Hyung Kim, Juhee Lee, Jiayan Liu, Cara Nelson, Emily Rabinsky, Hairat Sabit, Jing Sun and Zac Walls provided a great amount of help and guidance for my Ph.D. research, which I am immensely grateful for. I want to thank Gail Benninghoff for taking good care of the administrative business of the lab and Oluseyi Adeniyi, Allison Matyas and Laura Radecki along with everybody mentioned above for making “the fourth floor” such a delightful workplace.

I also want to thank the College of Pharmacy for the financial support and Dr. David Smith, Dr. Gus Rosania and Dr. Meihua Rose Feng for their advice and guidance in course work, research and career planning. I am deeply thankful for the administrative support provided by Terri Azar, Lynn Alexander, Jeanne Getty, Maria Herbel, Mark Nelson, Antoinette Hopper and Patrina Hardy; they made my academic and personal life at the University a whole lot easier. I would like to thank my colleagues and mentors during my internship at Genentech, especially Gauri Deshmukh, Dr. Xiao Ding, Dr. Bianca Liederer and Dr. Xingrong Liu for their detailed and rigorous instructions on bioanalytical techniques and pharmacokinetic data analysis. I want to thank my friends in Ann Arbor and all over the United States, especially Yuwen Liu, Wenfeng Qian, Di Ma, Dongbiao Shen, Xiang Wang, Ting Han, Yehua Xie and Yajun Liu, for all the lively times we spent together. I would also like to give thanks to the Michigan Wolverines football team for all the excitements and inspirations throughout the past six seasons.

Most importantly, to my parents, SUN Yong and KANG Xiaohui, and my dear wife, Ying: Thank you for all the support, tolerance and encouragement you have given me. Thank you for making me believe in myself and the path I chose. I am everything I am today because of the love from you.

TABLE OF CONTENTS

LIST OF FIGURES

LIST OF TABLES

LIST OF ABBREVIATIONS

A_x	absorption at x-nanometer wavelength
Abu	(α,L)-aminobutyric acid
Ac	acetyl
ACN	acetonitrile
AcPheAlaGCV	*N*-acetyl-(L)-phenylalanine-(L)-alanine-ganciclovir
AcPheAbuGCV	*N*-acetyl-(L)-phenylalanine-(α,L)-aminobutyric acid-ganciclovir
Ala, A	(L)-alanine
AMC	7-amino-4-methylcoumarin
ANOVA	analysis of variance
BA	bioavailability
BCA	bicinchoninic acid
BCS	Biopharmaceutics Classification System
Boc	*tert*-butyloxycarbonyl
BSA	bovine serum albumin
Cbz	benzyloxycarbonyl
CbzAlaGCV	*N*-benzyloxycarbonyl-(L)-alanine-ganciclovir
CbzAbuGCV	*N*-benzyloxycarbonyl-(α,L)-aminobutyric acid-ganciclovir
DCM	dichloromethane
DIPEA	N,N-diisopropylethylamine
DMEM	Dulbecco's Modified Eagle Medium
DMF	dimethylformamide
DMSO	dimethyl sulfoxide
DNA	deoxyribonucleic acid

DNase	deoxyribonuclease
DPBS	Dulbecco’s phosphate buffered saline
DTT	dithiothreitol
Et	ethyl
eq	equivalent
ESI	electrospray ionization
F_{abs}, F_a	fraction absorbed
FBS	fetal bovine serum
×g	g-force
GCV	ganciclovir
Gly, G	(L)-glycine
hCMV	human cytomegalovirus
hCMVP	human cytomegalovirus protease
HEPES	4-(2-hydroxyethyl)-1-piperazineethanesulfonic acid
His, H	(L)-histidine
HPLC	high-performace liquid chromatography
IC_{50}	half maximal inhibitory concentration
IPTG	isopropyl β-D-1-thiogalactopyranoside
LC-MS	liquid chromatography-mass spectrometry
Leu	(L)-leucine
µ	micro
m	milli
M	molar (mole per liter)
Me	methyl
MEM	Minimal Essential Medium
MES	2-(*N*-morpholino)ethanesulfonic acid
Met, M	(L)-methionine
MOPS	3-morpholinopropane-1-sulfonic acid
m/z	mass-to-charge ratio
MS	mass spectrometry

n	nano
NADP	nicotinamide adenine dinucleotide phosphate
NADPH	nicotinamide adenine dinucleotide phosphate (reduced form)
Nle	(L)-norleucine
NMR	nuclear magnetic resonance
NTA	nitrilotriacetic acid
OD	optical density
PBS	phosphate buffered saline
PCR	polymerase chain reaction
PEPT1	peptide transporter 1
Phe, F	(L)-phenylalanine
PIPES	1,4-piperazinediethanesulfonic acid
PK	pharmacokinetics
p-NP	*p*-nitrophenol
Pr	propyl
PVDF	polyvinylidene fluoride
RNA	ribonucleic acid
RNase	ribonuclease
rpm	revolutions per minute
SAF	selective activation factor
SD	standard deviation
SDS-PAGE	sodium dodecyl sulfate polyacrylamide gel electrophoresis
SEM	standard error of the mean
Ser, S	(L)-serine
Suc	succinyl
TAPS	3-[[1,3-dihydroxy-2-(hydroxymethyl)propan-2-yl]amino]propane-1-sulfonic acid
TB	Terrific Broth®
TEER	transepithelial electrical resistance
TFA	trifluoroacetic acid

Thr, T	(L)-threonine
TOF	time-of-flight
Tyr, Y	(L)-tyrosine
UV	ultraviolet
Val, V	(L)-valine
ValGCV	valganciclovir

ABSTRACT

The prodrug strategy has been frequently used as a chemical approach for the enhancement of certain disadvantages of parent drugs. In this dissertation, I synthesized prodrugs of two anti-infective agents, ganciclovir and ciprofloxacin, and demonstrated their potential advantages in targeting and biopharmaceutical profiles over the respective parent compounds. In the first project, it was demonstrated that four monoester prodrugs of ganciclovir, N-benzyloxycarbonyl-(L)-alanine-ganciclovir (CbzAlaGCV), N-benzyloxycarbonyl-(α,L)-aminobutyric acid-ganciclovir (CbzAbuGCV), N-acetyl-(L)-phenylalanine-(L)-alanine-ganciclovir (AcPheAlaGCV) and N-acetyl-(L)-phenylalanine-(α,L)-aminobutyric acid-ganciclovir (AcPheAbuGCV), could be hydrolyzed by the human cytomegalovirus (hCMV) protease, a serine protease that possesses intrinsic esterase activities. CbzAlaGCV and AcPheAlaGCV were found to be activated at a higher rate by the hCMV protease than CbzAbuGCV and AcPheAbuGCV. These ganciclovir prodrugs could potentially be targeted to selective activation by hCMV protease. Tissue stability and cellular uptake of these ganciclovir prodrugs were also characterized. The acetylated dipeptide prodrugs of ganciclovir were generally more stable than Cbz-amino acid prodrugs in cell homogenates, plasma and liver microsomes. Among the four prodrug candidates, AcPheAbuGCV was the most stable one in the uninfected tissue matrices and also possessed a superior cellular uptake profile. Since the targeted selective activation of a ganciclovir prodrug is governed by not only its rate of hydrolysis catalyzed by hCMV protease but also its stability in normal tissue matrices as well as the extent of its cellular uptake, AcPheAbuGCV was considered the best overall candidate among the four ganciclovir prodrugs for further development.

In another application of the prodrug strategy, I synthesized ciprofloxacyl-glycine methyl ester (Cipro-Gly-OMe), an amide prodrug of ciprofloxacin, the latter classified as a

Biopharmaceutical Classification System (BCS) class IV drug. Cipro-Gly-OMe displayed a potentially much higher solubility in the physiological pH range than ciprofloxacin does. Furthermore, Cipro-Gly-OMe may also have a higher intestinal permeability at neutral pH than that of the parent compound. Therefore, through the prodrug methodology, a BCS class IV drug was converted to a potential class I compound. Taken together, the versatility of the prodrug approach makes it an effective and promising strategy for improving the targeting and biopharmaceutical properties of existing anti-infective drugs.

CHAPTER I

PREAMBLE: A BRIEF REVIEW ON ESSENTIAL CONCEPTS

Serine Proteases: Classification and Catalytic Mechanisms

Hydrolases are enzymes that catalyze the hydrolysis of chemical bonds. In the Enzyme Commission (EC) number classification scheme, they are categorized as EC 3 [1]. Proteases (EC 3.4), also called peptidases or proteinases, are hydrolases that catalyze the hydrolysis of peptide (amide) bonds. They comprise a large part of the human proteome, with at least 703 different proteases being identified by the MEROPS database as of February, 2013 [2]. Proteases with known catalytic mechanisms are further classified by the species at their active sites into six groups: serine proteases, threonine proteases, cysteine proteases, aspartate proteases, glutamic proteases and metalloproteases [3, 4].

A serine protease (EC 3.4.16 and 3.4.21 [3]) is a protease with a serine (Ser) residue as the nucleophile at the protease's active site. Almost one third of all proteases are serine proteases [5]. They are known for the well-defined "catalytic triad" that serves as the charge relay system during the catalytic processes. The most commonly observed catalytic triad is the serine-histidine-aspartic acid (Ser-His-Asp) system, although novel catalytic triads like Ser-His-Glu and Ser-His-His have also been identified [5, 6]. Of the serine proteases that utilize the Ser-His-Asp triad, chymotrypsin-like proteases (family S1 as classified by MEROPS database) are the most abundant form of all proteases; over 684 among all species [7] and 144 in human [8] has been categorized as chymotrypsin-like proteases as of February, 2013.

The catalytic mechanism of the chymotrypsin-like serine proteases has been well-studied. **Figure 1.1** demonstrates the currently accepted mechanism of action. In the first phase of the reaction (acylation), the hydroxyl group of the serine residue attacks the carbonyl group of the substrate, forming a tetrahedral intermediate (Fig. 1.1a,b). The intermediate is partially stabilized by hydrogen bonding between the histidine and aspartic acid residues. The leaving group of the substrate is then discharged from the intermediate (Fig. 1.1b,c), yielding an acyl-protease (Fig. 1.1c). The second phase of the hydrolysis reaction is deacylation of the protease. A water molecule, activated by the histidine residue, attacks the acyl-protease (Fig. 1.1d) and another tetrahedral intermediate is formed. The serine residue is then expelled (Fig. 1.1e) and the carboxylic acid product leaves the enzyme's pocket as the deacylation process is completed (Fig. 1.1f).

Many serine proteases also possess catalytic activities against ester substrates [5]. For example, the esterase activities of chymotrypsin [9] and trypsin [10] were published before the catalytic mechanisms and crystal structures were known. It is now known that the hydrolysis of ester bonds catalyzed by serine proteases share a similar mechanism (**Figure 1.2**) with the hydrolysis of amide bonds (**Figure 1.1**), the only difference being the leaving group during the formation of acyl-enzyme. Moreover, it has been found that esters with the same substrate sequences are usually more reactive than their peptide counterparts. This has been attributed to the greater intrinsic reactivity of the ester bonds [5], as the alcohol leaving group is more readily discharged from the intermediate (Fig. 1.2b) than an amine group could be. In summary, the esterase-like activity of serine proteases could thus be utilized for the design of specific ester compounds that could be hydrolyzed by target serine proteases.

Viral Proteases: Examples and Importance

One unique biological feature of viruses is that they only replicate inside the hosts. For many viruses, during the synthesis of new viral proteomes a large, inactive precursor protein is initially translated from the viral mRNA. Such a polyprotein requires cleavage by proteases to release the mature, active forms of viral proteins. While many virus species utilize host cell protease mechanisms for this maturation process [11-13], plenty of others encode their own protease sequences in their genomes [14]. These viral proteases generally have the same

catalytic mechanisms as proteases expressed in eukaryotes [14]. Due to the essential roles of viral proteases in the life cycles of viruses, loss-of-function of these proteases, either natural or induced by xenobiotics, could lead to disruption in viral replication and propagation. Therefore, the proteases of viruses that cause important diseases are generally well studied; two examples are the human immunodeficiency virus-1 (HIV-1) protease and hepatitis C virus (HCV) protease.

The HIV-1 protease hydrolyzes the *Gag* and *Pol* polyproteins at ten cleavage sites and is crucial for the maturation of the virion. It is an aspartate protease with the active site amino acid residue at Asp25 [15]. Its active form is also a homodimer, with the substrate-binding site at the dimer interface [15, 16]. An octapeptide sequence, ranging from P4 to P4', is recognized by the protease [16]. It is generally accepted that during the hydrolysis of peptide substrates, a tetrahedral intermediate exists in the substrate envelope and interacts noncovalently with the protease [15, 16]. Knowledge of such catalytic mechanisms has led to the rational design and development of a number of inhibitor compounds. As of 2012, ten HIV-1 protease inhibitors have been approved by the United States Food and Drug Administration (US FDA): saquinavir, ritonavir, indinavir, nelfinavir, amprenavir, lopinavir, fosamprenavir, atazanavir, tipranavir, darunavir, although amprenavir was withdrawn from the market in 2004. These inhibitors generally bind to the protease at affinities of nanomolar (nM) to picomolar (pM) range [14]. Use of these inhibitors is generally combined with other drugs such as reverse-transcriptase inhibitors (RTIs) to form a highly active antiretroviral therapy (HAART).

The hepatitis C virus NS3/4A protease is a chymotrypsin-like serine protease with Ser139 as the amino acid residue at the active site [17]. It catalyzes four of the ten cleavages within the large precursor polyprotein [14]. The protease recognizes a peptide substrate sequence with ten amino acid residues, though only three of them are conserved: Cys or Thr at P1, Ser or Ala at P1', and Asp or Glu at P6 [17, 18]. The crystal structure of the HCV NS3/4A protease was also well studied [19] and understandings of the substrate-binding cleft have enabled the development of several inhibitors. Two of them, telaprevir and boceprevir,

were both approved for use by the US FDA in 2011 for treatment of genotype 1 hepatitis C, for which the traditional therapy with ribavirin / pegylated interferon is less effective [20].

Other important viral proteases with known crystal structures include, but are not restricted to, the dengue virus NS2B/NS3 protease, the rhinovirus 3C protease, the severe acute respiratory syndrome coronavirus (SARS-CoV) protease, the herpes simplex virus-1 (HSV-1) protease, the human cytomegalovirus (hCMV) protease and the influenza A virus PA protease (of which the proteolytic activity is still under debate). The hCMV protease and influenza A PA protein will be discussed in detail in later chapters. Taken together, viral proteases are important targets for drug development and it is critical to understand their structures, especially that around the active site, and substrate recognition patterns.

Biopharmaceutics and the Biopharmaceutics Classification System (BCS)

Biopharmaceutics is the discipline that studies the influences of the physiology of the route of administration of a drug product, the formulation of the product and chemical and physical properties of the product's active pharmaceutical ingredient (API) on the absorption, distribution, metabolism and excretion (ADME) of said drug product [21]. Orally administered drug products have been particularly well-studied in the context of biopharmaceutics. Upon intake into the gastrointestinal (GI) system, the drug product needs to dissolve into the fluids within the system and the API must then traverse the GI tract wall in order to be absorbed into the blood circulation. This process is characterized by the fraction absorbed (F_{abs} or F_a) parameter [22] and the oral bioavailability (BA, or F), which is defined as "the rate and extent to which the active ingredient is absorbed from a drug product and becomes available at the site of action" [23]. Generally speaking, a high fraction absorbed and bioavailability are desirable for all the immediate release (IR) oral drug products.

Extensive research has been devoted how to the physicochemical properties of a drug product and their interactions with the human GI tract could influence the absorption of the API through the gut walls. For IR solid oral dosage forms, dissolution, aqueous solubility and intestinal permeability are the three factors that are considered to govern the fraction absorbed (F_a) of the API of a drug product [24, 25]. While dissolution is affected by not only the API

but also the excipients and the manufacturing process [25], solubility and permeability are the two properties that are intrinsic to the drug substances themselves.

The Biopharmaceutical Classification System, first established by Amidon *et al*. in 1995, is a rational and scientific framework for the classification of drug compounds based on their aqueous solubility and intestinal permeability [26]. According to the BCS, the drug substances are classified as follows:

- Class I: High solubility, high permeability;
- Class II: Low solubility, high permeability;
- Class III: High solubility, low permeability;
- Class IV: Low solubility, low permeability.

An API is considered to have a "high solubility" if its highest dose strength is able to be solubilized in 250 mL aqueous media over the pH range of 1 to 7.5 [24]. It is considered highly permeable if the fraction absorbed number is above 90% of the administered dose [24]. A few examples of the BCS include metoprolol, propranolol and caffeine (BCS class I); carbamazepine and ketoprofen (class II); atenolol and cimetidine (class III); and amoxicillin and furosemide (class IV) [27, 28].

Arguably the most significant and important influence of BCS on the pharmaceutical industry and regulatory agencies is its incorporation into the biowaiver extensions for bioavailability and / or bioequivalence (BE) studies for IR solid oral drug products [24, 29]. In short, sponsors may request biowaivers for an IR solid oral dosage product with a BCS class I API that exhibit rapid *in vitro* dissolution (i.e. >85% of API dissolved within 30 min using standard apparatuses), with a few additional restrictions [24, 29]. While the regulatory policies and ongoing efforts regarding biowaivers of BCS II and III drugs are beyond the scope of this dissertation, it is apparent that the low solubility and low permeability for BCS IV compounds generate significant problems for development of effective oral delivery strategies, since their oral absorption is limited by both *in vivo* dissolution and intestinal permeation [26]. Therefore, during the pre-clinical design of new chemical entities (NCEs), for compounds with class IV properties, efforts should be directed to the optimization of its

solubility and / or permeability profiles, with the target being classes III / II or, potentially, class I drug substances.

Prodrugs

The term “pro-drug” was first introduced by Adrien Albert in 1958, as a “substance that has to be broken down to give the true drug” [30]. Currently, a prodrug is defined as a derivative of a pharmacologically active agent (“drug”) that must undergo *in vivo* enzymatic and / or chemical transformation(s) to be converted to the active drug, or parent compound [31]. If a prodrug is formed by covalently linking a functional group to the parent compound, such a group is called a promoiety. Not all prodrugs have promoieties; such exceptions, termed “bioprecursor prodrug”, results from molecular modifications of the active drug [31]. For example, lovastatin and simvastatin are both inactive prodrugs containing a lactone ring [32] and hydrolysis of the cyclic ester within the prodrug, catalyzed by enzymes like carboxylesterase 1 (CES1) [33], yields the active compound. Nevertheless, the prodrugs discussed in this dissertation are restricted to those formed by the chemical conjugation of promoieties to the respective parent compounds.

A conservative estimate placed approximately 7% of all the currently marketed drugs as prodrugs [31, 34]. However, as the mechanisms of action of more existing compounds become known, this percentage would almost certainly be higher. In recent years, in order to overcome the various physicochemical and / or biopharmaceutical disadvantages of the parent compounds, the prodrug strategy has been increasingly utilized in rational drug designs. Three of the major properties of the drug substances improved by these prodrugs are aqueous solubility, intestinal permeability and site-directed delivery [31, 34, 35].

Prodrugs for Improvement of Aqueous Solubility

Drugs with poor water solubility present problems for both parenteral and oral delivery [35, 36]. For parenteral formulations, low intrinsic aqueous solubility limits the concentration of API within the dosage and also could cause physicochemical instability such as spontaneous precipitation. As for oral delivery, the rate of absorption, and thus bioavailability, of the drug product is hampered by the slow dissolution of the API in the gut

lumen, especially when the dose is relatively large. Although numerous formulation approaches such as solubilizing excipients and salt formations could alleviate these problems to a certain degree, prodrugs often offer a better chance of enhancing the innate solubility because of the covalent nature of the chemical modification [36].

Most of the prodrugs for improving the aqueous solubility involve promoieties of a polar nature. These prodrugs are mostly ester or amide derivatives of their parent compounds and the promoieties are usually charged at neutral pH's [31, 36]. Phosphate is a very commonly used ionizable promoiety for such purposes. For example, fosphenytoin, a phosphate ester of the poorly soluble anticonvulsant drug phenytoin (aqueous solubility 20-25 μg/mL), exhibits a more than 5,000-fold increase in solubility at around 140 mg/mL [37]. The prodrug is also readily converted *in vivo* by alkaline phosphatases to phenytoin following the parenteral administration [38]. For orally delivered prodrugs, one example is fosamprenavir, which is the phosphate ester of amprenavir, a 1st-generation HIV-1 protease inhibitor. Fosamprenavir demonstrated a 10-fold increase in solubility and comparable or higher intestinal permeability relative to those of the parent compound [39]. As a result, the dosing regimen for fosamprenavir has been adjusted to half of that of amprenavir, leading to improved patient compliance [40]. Fosamprenavir is also rapidly hydrolyzed by alkaline phosphatases expressed in the cells of the gut wall [39, 40]. In addition to phosphate, other promoieties that have been researched on for improving solubility include hemisuccinate [41] and amino acyl [36]. These prodrugs achieve varying degrees of success in increasing the aqueous solubility, but for some of them the relatively slow conversion to parent compounds may pose a problem in terms of the longer duration required to reach their therapeutic indices [36].

Prodrugs for Improvement of Intestinal Permeability

The clinical use of many pharmaceutical compounds is also hampered by their low permeability across the gastrointestinal tract. This often results from the presence of polar chemical groups within the compounds such as hydroxyl, amine, carboxyl and phosphate groups [31, 35]. In prodrug designs, promoieties are thus frequently employed to "mask" some of these groups. Improvement of permeability of these prodrugs could generally be

attributed to either enhanced passive absorption through the GI tract or carrier-mediated transport.

Achieving better passive intestinal absorption by enhancing lipophilicity is a frequently employed prodrug strategy. Successful ester, amide, carbamate or phosphonate prodrugs created by masking the respective polar or ionizable group within the parent drug could greatly increase the compound's lipophilicity while not appreciably sacrificing their aqueous solubility [42]. These prodrugs exhibit increased passive diffusion across the GI tract wall and are generally readily converted to the active forms by tissue hydrolases [35]. As an example, tenofovir, a reverse transcriptase inhibitor (RTI) for treatment of HIV-1 infections, has oral bioavailability of less than 5%. Tenofovir disoproxil, a bis-carbonate ester prodrug of tenofovir, is able to increase the oral BA to approximately 39% [43]. Other well-characterized examples include famciclovir, adefovir dipivoxil and oseltamivir, all possessing increased lipophilicity and markedly improved oral bioavailability over their respective parent compounds, penciclovir, adefovir and oseltamivir carboxylate [31, 35, 42].

As another mechanism to enhance intestinal absorption, the carrier-mediated transport of prodrugs has been extensively utilized and researched since the late 1990s when the functions, structural characteristics and substrate preferences of transporter proteins in the intestine started to be elucidated [44, 45]. Of particular importance is the human peptide transporter 1 (PEPT1; also known as solute carrier family 15 member 1, SLC15A1) which is expressed on the brush border membrane of the epithelial cells lining the intestinal wall. While its native function is to facilitate the transport of di- and tripeptides produced from the digestion of dietary proteins, PEPT1 has been discovered to also transport a wide array of xenobiotics such as β-lactams [46] and bestatin [47]. These compounds all contain peptide bonds within their structures and are considered peptidomimetics. As a result of these discoveries, a great number of prodrugs have been designed with promoieties being amino acyls or short peptidyls so that their transport across the GI wall could potentially be facilitated by PEPT1.

One of the best-known examples for such PEPT1-transported prodrugs is valacyclovir, the (L)-valine ester for the anti-HSV drug acyclovir (structures shown in **Figure 1.3**).

Acyclovir itself is poorly absorbed in the GI tract; its oral bioavailability is 10% - 30% [48]. In contrast, valacyclovir is more than 10 times more permeable than acyclovir in Caco-2 cells settings [49] and more soluble in water as well [42]. As a result, valacyclovir is more than 60% absorbed when given orally [50]. The increased permeability of valacylovir has been definitively attributed to PEPT1-facilitated transport by transfection and kinetic inhibition studies [49, 51]. The prodrug is rapidly hydrolyzed to acyclovir by biphenyl hydrolase-like serine hydrolase (BPHL, also known as valacylovirase, VACVase) [52, 53], which is abundantly expressed in the intestine and liver where the first-pass metabolism of valacyclovir is likely to occur.

In summary, for pharmaceutical substances with polar groups, the prodrug strategy could be exploited to either increase its lipophilicity for passive transport, or generate a molecule transported by intestinal carriers. Such a strategy could potentially increase the fraction absorbed (F_a) and, therefore, oral bioavailability of the poorly absorbed drug substances.

Targeted Prodrug Strategy

The ultimate goal of drug delivery is to achieve site selectivity, that is, the delivery of a therapeutic agent specifically to the site(s) of a disease while minimizing the activity of the drug in organs and tissues not inflicted by said disease. Several promising strategies related to the prodrug concept are being exploited to address this challenge. These strategies could generally be categorized with respect to their target molecules, i.e. tissue-specific transporters, surface antigens and disease-specific enzymes [35].

Prodrugs targeted to tissue-specific transporters are different from those designed for carrier-mediated transport in that these transporters are not expressed in the GI tract but elsewhere in the body. One well-known example is levodopa, a prodrug of dopamine. Levodopa is transported across the blood-brain barrier (BBB) by large neutral amino acid transporter 1 (LAT1) at the BBB [54]. It is then decarboxylated by amino acid decarboxylases within the brain [55] to yield dopamine, which is unable to traverse out of the brain via the BBB because of its hydrophilic nature [54]. This subsequent “trapping” thus completes the targeting process for levodopa.

A second targeted prodrug scheme takes advantage of specific antigens expressed on the surfaces of target tissues, the majority of them being tumor cells. The resulting prodrugs are the so-called antibody-drug conjugates (ADCs), in which case the "promoiety" is an antibody that recognizes a cancer cell surface antigen and the parent compound an antitumor agent. As of February 2013, the only marketed ADC is brentuximab vedotin which has been approved for the treatment of anasplastic large cell lymphoma (ALCL) and Hodgkin's lymphoma (HL) [56]. It consists of brentuximab, a monoclonal antibody that recognizes and binds to the CD30 biomarker protein on ALCL and HL, and monomethyl auristatin E (MMAE or vedotin), a potent chemotherapeutic [57, 58] conjugated to the antibody by a short peptide linker [58]. After the ADC binds to the CD30-positive cells, it is internalized and the peptide linker is cleaved by endosomal proteases such as cathepsin B, releasing MMAE into the cytoplasm where it exerts its pharmacological effects [58]. In addition to brentuximab vedotin, other well-known ADCs include gemtuzumab ozogamicin (FDA-approved but later withdrawn from market) and trastuzumab emtasine (in phase III clinical trials) [59].

Disease-specific enzymes represent another promising target group for site-specific prodrug delivery and activation. In particular, proteases have been the subject of extensive research for their potential to specifically activate prodrugs with peptide substrate sequence as promoieties [60, 61]. In principle, when such a prodrug is delivered *in vivo*, the active therapeutic will be selectively enriched at sites of protease expression and thus greater efficacy is achieved; at the same time, relatively little or no active drug substance should be formed where the target protease is absent. In anticancer research, such a pro-compound is referred to as a "tumor-activated prodrug" (TAP). The development of TAPs has centered on certain proteases that are specifically upregulated in tumor tissues, including prolidase [62-65], legumain [66, 67], prostate-specific antigen (PSA) [68, 69] and the matrix metalloproteinase (MMP) family [70-72]. In a 2006 study, Wu *et al.* showed that the peptide-coupled prodrug LEG-3 (*N*-succinyl-β-alanyl-(L)-alanyl-(L)-asparaginyl-(L)-leucyl-doxorubicin) completely obliterates the growth of diverse multidrug-resistant and legumain-expressing tumors *in vivo* without systemic toxicity such as myelosuppression [67]. In studies published in 2007, Mittal *et al*. demonstrated that the bioconversion and cytotoxicity of (L)-prophalan, the (L)-proline prodrug of mephalan, is highly correlated to the expression of prolidase in cancer cells and

that the prodrug displays reduced toxicity as well as higher anti-tumor efficacy when administered *in vivo* to mouse models [62, 63]. Non-tumor-specific enzymes like puromycin-sensitive aminopeptidase (also PSA) have also been researched for their roles on targeted prodrug activation [73]. These results demonstrate that in pre-clinical studies, prodrugs with amino acids or peptides as promoieties could potentially achieve the goal of selective targeting as well as decreased systemic adverse events.

Viral proteases serve as unique types of enzymes for the targeted prodrug strategy because viruses are exogenic species and, in principle, the viral proteases are only expressed at the infected tissues or cells. Therefore, a prodrug with a specifically designed peptide as promoiety could hypothetically be activated by virally infected locales. Three crucial factors affect the viral protease-targeted prodrug strategy. First, a drug substance against the virus must exist and it cannot be an inhibitor of the protease. Second, the efficiency of the viral protease against the peptide substrate to be incorporated as promoiety needs to be efficient, i.e. a relatively high k_{cat} / K_m value in Michaelis-Menten kinetics. Third, the prodrug must be relatively stable in non-infected tissues; otherwise it cannot reach the target sites without being largely degraded by non-specific enzymes. In summary, if a prodrug candidate could meet these three prerequisites, it could be particularly promising for *in vivo* tests and subsequent clinical development [61].

FIGURES

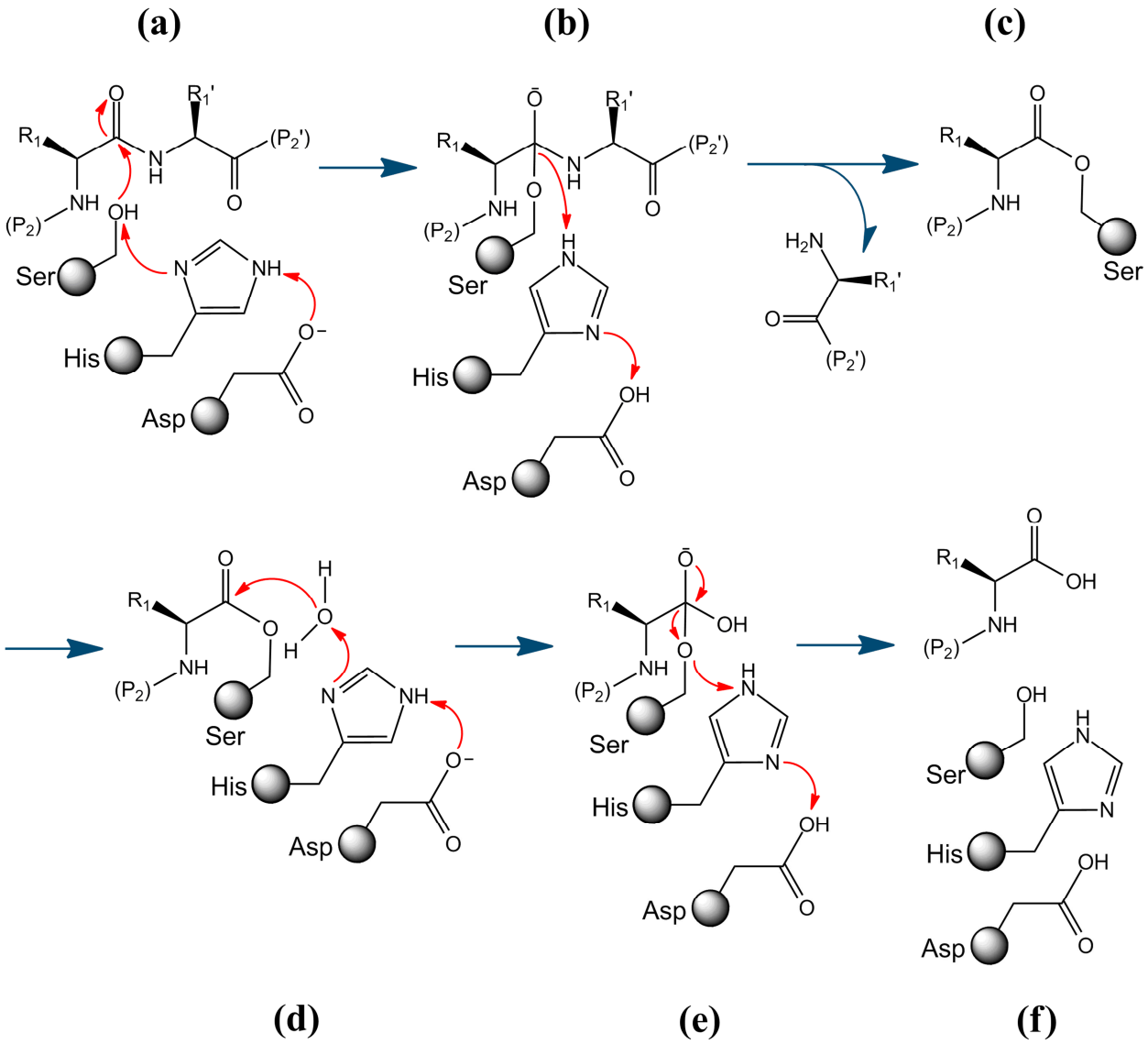

Figure 1.1. Reaction mechanism for the hydrolysis of a peptide bond catalyzed by a typical serine protease. This figure is created with ChemBioDraw Ultra 12.0, as an adaptation of Fig. 8-19 from [74].

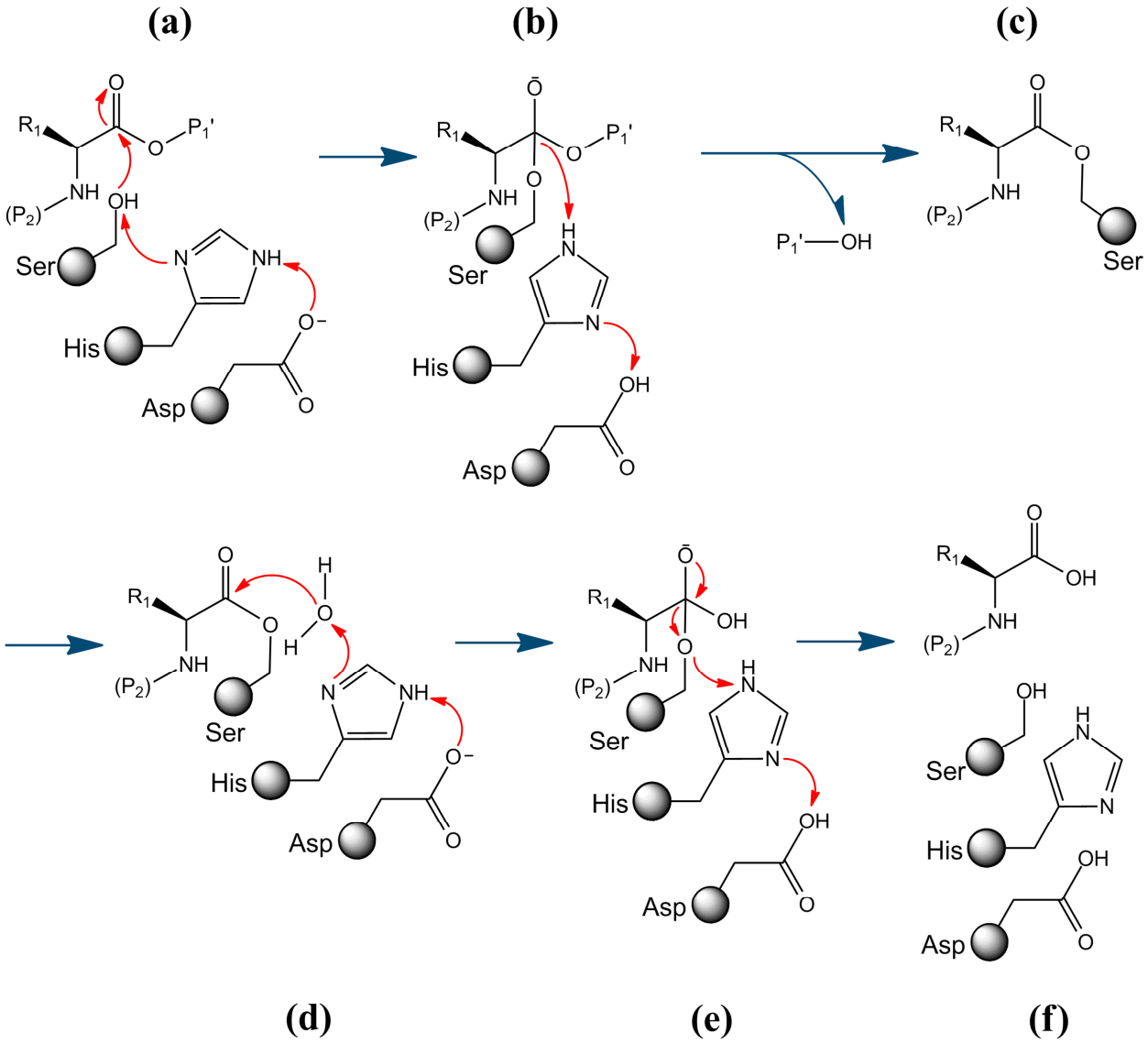

Figure 1.2. Reaction mechanism for the hydrolysis of an ester bond catalyzed by a typical serine protease. This figure is created with ChemBioDraw Ultra 12.0.

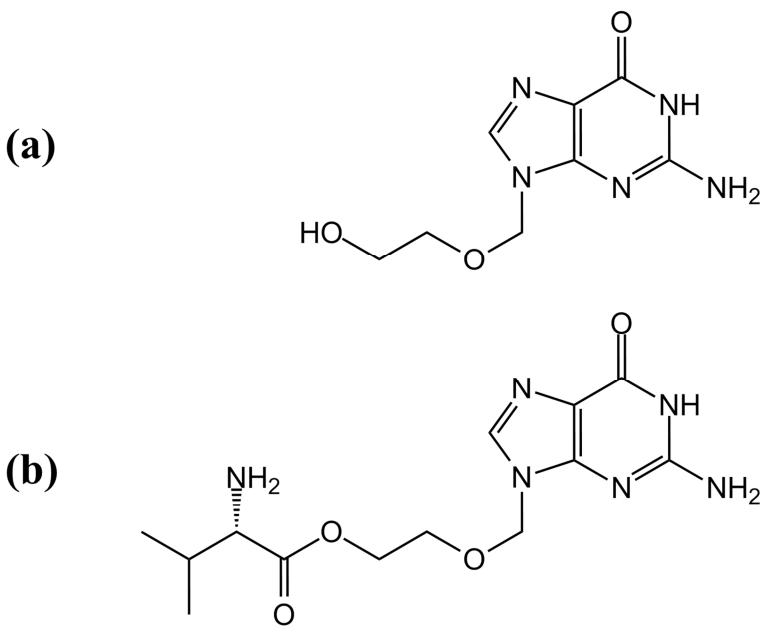

Figure 1.3. Chemical structures of **(a)** acyclovir and **(b)** valacyclovir.

REFERENCES

1. *Enzyme Nomenclature: Recommendations of the Nomenclature Committee of the International Union of Biochemistry and Molecular Biology on the Nomenclature and Classification of Enzymes by the Reactions they Catalyse. URL: http://www.chem.qmul.ac.uk/iubmb/enzyme/.*
2. *MEROPS database, peptidases, Homo sapiens. URL: http://merops.sanger.ac.uk/cgi-bin/speccards?sp=sp001823;type=peptidase.*
3. *EC 3: Hydrolase nomenclature. URL: http://www.chem.qmul.ac.uk/iubmb/enzyme/EC3/.*
4. *MEROPS database: Families of Proteolytic Enzymes. URL: http://merops.sanger.ac.uk/cgi-bin/family_index?type=P.*
5. Hedstrom, L., *Serine protease mechanism and specificity.* Chem Rev, 2002. **102**(12): p. 4501-24.
6. Dodson, G. and A. Wlodawer, *Catalytic triads and their relatives.* Trends Biochem Sci, 1998. **23**(9): p. 347-52.
7. *MEROPS database, Family S1. URL: http://merops.sanger.ac.uk/cgi-bin/famsum?family=S1.*
8. *MEROPS database, Family S1: Distribution among animals. URL: http://merops.sanger.ac.uk/cgi-bin/organism_famdist?family=S01;taxon=Animalia;id=peptidase.*
9. Kaufman, S., H. Neurath, and G.W. Schwert, *The specific peptidase and esterase activities of chymotrypsin.* J Biol Chem, 1949. **177**(2): p. 793-814.
10. Schwert, G.W., H. Neurath, and et al., *The specific esterase activity of trypsin.* J Biol Chem, 1948. **172**(1): p. 221-39.
11. Scheid, A. and P.W. Choppin, *Identification of biological activities of paramyxovirus glycoproteins. Activation of cell fusion, hemolysis, and infectivity of proteolytic cleavage of an inactive precursor protein of Sendai virus.* Virology, 1974. **57**(2): p. 475-90.
12. Irigoyen, N., J.R. Caston, and J.F. Rodriguez, *Host proteolytic activity is necessary for infectious bursal disease virus capsid protein assembly.* J Biol Chem, 2012. **287**(29): p. 24473-82.
13. Bertram, S., et al., *Novel insights into proteolytic cleavage of influenza virus hemagglutinin.* Rev Med Virol, 2010. **20**(5): p. 298-310.
14. Anderson, J., et al., *Viral protease inhibitors.* Handb Exp Pharmacol, 2009(189): p. 85-110.
15. Jaskolski, M., et al., *Structure at 2.5-A resolution of chemically synthesized human immunodeficiency virus type 1 protease complexed with a hydroxyethylene-based inhibitor.* Biochemistry, 1991. **30**(6): p. 1600-9.
16. Prabu-Jeyabalan, M., E. Nalivaika, and C.A. Schiffer, *Substrate shape determines specificity of recognition for HIV-1 protease: analysis of crystal structures of six substrate complexes.* Structure, 2002. **10**(3): p. 369-81.
17. Bartenschlager, R., *The NS3/4A proteinase of the hepatitis C virus: unravelling structure and function of an unusual enzyme and a prime target for antiviral therapy.* J Viral Hepat, 1999. **6**(3): p. 165-81.

18. Steinkuhler, C., et al., *Product inhibition of the hepatitis C virus NS3 protease.* Biochemistry, 1998. **37**(25): p. 8899-905.
19. Kim, J.L., et al., *Crystal structure of the hepatitis C virus NS3 protease domain complexed with a synthetic NS4A cofactor peptide.* Cell, 1996. **87**(2): p. 343-55.
20. *Hepatitis C Medications: Update on New Drugs. United States Department of Veteran Affairs. URL: http://www.hepatitis.va.gov/provider/topics/treatment-new-drugs.asp.*
21. Lobenberg, R. and G.L. Amidon, *Modern bioavailability, bioequivalence and biopharmaceutics classification system. New scientific approaches to international regulatory standards.* Eur J Pharm Biopharm, 2000. **50**(1): p. 3-12.
22. Varma, M.V., et al., *Physicochemical space for optimum oral bioavailability: contribution of human intestinal absorption and first-pass elimination.* J Med Chem, 2010. **53**(3): p. 1098-108.
23. *US FDA/CDER. Guidance for Industry: Bioavailability and Bioequivalence Studies for Orally Administered Drug Products - General Considerations. URL: http://www.fda.gov/downloads/Drugs/GuidanceComplianceRegulatoryInformation/Guidances/UCM070124.pdf.* 2003.
24. *US FDA/CDER. Waiver of In Vivo Bioavailability and Bioequivalence Studies for Immediate-Release Solid Oral Dosage Forms Based on a Biopharmaceutics Classification System. URL: http://www.fda.gov/downloads/Drugs/GuidanceComplianceRegulatoryInformation/Guidances/UCM070246.pdf.* 2000.
25. *US FDA/CDER. Dissolution Testing of Immediate Release Solid Oral Dosage Forms. URL: http://www.fda.gov/downloads/Drugs/GuidanceComplianceRegulatoryInformation/Guidances/UCM070237.pdf.* 1997.
26. Amidon, G.L., et al., *A theoretical basis for a biopharmaceutic drug classification: the correlation of in vitro drug product dissolution and in vivo bioavailability.* Pharm Res, 1995. **12**(3): p. 413-20.
27. *TSRL Inc. Biopharmaceutics Classification System database. URL: http://69.20.123.154/services/bcs/search.cfm.*
28. Takagi, T., et al., *A provisional biopharmaceutical classification of the top 200 oral drug products in the United States, Great Britain, Spain, and Japan.* Mol Pharm, 2006. **3**(6): p. 631-43.
29. Yu, L.X., et al., *Biopharmaceutics classification system: the scientific basis for biowaiver extensions.* Pharm Res, 2002. **19**(7): p. 921-5.
30. Albert, A., *Chemical aspects of selective toxicity.* Nature, 1958. **182**(4633): p. 421-2.
31. Rautio, J., et al., *Prodrugs: design and clinical applications.* Nat Rev Drug Discov, 2008. **7**(3): p. 255-70.
32. Alberts, A.W., *Lovastatin and simvastatin--inhibitors of HMG CoA reductase and cholesterol biosynthesis.* Cardiology, 1990. **77 Suppl 4**: p. 14-21.
33. Fukami, T., et al., *In vitro evaluation of inhibitory effects of antidiabetic and antihyperlipidemic drugs on human carboxylesterase activities.* Drug Metab Dispos, 2010. **38**(12): p. 2173-8.
34. Stella, V.J., *Prodrugs as therapeutics.* Expert Opinion on Therapeutic Patents, 2004. **14**(3): p. 277-280.

35. Ettmayer, P., et al., *Lessons learned from marketed and investigational prodrugs.* J Med Chem, 2004. **47**(10): p. 2393-404.
36. Stella, V.J. and K.W. Nti-Addae, *Prodrug strategies to overcome poor water solubility.* Adv Drug Deliv Rev, 2007. **59**(7): p. 677-94.
37. Varia, S.A. and V.J. Stella, *Phenytoin Prodrugs .6. Invivo Evaluation of a Phosphate Ester Prodrug of Phenytoin after Parenteral Administration to Rats.* Journal of Pharmaceutical Sciences, 1984. **73**(8): p. 1087-1090.
38. Browne, T.R., A.R. Kugler, and M.A. Eldon, *Pharmacology and pharmacokinetics of fosphenytoin.* Neurology, 1996. **46**(6 Suppl 1): p. S3-7.
39. Wire, M.B., M.J. Shelton, and S. Studenberg, *Fosamprenavir : clinical pharmacokinetics and drug interactions of the amprenavir prodrug.* Clin Pharmacokinet, 2006. **45**(2): p. 137-68.
40. Chapman, T.M., G.L. Plosker, and C.M. Perry, *Fosamprenavir: a review of its use in the management of antiretroviral therapy-naive patients with HIV infection.* Drugs, 2004. **64**(18): p. 2101-24.
41. Derendorf, H., et al., *Kinetics of methylprednisolone and its hemisuccinate ester.* Clin Pharmacol Ther, 1985. **37**(5): p. 502-7.
42. Li, F., H. Maag, and T. Alfredson, *Prodrugs of nucleoside analogues for improved oral absorption and tissue targeting.* J Pharm Sci, 2008. **97**(3): p. 1109-34.
43. Barditch-Crovo, P., et al., *Phase i/ii trial of the pharmacokinetics, safety, and antiretroviral activity of tenofovir disoproxil fumarate in human immunodeficiency virus-infected adults.* Antimicrob Agents Chemother, 2001. **45**(10): p. 2733-9.
44. Adibi, S.A., *The oligopeptide transporter (Pept-1) in human intestine: biology and function.* Gastroenterology, 1997. **113**(1): p. 332-40.
45. Broer, S., et al., *Characterization of the monocarboxylate transporter 1 expressed in Xenopus laevis oocytes by changes in cytosolic pH.* Biochem J, 1998. **333 (Pt 1)**: p. 167-74.
46. Ganapathy, M.E., et al., *Differential recognition of beta -lactam antibiotics by intestinal and renal peptide transporters, PEPT 1 and PEPT 2.* J Biol Chem, 1995. **270**(43): p. 25672-7.
47. Tomita, Y., et al., *Transport mechanisms of bestatin in rabbit intestinal brush-border membranes: role of H+/dipeptide cotransport system.* J Pharmacol Exp Ther, 1990. **252**(2): p. 859-62.
48. de Miranda, P. and M.R. Blum, *Pharmacokinetics of acyclovir after intravenous and oral administration.* J Antimicrob Chemother, 1983. **12 Suppl B**: p. 29-37.
49. Han, H.K., D.M. Oh, and G.L. Amidon, *Cellular uptake mechanism of amino acid ester prodrugs in Caco-2/hPEPT1 cells overexpressing a human peptide transporter.* Pharm Res, 1998. **15**(9): p. 1382-6.
50. Beauchamp, L.M., et al., *Amino-Acid Ester Prodrugs of Acyclovir.* Antiviral Chemistry & Chemotherapy, 1992. **3**(3): p. 157-164.
51. Ganapathy, M.E., et al., *Valacyclovir: a substrate for the intestinal and renal peptide transporters PEPT1 and PEPT2.* Biochem Biophys Res Commun, 1998. **246**(2): p. 470-5.
52. Kim, I., et al., *Identification of a human valacyclovirase: biphenyl hydrolase-like protein as valacyclovir hydrolase.* J Biol Chem, 2003. **278**(28): p. 25348-56.

53. Lai, L., et al., *Molecular basis of prodrug activation by human valacyclovirase, an alpha-amino acid ester hydrolase.* J Biol Chem, 2008. **283**(14): p. 9318-27.
54. Rautio, J., et al., *Prodrug approaches for CNS delivery.* AAPS J, 2008. **10**(1): p. 92-102.
55. Dairman, W., J.G. Christenson, and S. Udenfriend, *Decrease in liver aromatic L-amino-acid decarboxylase produced by chronic administration of L-dopa.* Proc Natl Acad Sci U S A, 1971. **68**(9): p. 2117-20.
56. *FDA News Release: FDA approves Adcetris to treat two types of lymphoma. URL: http://www.fda.gov/NewsEvents/Newsroom/PressAnnouncements/ucm268781.htm.* 2011.
57. Francisco, J.A., et al., *cAC10-vcMMAE, an anti-CD30-monomethyl auristatin E conjugate with potent and selective antitumor activity.* Blood, 2003. **102**(4): p. 1458-65.
58. Doronina, S.O., et al., *Development of potent monoclonal antibody auristatin conjugates for cancer therapy.* Nat Biotechnol, 2003. **21**(7): p. 778-84.
59. Sievers, E.L. and P.D. Senter, *Antibody-drug conjugates in cancer therapy.* Annu Rev Med, 2013. **64**: p. 15-29.
60. Atkinson, J.M., C.S. Siller, and J.H. Gill, *Tumour endoproteases: the cutting edge of cancer drug delivery?* British Journal of Pharmacology, 2008. **153**(7): p. 1344-1352.
61. Choi, K.Y., et al., *Protease-activated drug development.* Theranostics, 2012. **2**(2): p. 156-78.
62. Mittal, S., et al., *Proline prodrug of melphalan, prophalan-L, demonstrates high therapeutic index in a murine melanoma model.* Eur J Pharm Biopharm, 2007. **67**(3): p. 752-8.
63. Mittal, S., et al., *Proline prodrug of melphalan targeted to prolidase, a prodrug activating enzyme overexpressed in melanoma.* Pharm Res, 2007. **24**(7): p. 1290-8.
64. Bielawski, K., et al., *Proline-linked nitrosoureas as prolidase-convertible prodrugs in human breast cancer cells.* Pharmacol Rep, 2008. **60**(2): p. 171-82.
65. Mittal, S., et al., *Prolidase, a potential enzyme target for melanoma: design of proline-containing dipeptide-like prodrugs.* Mol Pharm, 2005. **2**(1): p. 37-46.
66. Liu, C., et al., *Overexpression of legumain in tumors is significant for invasion/metastasis and a candidate enzymatic target for prodrug therapy.* Cancer Res, 2003. **63**(11): p. 2957-64.
67. Wu, W., et al., *Targeting cell-impermeable prodrug activation to tumor microenvironment eradicates multiple drug-resistant neoplasms.* Cancer Res, 2006. **66**(2): p. 970-80.
68. Denmeade, S.R., et al., *Prostate-specific antigen-activated thapsigargin prodrug as targeted therapy for prostate cancer.* J Natl Cancer Inst, 2003. **95**(13): p. 990-1000.
69. Garsky, V.M., et al., *The synthesis of a prodrug of doxorubicin designed to provide reduced systemic toxicity and greater target efficacy.* J Med Chem, 2001. **44**(24): p. 4216-24.
70. Tauro, J.R., et al., *Matrix metalloprotease selective peptide substrates cleavage within hydrogel matrices for cancer chemotherapy activation.* Peptides, 2008. **29**(11): p. 1965-73.

71. Van Valckenborgh, E., et al., *Targeting an MMP-9-activated prodrug to multiple myeloma-diseased bone marrow: a proof of principle in the 5T33MM mouse model.* Leukemia, 2005. **19**(9): p. 1628-33.
72. Tauro, J.R. and R.A. Gemeinhart, *Extracellular protease activation of chemotherapeutics from hydrogel matrices: a new paradigm for local chemotherapy.* Mol Pharm, 2005. **2**(5): p. 435-8.
73. Tehler, U., et al., *Puromycin-sensitive aminopeptidase: an antiviral prodrug activating enzyme.* Antiviral Res, 2010. **85**(3): p. 482-9.
74. Lehninger, A.L., D.L. Nelson, and M.M. Cox, *Lehninger principles of biochemistry*. 3rd ed. 2000, New York: Worth Publishers.

CHAPTER II

CHARACTERIZATION OF THE ESTERASE ACTIVITIES OF HUMAN CYTOMEGALOVIRUS PROTEASE A143S

SUMMARY

The human cytomegalovirus (hCMV) infects a high percentage of the population and could cause serious, life-threatening diseases in immunocompromised patients. The hCMV protease, a serine protease encoded by the viral genome, plays an important role in the maturation of the virion. The crystal structure, catalytic mechanism, substrate preferences and *in vitro* proteolytic reaction conditions for the hCMV protease have all been well studied. Hypothetically, serine proteases like the hCMV protease could also exhibit hydrolytic activities toward ester substrates. In this chapter, I expressed and purified the relatively stable mutant of hCMV protease (A143S) and then characterized its esterase activities against an array of N-terminally protected (L)-amino acid-*p*-nitrophenol esters. It was discovered that some of those ester substrates could be preferentially hydrolyzed by hCMV protease A143S. The preference at the P_1 position of the ester substrate was alanine (Ala) > (α,L)-aminobutyric acid (Abu) = glycine (Gly) > methionine (Met) > all others, and at the N-terminal protecting group, benzyloxycarbonyl (Cbz) > butyloxycarbonyl (Boc). These results demonstrated the esterase activity of hCMV protease against selective small molecular esters and this knowledge would be used in designing the promoieties of ester prodrugs for targeted activation by the hCMV protease.

BACKGROUND

Human Cytomegalovirus (hCMV): Relevant Infections and Diseases

The human cytomegalovirus (hCMV; species name human herpesvirus 5, HHV-5) belongs to the *Herpesviridae* family and *betaherpesvirinae* subfamily of known viruses [1]. It was first named in 1957 by Weller *et al*. after frequent observations of enlarged fibroblast cells infected with this virus [2]. It has been estimated that hCMV infects on average over 58% of all individuals over 6 years old in the United States as determined by a study that employed serological testing of hCMV-specific immunoglobulins from over 21,000 individuals [3]. The same study also shows that the percentage of the population infected with hCMV steadily increases with age, from around 36% in 6-11 year-old humans to over 90% in 80 year-olds [3]. Congenital infection is an important route for the hCMV infection in newborns [4]; after childbirth the virus is primarily transmitted by sexual contact and via other bodily fluids such as transfused blood and breast milk [5].

In most immunocompetent individuals, hCMV causes few overt symptoms following the primary infection [6]. However, it has been established that hCMV is able to achieve latent infections of leukocytes with myeloid lineage, especially monocytes, and the bone marrow is one of the latent reservoirs for the virus [7, 8]. In healthy subjects, the period of viral latency is usually asymptomatic. However, when the infected subject becomes immunosuppressed or immunocompromised, hCMV in latency is readily reactivated and enters the lytic cycle, causing severe, sometimes fatal, infections [6, 9]. In solid organ and bone marrow transplant recipients, organs and tissues that could be infected by hCMV include lung (pneumonitis), retina (retinitis) and the entire gastrointestinal tract (esophagitis, gastritis and colitis) [9]. For high-risk recipients (hCMV-negative patients receiving transplants from hCMV-positive donors) without prophylaxis, up to 73% may develop infectious complications caused by hCMV; hCMV has also been shown to be a probable cause for acute graft rejections [10]. For acquired immunodeficiency syndrome (AIDS) patients, up to 90% of them may develop hCMV-related diseases from opportunistic infections [9]. HCMV retinitis is the most commonly observed hCMV-related infection in patients with AIDS (up to 40%);

hCMV-encephalitis, pneumonitis, adrenalitis and GI tract infections are also frequently encountered [9, 11].

Introduction to the Human Cytomegalovirus Protease

The human cytomegalovirus has a double-stranded DNA genome with a size of approximately 235 kilobase pairs (kbp) that encode up to 232 open reading frame (ORF) sequences that could potentially be translated as viral proteins [6]. Most of the hCMV ORFs are typically given the standardized names of "UL" or "US" followed by a designated alphanumeric code, of which UL and US refer to the U_L and U_S domains within the genome [6].

The human cytomegalovirus protease (hCMV protease, also known as hCMV assemblin) exert crucial roles during the assembly of newly synthesized virion: it degrades internal scaffolding proteins from the procapsid, thus aiding the maturation of the capsid for successful viral DNA incorporation [12]. The hCMV protease is encoded within the UL80 ORF of the viral genome. During the viral protein synthesis, the hCMV protease is translated from UL80 ORF first as a precursor protein, with 708 amino acid residues. The precursor protein has proteolytic activity: it first cleaves itself at the "maturational site" (M-site) of alanine 643 near the C terminus, then undergoes autoproteolysis again at Ala256 ("release site", R-site) [13]. The N-terminal product, sometimes called N_0, is the mature hCMV protease and cleavages at both the M- and R-sites are required for viral infectivity [14]. Another "internal cleavage" site ("I-site") for autoproteolysis has also been discovered within the mature protease at Ala143. It has been suggested that autoproteolysis at the I-site may be involved in the regulation of hCMV protease by the virus [12, 15]. The resulting two fragments from the autoproteolysis somewhat retain the catalytic activities of the hCMV protease [16]. Nevertheless, for the sake of uniformity and purity, it has been a general practice in biochemical studies to mutate Ala143 to other amino acid residues like glutamine (Q), serine (S), threonine (T) or valine (V) when the protease is to be overexpressed. As an example, the A143S mutant of hCMV protease is eight times more stable than the wild type protease but retains similar proteolytic activities as the wild type [16].

The mature hCMV protease has 256 amino acid residues and a molecular weight of around 28 kilodaltons. The crystal structure of hCMV protease has been determined at various resolutions [17-21] and it was discovered that hCMV protease is a serine protease, its catalytic triad being Ser 132, His 63 and His 157. Although this is different from the typical Ser-His-Asp catalytic triads of most serine proteases, the relative spatial positions of the catalytic triad of hCMV protease are especially similar to those of the chymotrypsin-like proteases [17], suggesting that hCMV protease indeed preserves the essential components for a typical serine protease. Interestingly, commonly used covalent serine protease inhibitors such as phenylmethylsulfonyl fluoride (PMSF) and tosylleucine chloromethyl ketone (TLCK) are not good inhibitors for the hCMV protease [22], indicating that its active site is still distinct from other serine proteases. The hCMV protease was also found to exhibit monomer-dimer equilibrium in solution and that its dimerization is essential for the proteolytic activities [23, 24]. In *in vitro* studies with purified hCMV protease, factors like high glycerol content, high ionic strength and a temperature of 30°C (in comparison to other temperatures) could all facilitate the dimerization of hCMV protease, thus greatly increasing its proteolytic activity [24-26].

The substrates and their recognition by the hCMV protease have also been well defined. Structural insights have demonstrated that the hCMV protease has a relatively small S_1 pocket, which only allows P_1 amino acid residues with a relatively small side chain [20, 21]. Alanine is the natural and preferred amino acid residue at the P_1 position. The side chains at the P_2 and P_4 positions could be more variable because they are facing away from the S_2 and S_4 substrate-binding pockets [20]. The S_3 pocket of the protease is relatively more spacious than S_1 and can tolerate various sizes of side chains for the P_3 position [20]. Such structure-activity relationship (SAR) studies have led to the development of several potent experimental inhibitors, some of them having IC_{50}'s of lower than 50 nM [21].

Potential Esterase Activities of the Human Cytomegalovirus Protease

In theory, the hCMV protease should only be present in the virally infected tissue and cells. This makes the hCMV protease a potential target enzyme for the activation of site-directed anti-hCMV prodrugs. As detailed in Chapter I, serine proteases could possess

inherent esterase activities toward peptidyl esters with specific substrate sequences. The hCMV protease, with its catalytic triad aligned in a similar fashion to chymotrypsin-like proteases, could likely harbor esterase-like activities as well. Identification of its esterase functions, especially substrate preferences, will be crucial for the design of hCMV-activated ester prodrugs with said substrates as promoieties. Another reason for characterization for hCMV protease's esterase activity stems from the chemical structures of currently used anti-CMV medications, including ganciclovir, foscarnet, cidofovir and acyclovir [27]. All four drugs have one or more hydroxyl groups, thus making development of ester prodrugs (as opposed to amides or others) of these compounds a logical choice.

The carboxylic esters of *p*-nitrophenol have long been used for characterization of the substrate preference of esterases and proteases [28]. In this chapter I planned to first overexpress and purify a stable mutated hCMV protease, then to test its esterase activities toward a library of *p*-nitrophenyl carboxylic esters. I aim to define the preference of ester substrates of hCMV protease at the P_1 and (less so) P_2 positions so that these substrate sequences could be used as promoieties for the development of activatable prodrugs.

MATERIALS AND METHODS

Materials

The plasmid pET29b-hCMVP(A143S)-His_6 was a generous gift from Dr. Hairat Sabit. *Escherichia coli* strain BL21(DE3)-RIPL was purchased from Stratagene (Santa Clara, CA). Kanamycin powder and agar were purchased from Fisher Scientific (Pittsburgh, PA). Isopropyl β-D-1-thiogalactopyranoside (IPTG), Triton X-100 and lysozyme powder were purchased from Sigma Aldrich (St. Louis, MO). Deoxyribonuclease (DNase) was purchased from New England Biolabs (Ipswich, MA). Ni^{2+}-NTA agarose resins were purchased from Qiagen (Gaithersburg, MD). Terrific Broth and Tris-glycine minigels used for sodium dodecyl sulfate polyacrylamide gel electrophoresis (SDS-PAGE) were purchased from Invitrogen (Grand Island, NY). Bicinchoninic acid (BCA) assay kits and Krypton staining kits were purchased from Pierce (Rockford, IL). PD-10 desalting columns were purchased from GE Healthcare Life Sciences (Piscataway, NJ).All the *N*-*tert*-butyloxycarbonyl-amino acid-*p*-nitrophenyl esters and *N*-benzyloxycarbonyl-amino acid-*p*-nitrophenyl esters were purchased from Chem-Impex (Wood Dale, IL).

Expression of hCMV Protease A143S by *Escherichia coli*

E. coli strain BL21(DE3)-RIPL transformed with the plasmid pET29b-hCMVP(A143S)-His_6 was grown in Terrific Broth (TB) medium with 30 µg/mL kanamycin. To induce the expression of hCMVP A143S in *E. coli*, a final concentration of 0.3 mM IPTG was added and the culture is shaken at 220 rpm, 30°C for 5 hours. The culture was then cooled down on ice and the bacterial pellets collected by centrifugation of the culture at 7,000×g at 4°C for 20 min.

Purification and Detection of hCMV Protease A143S

The aforementioned *E. coli* pellets were resuspended in wash buffer (50 mM NaH_2PO_4, 300 mM NaCl, 20 mM imidazole, pH 8.0) containing 1 mg/mL lysozyme, 0.01% DNase and 1% Triton X-100. The mixture was then sonicated and centrifuged. The cleared supernatant was incubated with pre-equilibrated Ni^{2+}-NTA agarose resin at 4°C for 90 min. The resins were then washed three times with wash buffer and then wash buffer containing 400 mM

imidazole was used to elute the His_6-tagged protein from the resins. The eluate was passed through a desalting PD-10 column for the removal of salts and eluted with protein storage buffer (20 mM Tris·HCl, 0.2 mM EDTA, 100 mM NaCl, 1 mM dithiothreitol, pH 7.9 at 25°C). The final eluate was aliquoted and frozen at -80°C before use. Quantification of protein concentrations was achieved with BCA assays. The expression of hCMV protease A143S is detected by Krypton staining of an SDS-PAGE Tris-glycine minigel (4-20%, 1.5 mm, 10-well) loaded with eluate samples, which was visualized on a Typhoon 9200 scanner at excitation / emission wavelengths of 525 / 580 nm. Band intensities were quantified using ImageQuant version 5.0.

Hydrolysis of Substrates Catalyzed by hCMV Protease A143S

N-*tert*-butyloxycarbonyl-(L)-amino acid-*p*-nitrophenyl esters (Boc-XAA-ONp, XAA: Abu, Ala, Asn, Gly, Ile, Leu, Met, Phe, Pro, Trp, Val) and *N*-benzyloxycarbonyl-(L)-amino acid-*p*-nitrophenyl esters (Cbz-XAA-ONp, XAA: Ala, norleucine (Nle)) substrates (structures shown in **Figures 2.1 and 2.2**) at 50 μM final concentrations were added to reaction buffers (50 mM Tris, pH 7.6 at 25 °C, with 0.5 M Na_2SO_4 and 10% glycerol) with or without 10 μg/mL hCMV protease A143S. The reactions were incubated at 30°C for one hour, during which time absorptions at 405 nm (A405) were periodically read and recorded by a Biotek Synergy HT plate reader for the quantification of the release of *p*-nitrophenol (*p*-NP) from their respective ester compounds (**Figure 2.3**).

Data Analysis

An A405 vs. *p*-nitrophenol polynomial standard curve was generated and concentrations of *p*-NP in substrate hydrolysis samples were calculated from their respective A405 values. To determine the amounts of hydrolyzed substrates catalyzed by the protease, the concentrations of *p*-NP released by a substrate in blank buffer were subtracted from that of the same substrate in hCMVP A143S-containing buffer. The percentage hydrolyzed for different substrates at 10 min after the initiation of the reactions were compared with others using one-way analysis of variance (ANOVA) with *post-hoc* Tukey's multiple comparison tests. The statistical analysis was performed with GraphPad Prism (v5.0).

RESULTS

Expression and Purification of hCMV Protease A143S

The protease was expressed relatively robustly in *E. coli*; the final yield, as quantified by BCA assays, was approximately 13 mg from 500 mL of bacterial culture. As shown in **Figure 2.4**, the prepared protease was also highly pure, as it was determined that the prepared batch of hCMV protease A143S had a minimum purity of 91% (mass ratio).

Hydrolysis of Ester Substrates Catalyzed by hCMV Protease A143S

The hCMV protease displays differential preferences toward the *p*-nitrophenyl ester substrates tested. 8 of the 13 substrates tested demonstrated no catalytic hydrolysis by hCMVP compared to buffer: Boc-Asn-ONp, Boc-Ile-ONp, Boc-Leu-ONp, Boc-Phe-ONp, Boc-Pro-ONp, Boc-Trp-ONp, Boc-Val-ONp and Cbz-Nle-ONp. Of the five that did display enzymatic hydrolysis (**Figure 2.5**), Cbz-Ala-ONp generated the most *p*-nitrophenol at 10 min, almost 60% more than Boc-Ala-ONp, which released the second highest amount. This clearly showed the effects of the "protecting group" of the substrates on their affinity to the protease. Boc-Abu-ONp, an ester containing the unnatural amino acid (α,L)-aminobutyric acid, and Boc-Gly-ONp, could also be hydrolyzed by hCMV protease, though the extent of hydrolysis is approximately 27% and 33% less than Boc-Ala-ONp, respectively. This observation reaffirmed that Ala is the preferred amino acid at P_1 position. In addition, Boc-Met-ONp could also be hydrolyzed by the protease, albeit at a rate much slower than the other four. In summary, within a limited scope this screening study identified hCMV protease's preference of specific components comprising the ester substrates, with benzyloxycarbonyl (Cbz) over butyloxy (Boc) at the N-terminus protecting group and, at the P_1 position, Ala over Abu, Gly and all others tested.

DISCUSSION

In this study I was able to express and purify from bacterial cultures C-terminally His_6-tagged hCMV protease A143S and the resulting batch contains said protease at a relatively high purity. I also managed to discover and quantitatively compare hCMVP A143S's esterase activities toward several protected amino acid-*p*-nitrophenol substrates. This knowledge would be directly used in subsequent designs of prodrugs that could be activated by hCMVP.

The purity of the hCMV protease A143S in the final eluate is relatively high (~91%), as determined by quantification of fluorescence intensities of bands in the Krypton-stained SDS-PAGE gel. Although measures had been taken to minimize protein degradation (such as shortening the total time spent on the purification process and performing almost all procedures at 4°C), autoproteolysis products of the hCMV protease A143S were still observed. In **Fig. 2.4**, the two bands located slightly above the 15-kD marker correspond to the 16- and 17-kD autoproteolytic products from the predicted internal cleavage at Ala143 of the 33-kD hCMV(A143S)-His_6 protein [12]. The total amounts of these products are relatively small (4.8%). Although previous studies reported that these products retain some degrees of proteolytic activity [12, 16], they would still be regarded to as impurities in all subsequent studies.

Previous reports have shown that the dimerization of hCMV protease is required for its proteolytic activity and influenced by factors like glycerol content, ionic strength and temperature [24-26]. Therefore, 0.5 M Na_2SO_4 and 10% glycerol were supplemented into the reaction buffer and reactions were also performed at 30°C, all these measures aiming at enhancing the dimerization of hCMV protease A143S and thus its activity in the *in vitro* environment. This condition would also be used in subsequent studies of prodrug activation by hCMV protease A143S in Chapter III.

The *p*-nitrophenyl esters have long been used to characterize enzymes' esterase activities due to their high reactivity [28]. In our study, it was observed that almost all the *p*-nitrophenyl esters tested could undergo some degree of spontaneous hydrolysis in the (blank) buffer (50 mM Tris, pH 7.6 at 25 °C, with 0.5 M Na_2SO_4 and 10% glycerol). Their rates of

chemical hydrolysis were also vastly different: while some of them, such as Boc-Ile-ONp and Boc-Pro-ONp, were relatively stable in buffer (< 1% hydrolyzed in buffer at 1 h), a few others like Boc-Asn-ONp were found to be very labile (> 70% hydrolyzed in buffer in less than 2 min), thus making them unsuitable for screening. As a result, at all the time points, the amounts of *p*-nitrophenol generated by hCMVP catalysis had to be derived from amounts of *p*-Np in hCMVP plus buffer subtracted by those in just buffer. Using Boc-Abu-ONp as a representative of substrates, its spontaneous hydrolysis and release of *p*-Np over a period of 45 min is shown in **Figure 2.6**.

The high reactivity of *p*-nitrophenyl esters in both buffer and hCMVP-containing systems also caused an unexpected problem: the initial "burst" of the reactions was so rapid that it could not be captured. As a result, the preferred parameter to characterize hydrolysis kinetics, the initial rate (v_0), could not be accurately determined. Instead, the hydrolysis percentage at 10 min was used as a surrogate because at this point sufficient amounts of substrates have been hydrolyzed and none had yet reached the "plateau". This percentage is proportional to the average rate of hydrolysis within the first 10 min and could reflect the protease's efficiency in catalyzing the breakdown of esters.

Eventually, I discovered several preferences of hCMV protease toward the components of the ester substrates. At the P_1 position, alanine, with a methyl on the side chain, is preferred over (α,L)-aminobutyric acid (ethyl side chain), glycine (no side chain) and methionine (methylthioethyl side chain). This finding could be explained by previous structure-activity relationship (SAR) studies [20]. The S_1 pocket of the protease was found to be small and could only tolerate methyl and (to a lesser degree) ethyl groups as P_1 side chains [20], or no side chain at all in the case of glycine. That Boc-Met-ONp was slowly hydrolyzed in buffer systems with hCMVP was surprising because the size of methionine's side chain is, in theory, too large to fit in the S_1 pocket of the protease. It was also observed that another substrate with structural similarity at P_1, Cbz-Nle-ONp (**Fig. 2.2**), could not be hydrolyzed at all by the protease. Therefore this may suggest a potentially new mechanism of hCMVP-mediated catalysis. More SAR studies could be carried out to further probe into this phenomenon.

The comparison between *tert*-butyloxy carbonyl (Boc) and benzyloxycarbonyl (Cbz) at the N-terminal protecting group of the *p*-nitrophenyl ester substrates was also made and Cbz was found to be preferred over Boc by the hCMV protease. The position of the protecting group within the substrates corresponds to that of the P_2 amino acid residue. Therefore, this knowledge could be translated to the design of promoieties of prodrugs: If an *N*-protected amino acid is to be used as the promoiety, the protecting group should be Cbz rather than Boc; or, in the case of a dipeptide prodrug, the P_2 amino acid residue should have a side chain that resembles the structure of Cbz instead of that of Boc.

CONCLUSIONS

The human cytomegalovirus (hCMV) protease A143S mutant possesses inherent *in vitro* esterase activities toward certain substrates N-terminally protected (L)-amino acid-*p*-nitrophenol esters. The preference at the P_1 position of the ester substrate was found to be alanine (Ala) > (α,L)-aminobutyric acid (Abu) = glycine (Gly) > methionine (Met). At the N-terminal protecting group, benzyloxycarbonyl (Cbz) is preferred over butyloxycarbonyl (Boc). These findings would be utilized for the designs of promoieties of ester prodrugs that could potentially be hydrolytically activated by the hCMV protease.

FIGURES

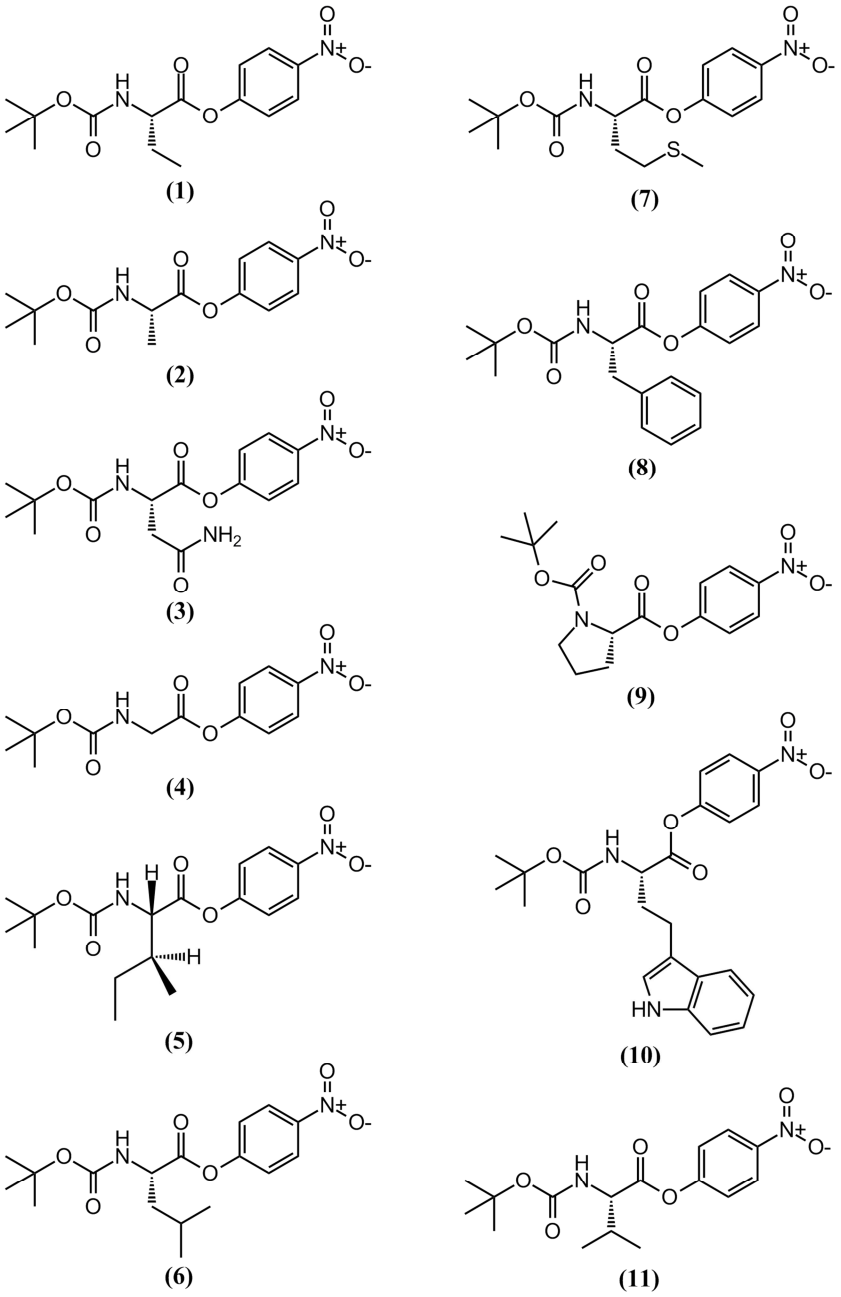

Figure 2.1. Chemical structures of *N-tert*-butyloxycarbonyl-(L)-amino acid-*p*-nitrophenyl esters (Boc-XAA-ONp). (1) Boc-Abu-ONp, Abu: (α)-aminobutyric acid; (2) Boc-Ala-ONp; (3) Boc-Asn-ONp; (4) Boc-Gly-ONp; (5) Boc-Ile-ONp; (6) Boc-Leu-ONp; (7) Boc-Met-ONp; (8) Boc-Phe-ONp; (9) Boc-Pro-ONp; (10) Boc-Trp-ONp; (11) Boc-Val-ONp. All amino acid residues are (L)-isomers.

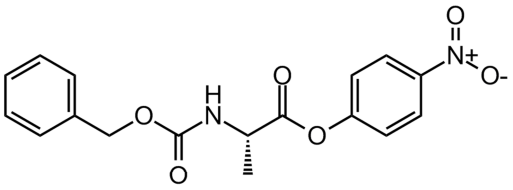

(1)

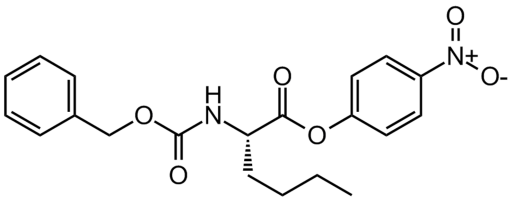

(2)

Figure 2.2. Chemical structures of *N*-benzyloxycarbonyl-(L)-amino acid-*p*-nitrophenyl esters (Cbz-XAA-ONp). (1) Cbz-Ala-ONp; (2) Cbz-Nle-ONp, Nle: norleucine.

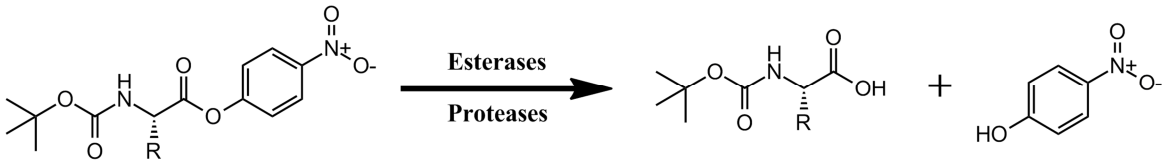

(1)

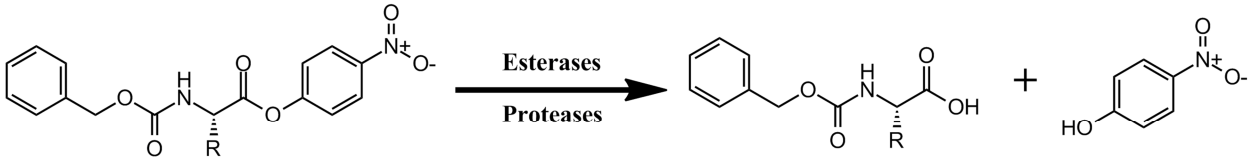

(2)

Figure 2.3. Hydrolysis of Boc-XAA-ONp (1) and Cbz-XAA-ONp (2). In aqueous solutions and under favorable conditions and in the presence of certain esterases and proteases, Boc-XAA-ONp and Cbz-XAA-ONp substrates could be catalytically hydrolyzed to release *p*-nitrophenol and Boc-XAA-OH and Cbz-XAA-OH carboxylic acids, respectively. The concentration of *p*-nitrophenol could be quantified from spectrophotometry absorbance readings at 405 nm.

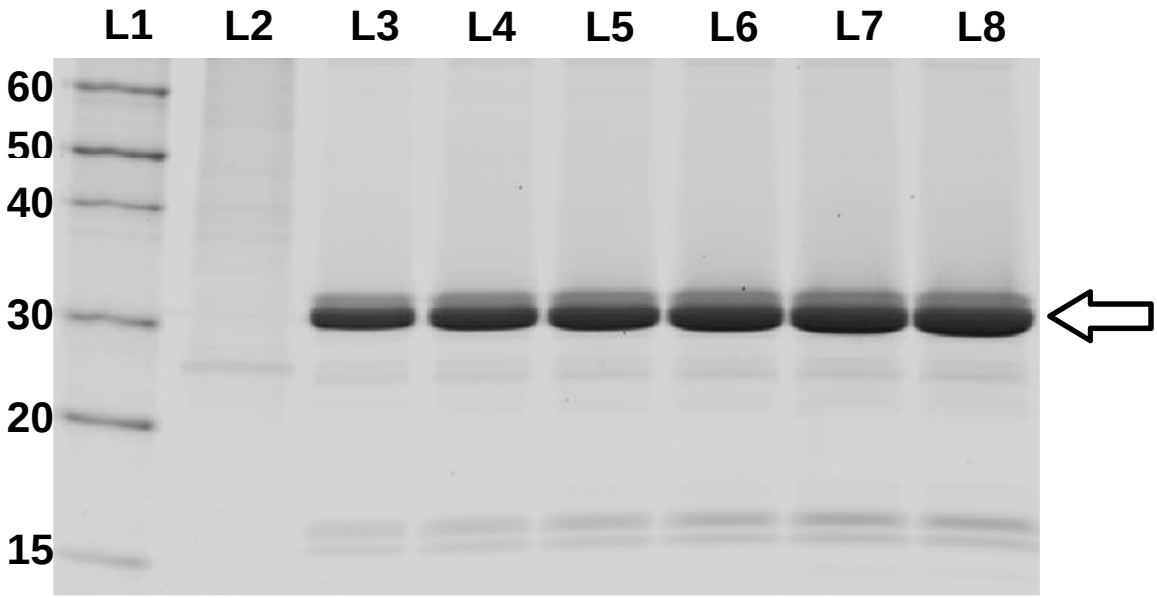

Figure 2.4. Representative Tris-glycine gel of purified His_6-tagged hCMV protease A143S stained with Krypton®. The protein samples loaded onto a 4%-20% Tris-glycine (1.5mm, 10 wells) minigel and electrophoresis was performed at 30 mA for 120 min. Krypton staining was performed for 1 h and the minigel was de-stained overnight. The minigel was then scanned on a Typhoon 9200 variable mode scanner, detecting fluorescence emission at 580 nm. Lane 1 (L1): 200 ng Novex Sharp unstained ladder; L2: 20 µL flowthrough after second wash of the protein-bound Ni^{2+}-NTA resin; L3 – L8: 300, 400, 500, 600, 700 and 750 ng final eluate from the PD-10 column. Arrow shows the band of His_6-tagged hCMV protease A143S (33 kD). The intensity of each band was quantified by ImageQuant software v5.0 and average purity of the 33kD main band was calculated among L3 through L8.

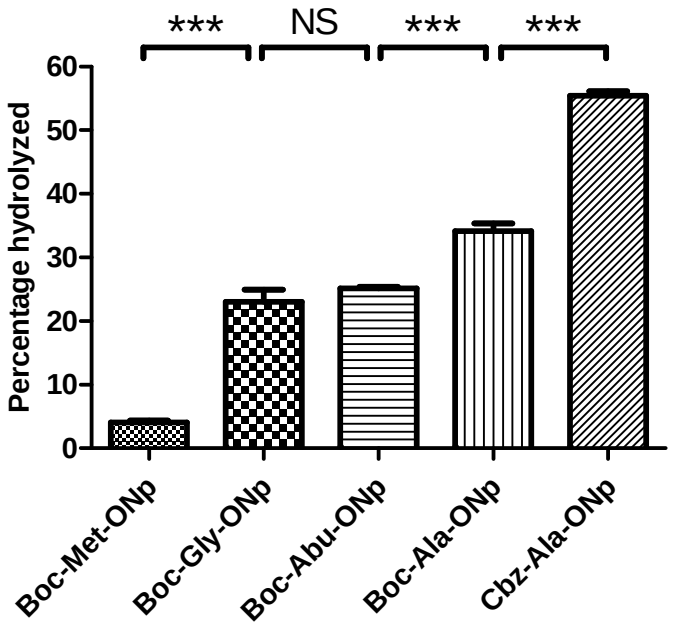

Figure 2.5. The percentages of 50 µM *p*-nitrophenyl ester substrates hydrolyzed by hCMV protease A143S at the 10-min time point. Enzymatic reactions were carried out in a 96-well plate setting. Following periodic shaking, A405 of each well was read and recorded by a Biotek Synergy HT plate reader. Concentrations of *p*-nitrophenol (*p*-Np) were calculated from a second-degree polynomial standard curve fitted to a plot of measured A405 vs. *p*-Np concentrations at 0, 10, 20, 35 and 50 µM. Concentrations of *p*-NP generated by hCMVP-catalyzed hydrolysis are derived from *p*-NP concentrations in wells with hCMVP subtracting by corresponding negative control wells with the same substrate but without hCMVP. Percentages hydrolyzed were calculated from *p*-Np concentrations divided by 50 µM. Only those substrates with significant hCMV-catalyzed hydrolysis were included in this graph. n =3 for all substrates; error bars represent SEM. One way analysis of variance (ANOVA) with *post-hoc* Tukey's tests was employed for statistical comparisons among the five substrates. NS, not significant; ***, $p < 0.001$.

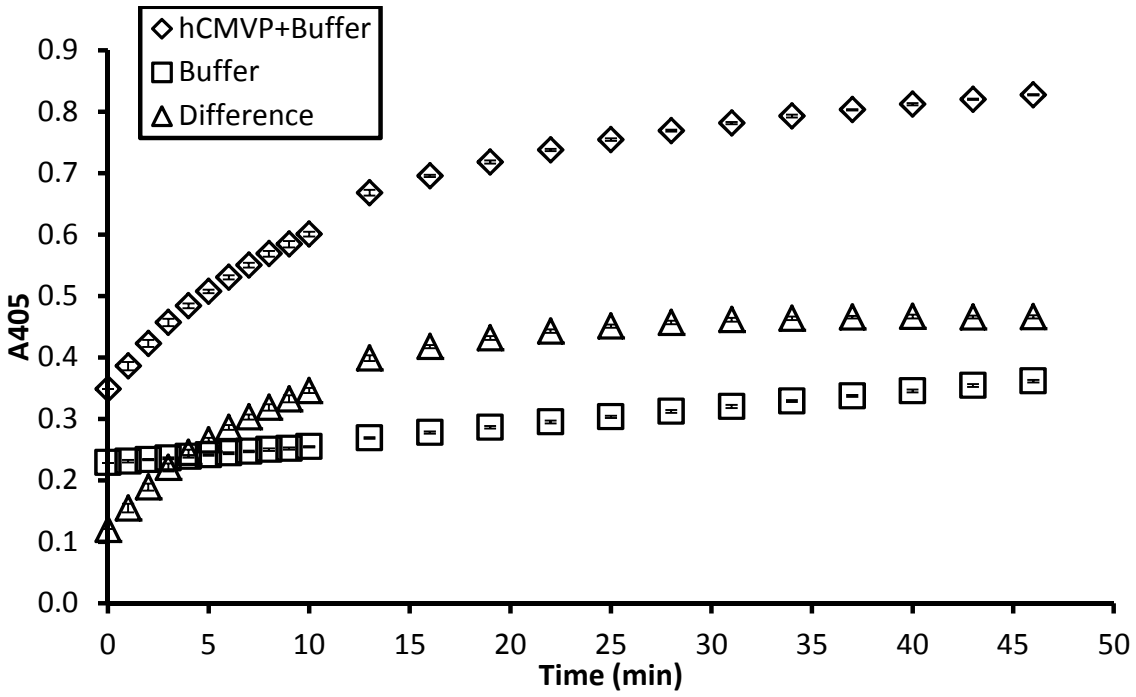

Figure 2.6. The time course of A405 readings from Boc-Abu-ONp in either buffer or buffer with hCMV protease A143S. “Difference” is calculated from subtraction of A405 in buffer from A405 in hCMV + buffer at each time point. n =3 for all time points; error bars represent standard deviations.

REFERENCES

1. *Virus taxonomy: 2011 release. International Committee on Taxonomy of Viruses. URL: http://www.ictvonline.org/virusTaxonomy.asp.* 2011.
2. Craig, J.M., et al., *Isolation of intranuclear inclusion producing agents from infants with illnesses resembling cytomegalic inclusion disease.* Proc Soc Exp Biol Med, 1957. **94**(1): p. 4-12.
3. Staras, S.A., et al., *Seroprevalence of cytomegalovirus infection in the United States, 1988-1994.* Clin Infect Dis, 2006. **43**(9): p. 1143-51.
4. Gaytant, M.A., et al., *Congenital cytomegalovirus infection: review of the epidemiology and outcome.* Obstet Gynecol Surv, 2002. **57**(4): p. 245-56.
5. Peckham, C.S., et al., *Early acquisition of cytomegalovirus infection.* Arch Dis Child, 1987. **62**(8): p. 780-5.
6. Shenk, T. and M. Stinski, *Human cytomegalovirus*. Current topics in microbiology and immunology. 2008, Berlin: Springer. xiii, 475 p.
7. Mendelson, M., et al., *Detection of endogenous human cytomegalovirus in CD34+ bone marrow progenitors.* J Gen Virol, 1996. **77 (Pt 12)**: p. 3099-102.
8. Taylor-Wiedeman, J., P. Sissons, and J. Sinclair, *Induction of endogenous human cytomegalovirus gene expression after differentiation of monocytes from healthy carriers.* J Virol, 1994. **68**(3): p. 1597-604.
9. Sissons, J.G.P. and A.J. Carmichael, *Clinical aspects and management of cytomegalovirus infection.* Journal of Infection, 2002. **44**(2): p. 78-83.
10. Lowance, D., et al., *Valacyclovir for the prevention of cytomegalovirus disease after renal transplantation. International Valacyclovir Cytomegalovirus Prophylaxis Transplantation Study Group.* N Engl J Med, 1999. **340**(19): p. 1462-70.
11. Drew, W.L., *Cytomegalovirus-Infection in Patients with Aids.* Clinical Infectious Diseases, 1992. **14**(2): p. 608-615.
12. Loveland, A.N., et al., *Cleavage of human cytomegalovirus protease pUL80a at internal and cryptic sites is not essential but enhances infectivity.* J Virol, 2005. **79**(20): p. 12961-8.
13. Welch, A.R., et al., *A herpesvirus maturational proteinase, assemblin: identification of its gene, putative active site domain, and cleavage site.* Proc Natl Acad Sci U S A, 1991. **88**(23): p. 10792-6.
14. Matusick-Kumar, L., et al., *Release of the catalytic domain N(o) from the herpes simplex virus type 1 protease is required for viral growth.* J Virol, 1995. **69**(11): p. 7113-21.
15. Jones, T.R., et al., *Proteolytic activity of human cytomegalovirus UL80 protease cleavage site mutants.* J Virol, 1994. **68**(6): p. 3742-52.
16. O'Boyle, D.R., 2nd, et al., *The effect of internal autocleavage on kinetic properties of the human cytomegalovirus protease catalytic domain.* J Biol Chem, 1995. **270**(9): p. 4753-8.
17. Tong, L., et al., *A new serine-protease fold revealed by the crystal structure of human cytomegalovirus protease.* Nature, 1996. **383**(6597): p. 272-5.
18. Chen, P., et al., *Structure of the human cytomegalovirus protease catalytic domain reveals a novel serine protease fold and catalytic triad.* Cell, 1996. **86**(5): p. 835-43.

19. Qiu, X., et al., *Unique fold and active site in cytomegalovirus protease.* Nature, 1996. **383**(6597): p. 275-9.
20. Tong, L., et al., *Conserved mode of peptidomimetic inhibition and substrate recognition of human cytomegalovirus protease.* Nat Struct Biol, 1998. **5**(9): p. 819-26.
21. Khayat, R., et al., *Structural and biochemical studies of inhibitor binding to human cytomegalovirus protease.* Biochemistry, 2003. **42**(4): p. 885-91.
22. Welch, A.R., et al., *Herpesvirus proteinase: site-directed mutagenesis used to study maturational, release, and inactivation cleavage sites of precursor and to identify a possible catalytic site serine and histidine.* J Virol, 1993. **67**(12): p. 7360-72.
23. Cole, J.L., *Characterization of human cytomegalovirus protease dimerization by analytical centrifugation.* Biochemistry, 1996. **35**(48): p. 15601-10.
24. Margosiak, S.A., et al., *Dimerization of the human cytomegalovirus protease: kinetic and biochemical characterization of the catalytic homodimer.* Biochemistry, 1996. **35**(16): p. 5300-7.
25. Darke, P.L., et al., *Active human cytomegalovirus protease is a dimer.* Journal of Biological Chemistry, 1996. **271**(13): p. 7445-7449.
26. Khayat, R., et al., *Characterization of the monomer-dimer equilibrium of human cytomegalovirus protease by kinetic methods.* Biochemistry, 2004. **43**(2): p. 316-22.
27. Chou, S.W., *Cytomegalovirus drug resistance and clinical implications.* Transpl Infect Dis, 2001. **3 Suppl 2**: p. 20-4.
28. Hedstrom, L., *Serine protease mechanism and specificity.* Chem Rev, 2002. **102**(12): p. 4501-24.

CHAPTER III

MONOESTER PRODRUGS OF GANCICLOVIR: TARGETED PROTEOLYTIC ACTIVATION AND TISSUE STABILITY

SUMMARY

Ganciclovir, a nucleoside analogue compound, remains the first line treatment as well as prophylactic agent for diseases caused by human cytomegalovirus (hCMV). Ganciclovir achieves its pharmacological effects by inhibition of viral DNA synthesis; however, it could also cause severe side effects, most notably hematotoxicity. Based on results from Chapter II, I synthesized four monoester prodrugs of ganciclovir, including *N*-benzyloxycarbonyl-(L)-alanine-ganciclovir (CbzAlaGCV), *N*-benzyloxycarbonyl-(α,L)-aminobutyric acid-ganciclovir (CbzAbuGCV), *N*-acetyl-(L)-phenylalanine-(L)-alanine-ganciclovir (AcPheAlaGCV) and *N*-acetyl-(L)-phenylalanine-(α,L)-aminobutyric acid-ganciclovir (AcPheAbuGCV). These prodrugs could be potentially targeted to activation by the hCMV protease expressed at hCMV infection sites, thereby possibly reducing the dosage needed and the systemic toxicities caused by ganciclovir. The hydrolysis of all four prodrugs by hCMV protease A143S, uninfected cytoplasm (represented by Caco-2 cell homogenates) and human plasma was characterized in a time-course setting. The stability of AcPheAlaGCV and AcPheAbuGCV in pooled human liver microsomes as well as the two prodrugs' Michaelis-Menten kinetic parameters for hydrolysis by both hCMV protease A143S and Caco-2 homogenates were also determined. Through statistical comparisons, it was concluded that the differentiated characteristics displayed by AcPheAlaGCV and AcPheAbuGCV rendered both of them as better candidates for further development in the targeted prodrug strategy.

AcPheAlaGCV could be activated by hCMV protease at a relatively high rate, but it was not as stable in normal tissue matrices as AcPheAbuGCV was. The latter was the most stable of all four prodrugs in all normal tissues matrices, but its hCMV protease-catalyzed hydrolysis rate was slower than AcPheAlaGCV. Altogether, I conducted a systematic characterization on the activation-stability interplay in the targeted prodrug strategy for hCMV protease and provided quantitative insights on how different factors in both activation and tissue stability of the prodrugs could influence their targeting efficiency.

BACKGROUND

As introduced in Chapter II, morbidity and mortality caused by infections related to human cytomegalovirus (hCMV) continue to pose a serious threat to immunosuppressed and immunocompromised patients. Currently, six pharmaceutical compounds have been approved by the US FDA for the treatment and / or prophylaxis of hCMV diseases. Ganciclovir [1, 2], valganciclovir [3], foscarnet [4], cidofovir [5] and fomivirsen [6] are used for the treatment of CMV retinitis in transplant and / or HIV patients. In addition, ganciclovir, valganciclovir and a biologic, CMV Immune Globulin Intravenous (Human) (CMV-IGIV) [7], are indicated for use of prophylaxis of hCMV diseases in transplant patients.

Ganciclovir: Clinical Anti-hCMV Efficacy

Ganciclovir was the first drug approved by the US FDA for antiviral management of cytomegalovirus diseases (in June 1989) [8] and remains the first-line treatment and prophylactic agent for hCMV [9]. It is currently available in two dosage forms, namely Cytovene-IV® (intravenous injection) [1] and Vitrasert® (intravitreal implant) [2]. Ganciclovir was found to clinically reduce the viral titer by more than 100-fold in at least 80% of patients with life- or sight-threatening hCMV infections [1]. In clinical studies on the treatment of CMV retinitis, ganciclovir was found to significantly delay the progression of retinitis compared to untreated controls [1, 2]. It was also found in prevention studies that ganciclovir could significantly reduce the incidences of hCMV diseases if it is given to transplant recipients immediately after they received solid organ or bone marrow engraftments [1, 10, 11]. Therefore, prophylaxis or preemptive treatment with ganciclovir is now considered a standard practice for transplant patients at high risks of developing hCMV infections [12].

Although treatment of CMV retinitis and prevention against hCMV diseases are the only two approved clinical usages for ganciclovir, the drug has also demonstrated efficacy against several other types of hCMV infections. Ganciclovir appeared to be effective against hCMV-related gastrointestinal tract infections, especially colitis, as it was shown to both reduce the viral counts in gut samples and improve symptoms such as diarrhea and weight loss [13-15]. In two other studies, ganciclovir combined with CMV-IGIV could significantly

reduce the symptoms and increase the survivability of bone marrow transplant patients inflicted with CMV pneumonia [16, 17]. Last but not least, the long-term benefits of treating hCMV hepatitis with ganciclovir are still uncertain, as patients displayed improved liver functions and decreased viral load in blood during the treatment but also relapses in infections after cessation of the drug therapy [18].

Ganciclovir: Physicochemical Properties, Mechanism of Action and Viral Resistance

Ganciclovir (9-[(1,3,-dihydroxy-2-propoxy)methyl]guanine, or DHPG; structure shown in **Figure 3.1a**) has a molecular formula of $C_{10}H_{13}N_5O_4$ and a molecular weight (MW) of 255.2. It is a polar compound with an *n*-octanol / water partition coefficient of 0.022 [1]. The "free base" form has a water solubility of 2.6 mg/mL at 25°C whereas the monosodium salt form is far more water-soluble at > 50 mg/mL (25°C) [1]. At physiological pH and 37°C, the sodium salt form has a solubility of 6 mg/mL [1].

Ganciclovir is an acyclic nucleoside with a structure mimicking that of deoxyguanosine (**Figure 3.1b**). It exerts its pharmacological effects by inhibition of viral DNA synthesis (**Figure 3.2**). After ganciclovir translocates into the hCMV-infected cells (mainly by passive diffusion [19]), it is first phosphorylated at one of its hydroxyl groups into ganciclovir monophosphate. This first step of phosphorylation is catalyzed by a protein kinase homologue encoded by the viral UL97 gene [20, 21] and estimated to be 10-fold faster in CMV-infected than uninfected cells [2, 22]. Ganciclovir monophosphate is then further phosphorylated by host cell kinases into ganciclovir diphosphate and, eventually, ganciclovir triphosphate [23]. Ganciclovir triphosphate is a competitive inhibitor of guanosine triphosphate (GTP) for the viral DNA polymerase (UL54, also known as *pol*). It is then incorporated into the viral DNA by the UL54 *pol* polymerase, but its acyclic structure slows down the elongation process of the DNA, thereby achieving the inhibitory effects on viral replication [9, 23]. The IC_{50} of ganciclovir on viral DNA replication generally falls in the range of 0.4 to 2.4 µM [12].

Ganciclovir-resistant hCMV strains (defined by IC_{50} > 3.0 mg/L or 12.0 µM) have been generated from laboratory-cultured strains as well as recovered from infected patients with or without prior treatment with ganciclovir [1, 12]. Subsequent studies discovered that

mutations or deletions in either one or both of the viral UL97 and UL54 genes lead to the resistance [24]. Deletions of 4 to 17 amino acid residues and a large variety of single amino acid mutations in the pUL97 kinase have been reported and the impaired phosphorylation of ganciclovir by the mutant pUL97 kinases confers viral resistance [24]. Mutations in the UL54 *pol* polymerase have also been reported to cause resistance to ganciclovir; some of these mutations may also have indications in the cross-resistance to cidofovir and / or foscarnet by certain virus strains [24]. Although the exact molecular mechanism of relationships between UL54 mutations and ganciclovir resistances is less clear, the decreased affinity of the mutated *pol* for ganciclovir triphosphate and the enhanced exonuclease activity of the mutant polymerase have been pointed to as the two most likely culprits [24, 25].

Ganciclovir: Dosing Regimens, Pharmacokinetics and Side Effects

The current FDA-approved routes of administration for ganciclovir are intravenous (IV) injection and intraocular injection [1, 2]. Its oral administration has now been discontinued due to its low bioavailability and the advent of valganciclovir [12]. For IV administration, it is typically given at doses of 2.5 or 5 mg/kg [26], although some studies suggested that 10 mg/kg might be optimal for achieving antiviral effects [27]. The pharmacokinetics of ganciclovir is largely linear during IV administration, with plasma c_{max} at 4.7 mg/L for 2.5 mg/kg dosage, 10 mg/L for 5 mg/kg and 20 mg/L for 10 mg/kg [1, 26, 27]. Plasma protein binding levels of ganciclovir are low, at 1% to 2% [1]. Ganciclovir is mainly eliminated in its unchanged form (> 90%) through renal excretion (via glomerular filtration and active tubular secretion) and has a half-life of approximately 3.5 h after IV administration [1].

Adverse events caused by ganciclovir have been well documented. Hematological toxicities, including neutropenia, anemia and thrombocytopenia, were commonly observed in patients administered with ganciclovir [1, 12, 26]. Bone marrow transplant (BMT) patients, with already low absolute neutrophil counts (ANCs), are particularly susceptible to neutropenia (ANC < 1000 / μL) after receiving ganciclovir as prophylactic or preemptive treatment [12]. It was found that 41% to 58% of all BMT patients treated with ganciclovir developed neutropenia, more than doubling the incidences in untreated subjects [10, 11]. In

addition, approximately 34% of patients at advanced stages of HIV infection could be inflicted with neutropenia after ganciclovir treatments [28]. These high frequencies clearly demonstrated the prevalence of ganciclovir-induced hematological side effects in specific patient groups.

The underlying causes of the hematological side effects of ganciclovir have been attributed to its toxicity toward bone marrow cells, especially the colony-forming hematopoietic progenitor cells [29]. In cell culture experiments, the IC_{50} of ganciclovir for bone marrow cells was 0.4 – 0.7 mg/L compared to 50 – 400 mg/L for other cell types like fibroblast and lung cells [23, 29, 30]. A few studies have demonstrated that the molecular mechanism of ganciclovir's toxicity on bone marrow cells is not dissimilar to that in virally infected cells. Although the first step of ganciclovir phosphorylation is catalyzed most efficiently by the UL97 viral kinase, it can also occur in uninfected cells, albeit at a slower rate [22]. However, ganciclovir triphosphate generated from later phosphorylation steps is still able to directly inhibit DNA synthesis and disrupt cell proliferation, as shown in an uninfected T lymphocyte model [31]. Findings from this study could be applied to hematopoietic progenitors, since they generally have higher rates of DNA replication and cellular proliferation than the mature T cells. In summary, the non-specific phosphorylation of ganciclovir and the eventual inhibition of DNA elongation are likely the causes for cytotoxicity of ganciclovir in bone marrow cells; as a result, hematotoxicity continues to be a routine occurrence in specific groups of patients treated with the drug.

Ganciclovir has also been reported to cause impaired renal functions, neurotoxicity and hepatotoxicity [12, 26]. However, the occurrence of these side effects is less frequent than hematotoxicity and these symptoms usually alleviate or disappear after the ganciclovir doses are reduced or stopped [12, 26]. The molecular mechanisms for these toxicities are still unclear. In addition, ganciclovir was seen in animal studies to inhibit spermatogenesis and impair fertility, although this was not observed in humans [1]. It is also a possible teratogen and thus listed as a Pregnancy Category C drug [1].

Other Therapeutic Agents against Human Cytomegalovirus

Valganciclovir (trade name Valcyte®), as a separate molecular entity, is the (L)-valine ester prodrug for ganciclovir (**Figure 3.3a**). The main advantage of valganciclovir over the parent compound ganciclovir is its increased intestinal permeability and oral bioavailability. Compared to approximately only 7% for ganciclovir [12], valganciclovir has shown an absolute oral bioavailability of around 60% in clinical trials [3]. The biopharmaceutical properties of valganciclovir will be discussed in detail in Chapter IV.

Foscarnet (trade name Foscavir®; structure shown in **Fig. 3.3b**) was the second drug approved by FDA for treatment of CMV retinitis. It is an analogue of pyrophosphate and binds to the pyrophosphate binding site of the UL54 polymerase (*pol*) of cytomegalovirus [4, 9]. Such binding prevents *pol* from cleaving the pyrophosphate group off of the terminal nucleotide in the DNA chain undergoing synthesis, thereby inhibiting viral DNA replication. Foscarnet is a second-line treatment for hCMV diseases and is mainly used on patients with viral resistance to ganciclovir (because of mutations in the viral UL97 gene) and those who developed dose-limiting hematotoxicity from ganciclovir therapies [9]. However, the use of foscarnet is limited by substantial nephrotoxicity associated with the drug. Severe electrolyte and mineral abnormalities are often observed and could lead to cardiac disorders, seizures and even death [4, 9]. Therefore, patients receiving foscarnet must be properly hydrated and their creatinine clearance constantly monitored [4].

Cidofovir (trade name Vistide®; **Fig. 3.3c**) is another FDA-approved anti-CMV retinitis therapeutic agent. It is an acyclic analogue of cytidine monophosphate and is phosphorylated by cellular kinases to the active form, cidofovir diphosphate [5]. Cidofovir diphosphate, when incorporated into the elongating viral DNA by the UL54 polymerase, causes premature termination of the DNA synthesis because of its lack of a 3'-hydroxyl group [5, 9]. Cidofovir's advantage over other anti-hCMV drugs lies in the higher stability of its active form and, as a result, less frequent dosing is required to achieve the therapeutic efficacy [32]. Nevertheless, severe renal toxicities caused by cidofovir limit its use and it must be administered together with probenecid in order to prevent irreversible damage to the kidneys [5, 9]. Cidofovir is also a possible carcinogen and teratogen and it remains a second-line treatment for CMV diseases [5].

Fomivirsen (trade name Vitravene®) was the first antisense compound approved by the US FDA [33]. It is a phosphorothioate oligonucleotide with a 21-nucleotide sequence, 5'-GCG TTT GCT CTT CTT CTT GCG-3', which complements the viral mRNA transcripts of the immediate-early region 2 (IE2) [6, 9]. Base-pairing between fomivirsen and the viral IE2 mRNA thus prevents protein translation from the mRNA [6]. The drug is administered locally by direct intravitreal injection and indicated for use against CMV retinitis resistant to other therapies [6]. Fomivirsen was later withdrawn from the European market for commercial reasons [34].

CMV Immune Globulin Intravenous (Human) (CMV-IGIV, trade name CytoGam®) contains immunoglobulin Gs (IgGs) against the human cytomegalovirus [7]. It is purified from pooled human plasma from healthy adults with high titers of antibodies against hCMV [7, 35]. The sterile liquid formulation of the antibodies is approved by the FDA for prophylaxis against hCMV diseases in solid organ transplant recipients [7]. Although CMV-IGIV is considered to be generally well tolerated in patients, its use has been hampered by its very high costs and fluctuating availability of supplies, which result from its human origins and the complicated purification and manufacturing processes [36].

In addition to the aforementioned small and macromolecular drugs, several other compounds have demonstrated *in vitro* and *in vivo* anti-hCMV efficacies and a few are undergoing clinical trials. Cyclopropavir, a nucleoside analog, has been found to inhibit both viral DNA synthesis and the normal functions of the viral UL97 kinase [37, 38]. It has demonstrated efficacy in a mouse model [38] as well as low cytotoxicity [39]. Maribavir, an (L)-ribosyl benzimidazole, appears to inhibit both the viral DNA replication and egress of nucleocapsid from the host cell nucleus [40, 41]. It has been tested for treatment of patients with ganciclovir-resistant hCMV infections, showing mixed results [42]. It subsequently failed to meet goals for the phase III clinical trials for prophylaxis against hCMV infections in stem cell transplant patients [43]. However, its efficacy in the treatment of hCMV infections in transplant recipients is currently being evaluated in another ongoing phase II trial [44]. Leflunomide, a drug used for rheumatoid arthritis, could inhibit hCMV capsid assembly and was found to have activity against ganciclovir-resistant strains [45, 46]. Another experimental

compound, letermovir (AIC246), interferes with viral DNA packaging by inhibiting the viral DNA terminase (UL56) complex [47]. It was reported to drastically reduce symptoms of a patient infected with an hCMV strain that was resistant to all known therapies [48]. Last but not least, acyclovir and valacyclovir share similar structures and mechanisms of action to those of ganciclovir and valganciclovir, respectively [49], and has been studied for prophylaxis against hCMV diseases after transplantation [50]. Nevertheless, ganciclovir is still deemed a far more superior inhibitor of viral DNA replication when compared to acyclovir, because not only is ganciclovir a much better substrate for the viral UL97 kinase, but also ganciclovir triphosphate has a much longer intracellular half-life than acyclovir triphosphate does [49].

Targeting Ester Prodrugs of Ganciclovir to Specific Activation by hCMV Protease

As explained in Chapter II, viral proteases harbor great potentials in the targeted prodrug strategy as the target enzymes for prodrug activation. The hCMV protease is an ideal protease for targeted activation of prodrugs of anti-hCMV compounds, as it has a catalytic structure distinct from other serine proteases, a well-defined substrate preference and is only expressed in hCMV-infected tissues. If a prodrug could be relatively stable in systemic circulation and preferably activated at the hCMV infection sites by the hCMV protease, the prodrug dosage required to achieve equivalent pharmacological effects would be greatly reduced compared to the original dosing regimen with the parent compound, therefore potentially reducing the related systemic toxicities.

Among all the marketed or experimental drugs for the management of hCMV, ganciclovir was eventually chosen as the parent compound, mainly for two reasons. First and foremost, it is the first-line treatment for hCMV infections as well as the standard therapeutic for prophylaxis against hCMV, with the largest amount of published data for reference. Second, among the three FDA-approved small molecular anti-hCMV compounds, ganciclovir possesses the most favorable physicochemical properties for analytical purposes. Its hydrophilicity is moderate (logP 0.022 [1]) compared to that of foscarnet (logP -2.1 [51]) and cidofovir (logP -3.3 [5]). It also has an adequate molecular weight (255.2) for mass spectrometry and strong UV absorption at 254 nm [52]. These profiles and properties of

ganciclovir render it the most preferable candidate for prodrug development among all small molecular anti-hCMV compounds.

In Chapter II, I explored the hCMV protease's preference of amino acyl ester substrates at their P_1 and P_2 positions. For the P_1 position, alanine (Ala) was the preferred amino acid residue over (α,L)-aminobutyric acid (Abu) and glycine (Gly). While Ala has long been known to be the naturally occurring P_1 amino acid residue for hCMV protease substrates, for Abu and Gly this was the first time that direct evidence was demonstrated for them also being acceptable P_1 residues. Ultimately, Ala and Abu were chosen as the P_1 site amino acid residues for designing promoieties. Abu is not a standard amino acid with a genetic code and it cannot be efficiently converted to other amino acids and does not take part in protein synthesis in humans [53, 54]. Therefore, hypothetically there should be lower amounts of enzymes in the body that could efficiently hydrolyze Abu-containing substrates than Ala- or Gly-containing ones. As a result, Abu-containing prodrugs are potentially more stable than the Ala- or Gly-containing counterparts and could possibly remain in their unchanged form for a longer duration in circulation. As for the P_2 residue of the substrate, which corresponds to the N-terminus protecting group, benzyloxycarbonyl (Cbz) was found to be superior to *tert*-butyloxycarbonyl (Boc) in terms of hydrolytic activity catalyzed by hCMV protease. Therefore, Cbz was selected as the protecting group within the promoieties of the proposed prodrugs. Nevertheless, the inherent reactivity within the Cbz at the oxycarbonyl part is likely to make it labile in tissues abundantly expressing esterases. In light of this possibility, I then designed two dipeptide promoieties, *N*-acetyl-(L)-phenylalanine-(L)-alanine (AcPheAla) and *N*-acetyl-(L)-phenylalanine-(α,L)-aminobutyric acid (AcPheAbu), which correspond to modifications to CbzAla and CbzAbu, respectively. Their structures are similar at the P_2 position (**Figure 3.4**) but the acetylated dipeptide promoieties, with amide linkages between the residues, are likely to be much more stable than the benzylcarbonyls as well as prodrugs with unprotected N-termini in uninfected tissues and cells [55].

In this chapter, I aimed to synthesize four different monoester prodrugs of ganciclovir. These prodrugs would then be characterized by their activation by purified hCMV protease A143S as well as stability in uninfected tissues such as cell homogenates, plasma and liver

microsomes. I also attempted to elucidate a quantitative relationship between the amount of hCMV protease expressed in tissues and the selective activation of ganciclovir prodrugs.

MATERIALS AND METHODS

Materials

The NH_2-protected amino acid compounds *N*-benzyloxycarbonyl-(L)-alanine (CbzAla) and *N*-benzyloxycarbonyl-(α,L)-aminobutyric acid (CbzAbu) were purchased from Chem-Inpex (Wood Dale, IL). The *N*-acetyl dipeptide compounds *N*-acetyl-(L)-phenylalanine-(L)-alanine (AcPheAla) and *N*-acetyl-(L)-phenylalanine-(α,L)-aminobutyric acid (AcPheAbu) were synthesized by and purchased from Genscript (Piscataway, NJ) and Chem-Inpex, respectively. 4-dimethylamino-pyridine (DMAP) and anhydrous *N*,*N*'-dicyclohexylcarbodiimide (DCC), caffeine and (S)-(-)-propranolol were purchased from Sigma-Aldrich (St. Louis, MO). All organic solvents were purchased from Fisher Scientific (Fair Lawn, NJ). Ganciclovir was purchased from Bosche Scientific (New Brunswick, NJ). Methanol-D4 (CD_3OD) was purchased from Cambridge Isotope Laboratories (Andover, MA). For tissue culture-related work, Caco-2 cells were acquired from American Type Culture Collection (ATCC; Rockville, MD) (catalog number HTB-37). Dulbecco's Modified Eagle Medium (DMEM), Minimal Essential Medium with non-essential amino acids (MEM NEAA) and fetal bovine serum (FBS) were purchased from Gibco (Grand Island, NY). Cell culture dishes and plates, cell scrapers and tissue homogenizer were purchased from Corning, Inc (Corning, NY). Human plasma was a gift from the University of Michigan Hospital. Pooled human liver microsomes (20 mg/mL) and RapidStart® NADPH regenerating system were purchased from Xenotech (Lenexa, KS). Unifilter® 800 PVDF hydrophilic filter plates were purchased from Whatman (Piscataway, NJ). All other materials that had been used in the experiments of Chapter II were acquired from the same sources.

Synthesis and Purification of Monoester Prodrugs of Ganciclovir

Chemical structures of the ganciclovir prodrugs are shown in **Figure 3.5**. 1.1 molar equivalent (eq.) of CbzAla, CbzAbu, AcPheAla or AcPheAbu carboxylic acid was reacted with 2 eq. of ganciclovir in the presence of DMAP and 1.5 eq. of DCC in dimethylformamide (DMF) under argon gas. After 24-72 hours, solvent was removed *in vacuo* and the pellets were dissolved in ethyl acetate / water mixtures. The water content was extracted and concentrated by aspiration to less than 10 mL, then injected into a Shimadzu preparatory

HPLC (Shimadzu America, Columbia, MD) with a Waters XBridge BEH C18 prep column (30 mm × 250 mm; Waters Corporation, Milford, MA) using water (1‰ v/v TFA) and acetonitrile (1‰ v/v TFA) as mobile phases A and B, respectively. Fractions with different chromatographic peaks at 254 nm were eluted and collected individually from the fraction collector; possible diastereomers of the prodrugs in particular were rigorously separated. The compounds in each fraction were first identified by electrospray ionization (ESI) mass spectrometry (MS), which was performed on an LCT Micromass time-of-flight (TOF) mass spectrometer. Solvents of the prodrug-containing fractions were then removed *in vacuo*. Proton nuclear magnetic resonance (^{1}H-NMR) spectra of the synthesized chemicals were obtained from a Varian INOVA 400 MHz NMR spectrometer with methanol-D4 (CD_3OD) as solvent. Purity of the compounds was evaluated by high performace liquid chromatography (HPLC). Prodrug powders are ultimately dissolved in dimethyl sulfoxide (DMSO) to a concentration of 20 mM and frozen at -20°C before use.

***N*-benzyloxycarbonyl-(L)-alanine-ganciclovir** (**CbzAlaGCV**). ^{1}H-NMR (400 MHz, methanol-D_4): δ 1.29-1.37 (3H, m, Ala CH_3), 3.50 (2H, m, GCV O-C_αH, GCV C_α-CH_2-O(H)), 3.95-4.21 (4H, m, GCV C_α-CH_2-O(H), GCV C_α-CH_2-OC=O, Ala C_α-H), 5.05 (2H, s, Cbz O-CH_2), 5.62 (2H, s, GCV N-CH_2-O), 7.28 (5H, m, Phe Ph), 8.61 (1H, s, GCV N-CH=N). ESI-MS: $[M+H]^+$ 461.2. Purity by HPLC: 91%.

***N*-benzyloxycarbonyl-(α,L)-aminobutyric acid-ganciclovir** (**CbzAbuGCV**). ^{1}H-NMR (400 MHz, methanol-D_4): δ 0.92 (3H, t, Abu CH_3, J = 8 Hz), 1.60-1.76 (2H, m, Abu CH_2), 3.49-3.57 (2H, m, GCV O-C_αH, GCV C_α-CH_2-O(H)), 3.95-4.23 (3H, m, GCV C_α-CH_2-O(H), GCV C_α-CH_2-OC=O), 4.30 (1H, m, Abu C_α-H), 5.05 (2H, d, Cbz O-CH_2, J = 4 Hz), 5.62 (2H, s, GCV N-CH_2-O), 7.26 (5H, m, Phe Ph), 8.64 (1H, s, GCV N-CH=N). ESI-MS: $[M+H]^+$ 473.2. Purity by HPLC: 93%.

***N*-acetyl-(L)-phenylalanine-(L)-alanine-ganciclovir** (**AcPheAlaGCV**). Diastereomer "A-4" ^{1}H-NMR (400 MHz, methanol-D_4): δ 1.31 (3H, t, Ala CH_3, J = 5.4 Hz), 1.89 (3H, m, Ac CH_3), 2.83 (1H, m, Phe CH_2), 3.14 (1H, d, Phe CH_2, J = 14 Hz), 3.58 (2H, m, GCV O-C_αH, GCV C_α-CH_2-O(H)), 3.98 (2H, m, GCV C_α-CH_2-O(H), GCV C_α-CH_2-OC=O), 4.30 (2H, m, GCV C_α-CH_2-OC=O, Ala C_α-H), 4.63 (1H, t, Phe C_α-H, J = 8 Hz), 5.64 (2H, s,

GCV N-CH_2-O), 7.24 (5H, m, Phe Ph), 8.50 (1H, d, GCV N-CH=N, J = 8 Hz). ESI-MS: $[M+H]^+$ 516.1. Purity by HPLC: 96% for diastereomer "A-4" and 95% for "A-5".

***N*-acetyl-(L)-phenylalanine-(α,L)-aminobutyric acid-ganciclovir** (**AcPheAbuGCV**). Diastereomer "B-3" ^{1}H-NMR (400 MHz, methanol-D_4): δ 0.72 (3H, t, Abu CH_3, J = 6 Hz), 1.60 (2H, m, Abu CH_2), 1.90 (3H, m, Ac CH_3), 2.89 (1H, m, Phe CH_2), 3.03 (1H, m, Phe CH_2), 3.52 (2H, m, GCV O-C_αH, GCV C_α-CH_2-O(H)), 4.13-4.28 (4H, m, GCV C_α-CH_2-O(H), GCV C_α-CH_2-OC=O, Abu C_α-H), 4.65 (1H, t, Phe C_α-H, J = 8 Hz), 5.63 (2H, s, GCV N-CH_2-O), 7.22 (5H, m, Phe Ph), 8.56 (1H, d, GCV N-CH=N, J = 8 Hz). ESI-MS: $[M+H]^+$ 530.1. Purity: > 99% for diastereomer "B-2" and 97% for "B-3".

Cell Culture and Homogenization

Caco-2 cells (passage 22 – 36) were routinely maintained in DMEM supplemented with 9.1% (v/v) FBS and 1% (v/v) NEAA in an atmosphere of 5% CO_2 and 90% relative humidity at 37°C. Before being harvested for homogenization, cells were cultured to 14-16 days post-confluence in 250-mm dishes. They were collected with a cell scraper in cold 50 mM Tris·HCl (pH 7.6 at 25°C) and immediately homogenized on ice by a tissue homogenizer. The mixture was centrifuged at 18,000 rpm in an Allegra 64R centrifuge at 4°C and the clear supernatant (S9 fraction) was removed and frozen at -80°C for later use. The protein concentrations of the Caco-2 cell homogenates were determined by BCA assays.

Stability of Prodrugs in Buffers

Prodrugs were diluted to 200 μM in hCMV protease reaction buffer (50 mM Tris HCl, pH 7.6 at 25°C, 0.5 M sodium sulfate, 10% v/v glycerol) and incubated at 30°C for 120 min. Half sample volumes of acetonitrile (ACN) with 40 μM caffeine was then added to each sample and all 0-min and 120-min samples were analyzed by HPLC.

Hydrolysis of Prodrugs in hCMV Protease (A143S)-containing System

Time-course hydrolysis studies. A final concentration of 40 μg/mL hCMV protease (hCMVP, A143S mutant) was added to the aforementioned hCMV protease reaction buffer and the mixture was pre-incubated for 5 min at 30°C. To initiate prodrug hydrolysis, prodrug

stock solutions were added to a final concentration of 200 μM and the reactions were incubated at 30°C. Samples were removed from the reaction pool at 15, 30, 60 and 90 min and quenched by half sample volumes of acetonitrile (ACN) with 40 μM caffeine as the internal standard for HPLC analysis. The mixtures were filtered through a 0.45 μm Whatman PVDF filter plate by centrifugation and the filtrates were then injected into HPLC to assay the extent of prodrug disappearance.

Hydrolysis kinetics studies (AcPheAlaGCV and AcPheAbuGCV only). Similarly to time-course studies, experiments were performed with 50 – 1000 μM prodrugs and samples were taken out at various time points during the first 10.5 min. Subsequent sample preparation steps were similar to time-course experiments. Initial rates (v_0) of hydrolysis were calculated from the linear time course of the disappearance of prodrugs, which was assayed by HPLC. The kinetic parameters v_{max} and K_m were obtained by fitting the initial rate versus concentration data to the Michaelis-Menten equation, using non-linear regression analysis (least-squares method) in GraphPad Prism (v5.0). k_{cat} was calculated from v_{max} / [hCMVP].

Hydrolysis of Prodrugs in Caco-2 Cell Homogenates

Time-course hydrolysis experiments. A final concentration of 1 mg/mL Caco-2 homogenate was prepared in 50 mM Tris·HCl (pH 7.6 at 25°C) and the homogenate pre-incubated for 5 min at 37°C. Prodrug stock solutions were then added to a final concentration of 200 μM and the reactions were incubated at 37°C. Sample collections and analysis were similar to hCMVP-mediated hydrolysis studies.

Hydrolysis kinetics experiments (AcPheAlaGCV and AcPheAbuGCV only). Reaction conditions were similar to time-course studies; 50 – 1000 μM prodrugs were used in assays for initial rates. Sample collection, analysis and curve fitting were performed in a similar fashion to hCMVP-catalyzed kinetic hydrolysis studies. k_{cat} was calculated from v_{max} / $[enzyme]_T$, of which $[enzyme]_T$ is the apparent total protein concentration of the homogenate, 1 mg/mL.

Stability of Prodrugs in Human Plasma

Prodrugs were added to 80 μM final concentrations in undiluted human blood plasma and the reactions were incubated at 37°C. Samples were taken out at 30, 60, 120, 180 and 240 min and quenched by adding two volumes of acetonitrile (ACN) with 40 μM caffeine. The mixtures were filtered through PVDF filter plates and the filtrates were added with equal volumes of water. The contents of prodrugs in samples at each time point were then analyzed by HPLC.

Stability of Prodrugs in Pooled Human Liver Microsomes

Pooled human liver microsomes were diluted to 1 mg/mL in Dulbecco's phosphate buffered saline (DPBS, pH 7.4) supplemented with NADPH regenerating system (1 mM NADP, 5 mM glucose-6-phosphate, 1 mM glucose-6-phosphate dehydrogenase) and the mixture was pre-incubated at 37°C for 5 min. AcPheAlaGcv or AcPheAbuGcv was added to a concentration of 2 μM and samples were taken out at 15, 30, 60 and 120 min and quenched with two volumes of ACN with 250 nM (S)-(-)-propranolol as internal standard. After the processed samples are mixed with equal volumes of water, the disappearance of prodrugs was analyzed by LC-MS.

HPLC Analysis

The Agilent 1100 / 1200 series HPLC system (Agilent Technologies, Santa Clara, CA) is equipped with a degasser, a quaternary pump, an autosampler (temperature at 4°C) and a diode array detector (DAD). Water (with 1‰ TFA) and acetonitrile (1‰ TFA) were used as mobile phases and the flow rate was 1.0 mL/min. An Agilent Zorbax Eclipse XDB-C18 (3.5 μm, reversed phase) 4.6×150 mm column was used for chromatographic separation of chemicals. The mobile phase B (ACN) content versus time diagram is set up as follows: 0 min, 0.1%; 3 min, 0.1%; 5 min, 8.0%; 14 min, 84.0%. All compounds were detected at UV 254 nm. A standard curve containing at least five points was utilized to calculate concentrations from peak area values. The accuracy of the HPLC assay was 90% to 110%.

LC-MS Analysis

Samples from prodrug stability in liver microsomes studies were analyzed with a Shimadzu LC-MS system. The system consists of a CBM-20A control module, a degasser, a

LC-20AD binary pump, a SIL-20A HT autosampler and a LCMS 2010A mass spectrometer with an ESI probe. A Waters XTerra C18 (5 µm, reversed phase) 2.1×50 mm column was used for chromatographic separation of chemicals. Water (1‰ formic acid) and acetonitrile (1‰ formic acid) were used as mobile phases and the flow rate was 0.2 mL/min. The mobile phase B content versus time diagram is set up as follows: 0 min, 0.5%; 1 min, 0.5%; 4 min, 20%; 9.5 min, 85%. Mass-to-charge ratios (m/z's) for chemical species in addition to the prodrugs: ganciclovir $[M+H]^+$ 256.1, (S)-(-)-propranolol $[M+H]^+$ 260.1. A standard curve containing at least five points was utilized to calculate concentrations from peak area values. The accuracy of the LC-MS assay was 75% to 125%.

Statistical Analysis

All the aforementioned hydrolysis and stability experiments were performed in triplicate and percentages remaining were expressed in mean ± SEM. For stability in plasma and liver microsomes studies, elimination rate constants (k) were derived from fitting the average percentages remaining vs. time data to a first-order elimination equation ($C(t) / C_0 = e^{-kt}$). Half-lives were calculated as $t_{1/2} = 0.693 / k$. For time-course hydrolysis studies, at each time point the percentage remaining of each prodrug was compared to others' using one-way analysis of variance (ANOVA) with *post hoc* Tukey's multiple comparison tests; $p < 0.05$ was considered significant.

Quantitative Modeling for the Selective Activation of Prodrugs and Calculations of Selective Activation Factors (SAFs)

The selective activation for a specific prodrug was characterized by the ratio of the initial rates of hydrolysis catalyzed by hCMV protease (v_{hCMVP}) over that by Caco-2 homogenate ($v_{Caco\text{-}2}$). Initial rates were assumed to follow the Michaelis-Menten model. For hCMV protease- and Caco-2 non-specific enzyme-catalyzed hydrolysis,

$$v_{hCMVP} = \frac{k_{cat,hCMVP}[hCMVP]_T[S]}{K_{m,hCMVP} + [S]} \qquad \text{(Equation 3.1)}$$

$$v_{Caco-2} = \frac{k_{cat,Caco-2}[Cellular\ Protein]_T[S]}{K_{m,Caco-2} + [S]} \quad \text{(Equation 3.2)}$$

Therefore,

$$\frac{v_{hCMVP}}{v_{Caco-2}} = \frac{\frac{k_{cat,hCMVP}[hCMVP]_T[S]}{K_{m,hCMVP} + [S]}}{\frac{k_{cat,Caco-2}[Cellular\ Protein]_T[S]}{K_{m,Caco-2} + [S]}} \quad \text{(Equation 3.3)}$$

Let $MFE(hCMVP) = \frac{[hCMVP]_T}{[Cellular\ Protein]_T}$, where *MFE* stands for "mass fraction expressed":

$$\frac{v_{hCMVP}}{v_{Caco-2}} = \frac{\frac{k_{cat,hCMVP}}{K_{m,hCMVP} + [S]}}{\frac{k_{cat,Caco-2}}{K_{m,Caco-2} + [S]}} \cdot MFE(hCMVP) \quad \text{(Equation 3.4)}$$

When [S] is small ([S] << $K_{m,hCMVP}$ and [S] << $K_{m,Caco\text{-}2}$), Eq. 3.4 becomes

$$\frac{v_{hCMVP}}{v_{Caco-2}} = \frac{k_{cat,hCMVP} \cdot K_{m,Caco-2}}{K_{m,hCMVP} \cdot k_{cat,Caco-2}} \cdot MFE(hCMVP) \quad \text{(Equation 3.5)}$$

The k_{cat} and K_m values have been determined from the hydrolysis kinetics studies. The **selective activation factor** (SAF) of a prodrug "X" is thus defined as

$$\boldsymbol{SAF}(\text{prodrug X}) = \frac{k_{cat,hCMVP}(\text{prodrug X}) \cdot K_{m,Caco-2}(\text{prodrug X})}{K_{m,hCMVP}(\text{prodrug X}) \cdot k_{cat,Caco-2}(\text{prodrug X})} \quad \text{(Equation 3.6)}$$

The SAF is a dimensionless quantity and also a unique characteristic for different prodrugs. It serves as an indicator of how much prodrug could be activated by hCMV protease **in addition to** the prodrug hydrolyzed by cellular hydrolases. Assuming the rate of non-specific

hydrolysis is unchanged in virally infected cells when compared to normal, uninfected cells, i.e. $v_{\text{infected cells}} = v_{\text{hCMVP}} + v_{\text{Caco-2}}$ and $v_{\text{uninfected cells}} = v_{\text{Caco-2}}$, Eq. 3.5 becomes

$$\boldsymbol{v_{infected\ cells} = \left(1 + \frac{k_{cat,hCMVP} \cdot K_{m,Caco-2}}{K_{m,hCMVP} \cdot k_{cat,Caco-2}} \cdot MFE(hCMVP)\right) \cdot v_{uninfected\ cells}}$$

(Equation 3.7)

Eq. 3.7 therefore provides a quantitative relationship between the ratios of prodrugs' hydrolysis rates in infected over uninfected cells and the mass fraction of hCMV protease expressed in the infected cells.

RESULTS

Diastereomers of Ganciclovir Prodrugs

During the purification process by preparatory HPLC, diastereomers of CbzAlaGcv and CbzAbuGcv were observed but unable to be efficiently separated. Therefore, the resulting products were likely racemic mixtures of (R)- and (S)-conformations at the acquired chiral center in the ganciclovir structure (Fig. 3.5). The diastereomers for AcPheAlaGCV and AcPheAbuGCV, however, were separated and each fraction was relatively pure (see Materials and Methods). The resulting stereoisomers were given code names of "A-4" and "A-5" for AcPheAlaGCV (**Figure 3.6**) and "B-2" and "B-3" for AcPheAbuGCV (**Figure 3.7**). Time-course hydrolysis of these four fractions by hCMV protease A143S were shown in **Figure 3.8**. It was evident that AcPheAlaGCV "A-4" could be hydrolyzed by hCMV protease A143S whereas "A-5" could not, and AcPheAbuGCV "B-3" could be hydrolyzed by the protease while "B-2" remained largely intact throughout the 90-min incubation period. Therefore, only AcPheAlaGCV fraction "A-4" and AcPheAbuGCV fraction "B-3" were used in all subsequent experiments. **All mentions of "AcPheAlaGCV" and "AcPheAbuGCV" throughout Chapters III and IV only refer to the "A-4" and "B-3" fractions, respectively, unless specified otherwise**.

Stability of Prodrugs in Buffers

All four prodrugs (CbzAlaGCV, CbzAbuGCV, AcPheAlaGCV and AcPheAbuGCV) were relatively stable in the hCMV protease reaction buffer. At 120 min, all four have greater than 95% remaining with respect to the zero-minute time point.

Time-course Hydrolysis of Prodrugs in hCMV protease (A143S)-containing System

As shown in **Figure 3.9**, all four monoester prodrugs of ganciclovir could be hydrolyzed by hCMV protease A143S. They also displayed differential rates of hydrolysis, with CbzAlaGCV and AcPheAlaGCV being hydrolyzed at higher rates than CbzAbuGCV and AcPheAbuGCV are. This confirmed that Ala is preferred over Abu at the P_1 site of the ester substrate by the hCMV protease. On the other hand, the progress of hydrolysis of CbzAlaGCV was not found to be significantly different from that of AcPheAlaGCV, nor was

the reaction progress of CbzAbuGCV significantly different from that of AcPheAbuGCV. This phenomenon demonstrated that the structural likeness between CbzXaa and AcPheXaa (Xaa = Ala or Abu) promoieties could translate into similarities in the rates of hCMV protease-catalyzed hydrolysis of the corresponding prodrugs.

Time-course Hydrolysis of Prodrugs in Caco-2 Homogenates

The four monoester prodrugs of ganciclovir possess varying degrees of stability in Caco-2 cell homogenates (**Figure 3.10**). AcPheAbuGCV is the most stable of all four: at 30, 60 and 90 min, significantly higher percentages of AcPheAbuGCV remain in the homogenate than CbzAlaGcv, CbzAbuGcv and AcPheAlaGCV. To offer a more direct comparison of specificity–stability interplay among the four ganciclovir prodrugs, data from studies of the time-course hydrolysis of prodrugs by both hCMVP A143S and Caco-2 homogenates were combined (**Figure 3.11**). The ratio of percentage of prodrug hydrolyzed by 40 µg/mL hCMVP over that by 1 mg/mL Caco-2 homogenate is used as an indicator to gauge a prodrug's specific activation by hCMVP. The higher this ratio is, the more likely a prodrug is activated by hCMV protease rather than being degraded non-specifically in uninfected cells. As shown in Fig. 3.11, at 30, 60 and 90 min, AcPheAbuGCV has higher hydrolyzed by hCMVP / hydrolyzed by Caco-2 ratios than the other three. These results demonstrated that the undesired slower hydrolysis of AcPheAbuGCV by hCMVP could be compensated by its higher stability in normal tissues, which becomes more apparent with the passing of time.

Stability of Prodrugs in Undiluted Human Plasma

The four ganciclovir prodrugs display varying rates of degradation in human plasma (**Figure 3.12**; elimination rate constants and half-lives in **Table 3.1**). The N-terminally protected amino acyl ester prodrugs are degraded rapidly in plasma, with no more than 50% remaining after 30 min. AcPheAlaGCV and AcPheAbuGCV are more stable with half-lives of 148 min and 210 min, respectively. Once again, AcPheAbuGCV demonstrated that it has the best stability among the four compounds in another tissue matrix that is plasma.

Stability of Prodrugs in Pooled Human Liver Microsomes

Due to the instability of CbzXaaGCV prodrugs in Caco-2 cell homogenates and plasma, they were not characterized for stability in liver microsomes because it is very likely that they are less stable than their counterparts with acetylated dipeptide promoieties. Between AcPheAlaGCV and AcPheAbuGCV, the latter was found to be more resistant to hydrolysis catalyzed by microsomal enzymes (**Figure 3.13**), with a half-life of 250 min compared to 97 min for AcPheAlaGCV (**Table 3.2**). Therefore, AcPheAbuGCV established itself as the most stable prodrug among the four in normal cells and tissue matrices.

Hydrolysis Kinetics Studies for Acetylated Dipeptide Prodrugs of Ganciclovir

Although the aforementioned time-course hydrolysis studies demonstrated the differential hydrolysis of ganciclovir prodrugs by hCMV protease A143S and non-specific enzymes, they were carried out using arbitrary, fixed amounts of enzymes and thus could not accurately reflect the physiological situations in which the concentrations of prodrugs and enzymes are almost certain to be dynamic. To address this problem, studies based on Michaelis-Menten kinetics were performed on the prodrugs' hydrolysis by hCMV protease and Caco-2 homogenates. The Michaelis-Menten kinetic parameters for hCMV protease A143S- or Caco-2 homogenate-catalyzed hydrolysis of AcPheAlaGCV or AcPheAbuGCV were determined by non-linear regressions of initial rates vs. concentrations data (**Figures 3.14** and **3.15**). The k_{cat}, K_m as well as k_{cat} / K_m values derived from the curve-fitting are listed in **Table 3.3**. For hydrolysis catalyzed by hCMV protease, AcPheAlaGCV has both a higher k_{cat} and a lower K_m than AcPheAbuGCV, resulting in an almost 60% higher k_{cat} / K_m (5.08 $(\text{min}\cdot(\mu\text{g/mL protein}))^{-1}$ for AcPheAlaGCV vs. 3.19 $(\text{min}\cdot(\mu\text{g/mL protein}))^{-1}$ for AcPheAbuGCV). This finding confirmed that, kinetically, AcPheAlaGCV is indeed a better substrate for the hCMV protease than AcPheAbuGCV is. Conversely, in Caco-2 cell homogenates, the k_{cat} for AcPheAbuGCV is slightly higher that of AcPheAlaGCV, but the K_m for AcPheAbuGCV is much higher than the K_m for AcPheAlaGCV. Consequently, AcPheAlaGCV has a 74% higher k_{cat} / K_m than AcPheAbuGCV does in hydrolytic reactions in Caco-2 homogenate (AcPheAlaGCV: 1.83×10^{-5} $(\text{min}\cdot(\mu\text{g/mL protein}))^{-1}$ vs. 1.05×10^{-5} $(\text{min}\cdot(\mu\text{g/mL protein}))^{-1}$ for AcPheAbuGCV). These kinetic parameters thus provided

quantitative details on why AcPheAbuGCV is more stable than AcPheAlaGCV is in Caco-2 homogenates.

Quantitative Models for the Selective Activation of Prodrugs

Selective activation factors (SAF) for AcPheAlaGCV and AcPheAbuGCV were calculated based on **Eq. 3.6**, using the kinetic parameters determined in the aforementioned studies. As a result, AcPheAlaGCV was found to have an SAF of **27.8** and AcPheAbuGCV an SAF of **30.3**. Therefore, AcPheAbuGCV has a roughly 9% higher SAF than AcPheAlaGCV. The quantitative models for the selective activation of the two prodrugs were then derived according to **Eq. 3.7**, when assuming concentrations of both prodrugs are much smaller than the K_m values (see Table 3.3):

For AcPheAlaGCV:

$$\frac{\boldsymbol{v_{infected\ cells}}}{\boldsymbol{v_{uninfected\ cells}}} = \mathbf{1} + \mathbf{27.8} \cdot \boldsymbol{MFE(hCMVP)} \qquad \text{(Equation 3.8)}$$

For AcPheAbuGCV:

$$\frac{\boldsymbol{v_{infected\ cells}}}{\boldsymbol{v_{uninfected\ cells}}} = \mathbf{1} + \mathbf{30.3} \cdot \boldsymbol{MFE(hCMVP)} \qquad \text{(Equation 3.9)}$$

DISCUSSION

In this chapter, I first synthesized four monoester prodrugs of ganciclovir: CbzAlaGCV, CbzAbuGCV, AcPheAlaGCV and AcPheAbuGCV. The diastereomers of AcPheAlaGCV and AcPheAbuGCV were rigorously separated and purified and the "A-4" fraction of AcPheAlaGCV and "B-3" fraction of AcPheAbuGCV were found to be reactive in hCMV protease A143S-containing buffer systems; the other two fractions were relatively inert. The two stereomerically pure fractions of "A-4" and "B-3" were thus selected to be used in later studies solely based on their reactivity in the hCMV protease-catalyzed hydrolysis. Due to limitations in the small amounts of available prodrugs (< 15 mg each) as well as in analytical instrumentation, the absolute configurations at the introduced chiral carbon of the prodrugs (Fig. 3.5) were not determined as of this moment. However, it is known that techniques such as X-ray powder diffraction (XRPD) and circular dichroism (CD) have been widely used for the determination of chirality [56]. These studies could be performed once enough spare compounds and the necessary equipment become available.

I first performed characterizations of the time-course hydrolysis and stability of the four ganciclovir prodrugs. It was not surprising to find that Ala-containing prodrugs were hydrolyzed at faster rates than Abu-containing ones (Fig. 3.9) because Ala has been confirmed in previous publications as well as in Chapter II to be the preferred residue at the substrates' P_1 position. Interestingly, the supposedly racemic CbzAlaGCV did not behave like the diastereomers of AcPheAlaGCV did in hydrolysis catalyzed by hCMV protease (i.e. if the hCMV protease distinguishes between the two isomers of CbzAlaGCV, its percentage remaining value should not drop much below 50% at any time point). Further structure-relationship studies may be needed to explain this phenomenon.

Nevertheless, the rate of activation of a prodrug by the target protease is just the first criterion for judging its "targetability"; it is also imperative that the prodrug is stable enough in normal, uninfected tissues in order to remain in its original form for long enough to reach the infected locales by circulation. Therefore, I also tested the stability of the prodrugs in various matrices. Caco-2 cells are known to highly express esterases and they have been used as a representative cell line to test hydrolysis of ester prodrugs [57, 58]; the homogenate of

Caco-2 was thus chosen to represent the cytoplasm of uninfected cells. Human plasma was selected to represent the main route of circulation; it has been known since as early as 1895 that the blood plasma harbors esterase activities [59]. Pooled human liver microsomes were selected as a model for liver, which contains abundant amounts of esterases [60]. In subsequent stability experiments with these tissue matrices, I first discovered that CbzAlaGCV and CbzAbuGCV were unstable in Caco-2 homogenates and plasma, presumably because the carbonyl group within Cbz is very prone to nucleophilic attack. These two were thereby excluded from all follow-up studies in Chapters III and IV. Secondly, AcPheAbuGCV was found to be more stable than all other prodrugs in all three tissue matrices (Fig. 3.10, 3.12, 3.13). Particularly, in Caco-2 homogenates the difference between AcPheAbuGCV and others was pronounced (Fig. 3.10). The reaction seemed to have slowed down as time elapsed. I thus suspect that in addition to typical kinetic mechanisms, a feedback regulation may be taking simultaneous actions, with the product(s) of AcPheAbuGCV hydrolysis inhibiting the hydrolyzing enzyme(s) within the homogenate. Such a mechanism is nonetheless desirable: by whatever means, the more stable a ganciclovir prodrug is in normal cells, the more likely it could be transported out of that cell and back into circulation, because once ganciclovir is generated and then phosphorylated by cellular kinases, it could not permeate through the cell membrane due to its polar nature.

The exact reason why the Abu residue within AcPheAbuGCV makes the prodrug possess higher stability than its Ala-containing counterpart is unclear. (α,L)-aminobutyric acid (also known as α-aminobutyrate, 2-aminobutyric acid, α-aminobutanoic acid and ethylglycine) is a non-standard amino acid that little systematic research has been devoted to, in stark contrast to one of its isomers, the well-known γ-aminobutyric acid (GABA). Free (α,L)-aminobutyric acid is naturally found in plasma but at very low concentrations compared to other “canonical” amino acids [61, 62] and it was identified as a product of metabolisms of other amino acids [63]. Elevated levels of Abu in plasma have been indicated as a possible marker for liver dysfunction [54]. Abu is not found to be a building block for proteins and cannot be efficiently converted to other amino acids [53, 54]. Ophthalmic acid (ophthalmate), a tripeptide analogue of glutathione, is the only known naturally occurring substance to be synthesized from Abu [64]. The physiological role of ophthalmic acid is not established either,

but it has also been discovered to be a possible indicator of oxidative stress in the body [65]. Proteases involved in the degradation of ophthalmate are currently unknown. These past findings highlight the fact that our knowledge on (α,L)-aminobutyric acid is very limited, which may result from the fact that Abu usually does not participate in physiological functions in the body under normal circumstances. It is likely that either there are no proteases or other hydrolases with Abu as the preferred P_1 residue, or, if such hydrolases do exist, their expression is regulated at a low level due to the body's very little need for them. This might shed a light on why AcPheAbuGCV is more stable than other prodrugs in the several tissue matrices I tested.

Despite the promising results from the time-course studies with hCMV protease A143S and Caco-2 homogenates, they were all performed with fixed amounts of enzymes and arbitrary concentrations of prodrugs; neither could reflect the likely dynamic nature of these two components in physiological conditions. To mimic such conditions, I did attempt to create a cell system transfected with a plasmid vector containing hCMV protease, but the expression of the protease in the transfected cells was inconsistent and, generally speaking, at very low levels (≤ 1‰ mass of cellular proteins). Therefore, I did not proceed further with such a system. Another possible *in vitro* model, cell lines infected with live human cytomegalovirus, have long been used to characterize the potency and efficacy of antiviral compounds against hCMV [39], although no published study has used them for prodrug activation. Due to the unavailability of such a system, I could not test the activation of ganciclovir prodrugs with live hCMV. Nevertheless, the virally infected cells should be the penultimate system to use for the determination of the selectiveness of prodrug activation, before the prodrugs are subjected to *in vivo* testing with infected animal models.

Eventually, I utilized Michaelis-Menten modeling to simulate a comparison of prodrug hydrolysis rates between infected and uninfected cell environments. Because there have been no published data on the amount of hCMV protease expressed in infected cells, it becomes a crucial variable in the model. As shown in Eq. 3.5 and 3.7, this variable is presented as a mass fraction expressed (MFE) of the total amount of cellular protein. Naturally, the higher the MFE of hCMV protease is, the higher the rate of prodrug hydrolysis in infected cells will be

when compared to uninfected cells. The final equations (Eq. 3.8 and 3.9) assume that prodrug concentrations are much lower than the K_m values and the hCMV protease is merely an "additive" to the uninfected cells' inherent hydrolytic machinery. These simplified models contain only MFE(hCMVP) as the independent variable. For example, if the hCMV protease constitutes 1% of total protein in infected cells, for AcPheAlaGCV (Eq. 3.8), it would be hydrolyzed 27.8% faster in infected cells than normal cells, whereas for AcPheAbuGCV (Eq. 3.9), its rate would be 30.3% higher in infected tissues. These numbers and the related equations, while not spectacular, do provide a quantitative insight into the relationships between the amount of hCMV protease expression, the structures of prodrug substrates and the extent of selective activation of those substrates. Moreover, this model could be used as a surrogate for the analysis of selective activation of prodrugs when more physiologically relevant models, such as infected cell lines, are unavailable.

Overall, the studies in Chapter III provided a proof-of-concept on the design of ganciclovir monoester prodrugs and how to quantitatively characterize their selective activation by the hCMV protease as well as stability in normal, uninfected tissues. As mentioned in Background, ganciclovir is phosphorylated on one of its hydroxyl groups by viral UL97 kinase or unspecified cellular kinase(s), and then incorporated into the elongating DNA by viral UL54 polymerase or the host cell DNA polymerase complex. Such a mechanism is essential for both anti-hCMV efficacy as well as toxicity to normal cells such as hematopoietic progenitors. By conjugating a promoiety to one of the hydroxyl groups in ganciclovir, thus effectively "blocking" the hydroxyl, the ganciclovir monoester prodrugs are potentially less toxic than the parent compound is. This would presumably be because the spatial occupation by the bulky promoiety would likely make the other (free) hydroxyl group less accessible to cellular kinases, thereby decreasing the rate of its phosphorylation. Moreover, even if the other hydroxyl group is phosphorylated, the existence of the promoiety could possibly hinder the binding of the DNA polymerase complex to the phosphorylated prodrug, making it less likely to be incorporated into the elongating DNA chain. To test this hypothesis, dose-dependent studies on the toxicity of ganciclovir prodrugs toward colony-forming hematopoietic cells, as well as their inhibition of DNA synthesis, would need to be performed and the results compared to those of ganciclovir itself [29, 31]. If the prodrugs are

indeed found to be less toxic to those cells, it would be a big step for the targeted prodrug strategy toward testing in clinical settings.

Finally, although the four ganciclovir monoester prodrugs could all be activated by hCMV protease at varying efficiencies and display differential stability profiles in normal tissue matrices, it is entirely plausible that prodrugs with other promoieties could be superior in both their activation by hCMV protease as well as in their tissue stability. The P_2 side chain of the hCMV protease substrate has been shown to be more tolerated by the protease [66]. Therefore, if an unnatural amino acid residue is introduced as the P_2 residue (**Figure 3.16**), hypothetically the promoiety would be less recognizable to certain tissue hydrolases and the prodrug would thus be more stable. The protecting group at the N-terminus could also be modified to cater to the hCMV protease's preference. As shown in Fig. 3.16, this proposed prodrug of ganciclovir contains a P_1 residue of either Ala or Abu, a P_2 residue of (*N*',*N*')-dimethylasparagine, which is theoretically the most preferred residue at P_2 site by hCMV protease [66]. The *tert*-butyloxycarbonyl protecting group at the N-terminus corresponds to a *tert*-butyl P_3 side chain that is, hypothetically, also the preferred one by the hCMV protease. The first proposed compound, Boc-Asn(Me_2)-Ala-GCV (Fig. 3.16a), could potentially be more rapidly activated by hCMV protease and more stable in tissues than AcPheAlaGCV is. Boc-Asn(Me_2)-Abu-GCV (Fig. 3.16b) is likely to possess similar advantages when compared to AcPheAbuGCV. In summary, more efforts in medicinal chemistry could be dedicated to modify the structure of the promoiety, so that both the hCMV-mediated activation as well as tissue stability of the resulting ganciclovir monoester prodrug could be further optimized.

CONCLUSIONS

Four synthetic monoester prodrugs of ganciclovir, *N*-benzyloxycarbonyl-(L)-alanine-ganciclovir (CbzAlaGCV), *N*-benzyloxycarbonyl-(α,L)-aminobutyric acid-ganciclovir (CbzAbuGCV), *N*-acetyl-(L)-phenylalanine-(L)-alanine-ganciclovir (AcPheAlaGCV) and *N*-acetyl-(L)-phenylalanine-(α,L)-aminobutyric acid-ganciclovir (AcPheAbuGCV), could be hydrolytically activated by the human cytomegalovirus (hCMV) protease. The two Ala-containing prodrugs were hydrolyzed by the hCMV protease at higher rates than the two Abu-containing prodrugs. The four prodrugs of ganciclovir also displayed different stability profiles in uninfected ("normal") tissue matrices. The *N*-acetylated dipeptide prodrugs were discovered to be generally more stable than their counterparts with *N*-benzyloxycarbonyl-amino acid promoieties. Moreover, among the four prodrugs, AcPheAbuGCV was the most stable one in uninfected tissue matrices. These findings presented qualitative as well as quantitative *in vitro* methodologies and results for the hydrolytic activation of prodrugs that are designed to be targeted to the hCMV infection sites. Future studies using more physiologically relevant models should be conducted in order to characterize the potential selective activation of these ganciclovir prodrugs at the locales of hCMV infections.

FIGURES

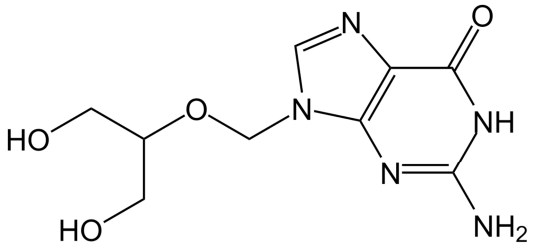

(a)

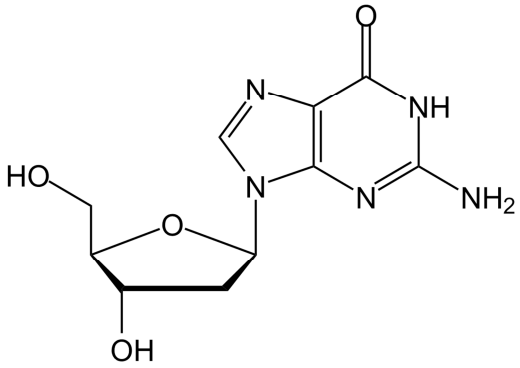

(b)

Figure 3.1. Chemical structures of (a) ganciclovir and (b) deoxyguanosine.

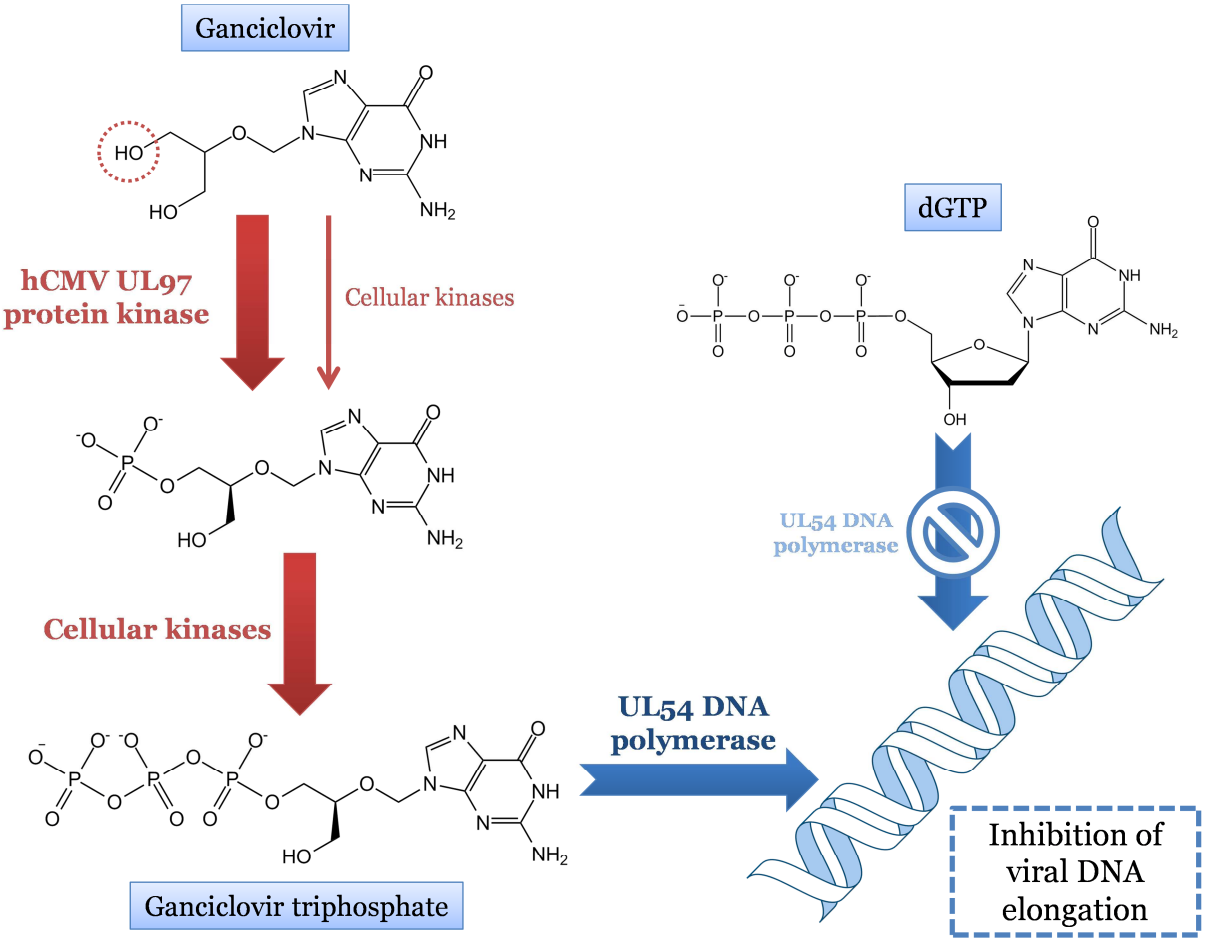

Figure 3.2. Activation of ganciclovir within the nucleus of hCMV-infected cells. Figure is adapted from Fig. 1 of [26] and created with ChemBioDraw Ultra 12.0 and PowerPoint 2010.

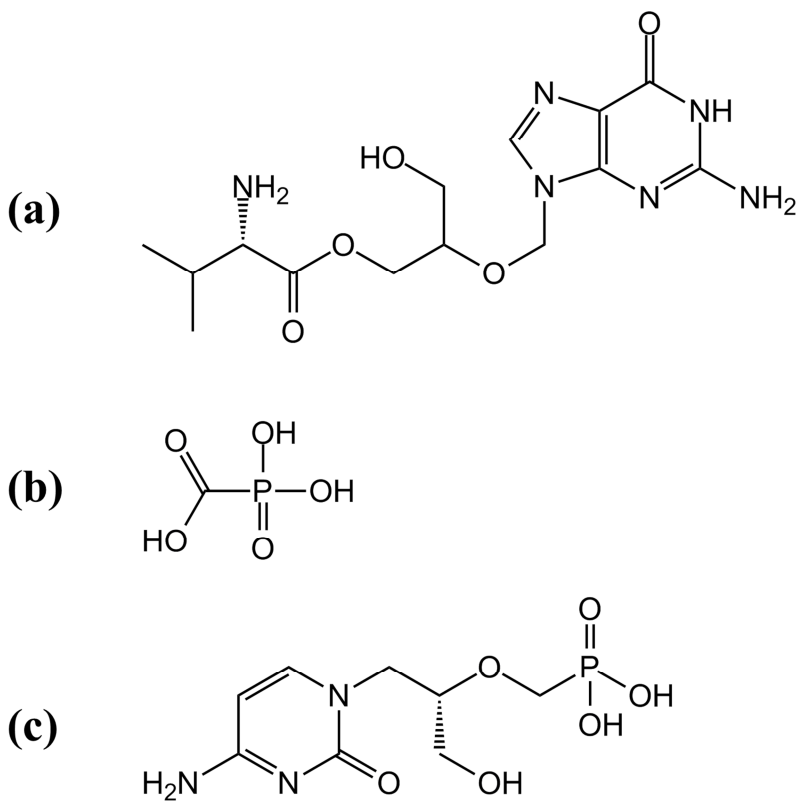

Figure 3.3. Chemical structures of other FDA-approved anti-hCMV compounds: (a) valganciclovir, (b) foscarnet and (c) cidofovir.

(a)

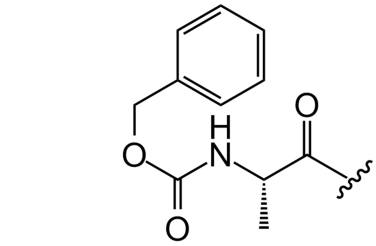

(b)

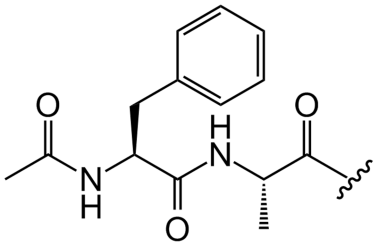

Figure 3.4. Comparison of promoieties: (a) *N*-benzyloxycarbonyl-(L)-alanine (CbzAla) and (b) *N*-acetyl-(L)-phenylalanine-(L)-alanine.

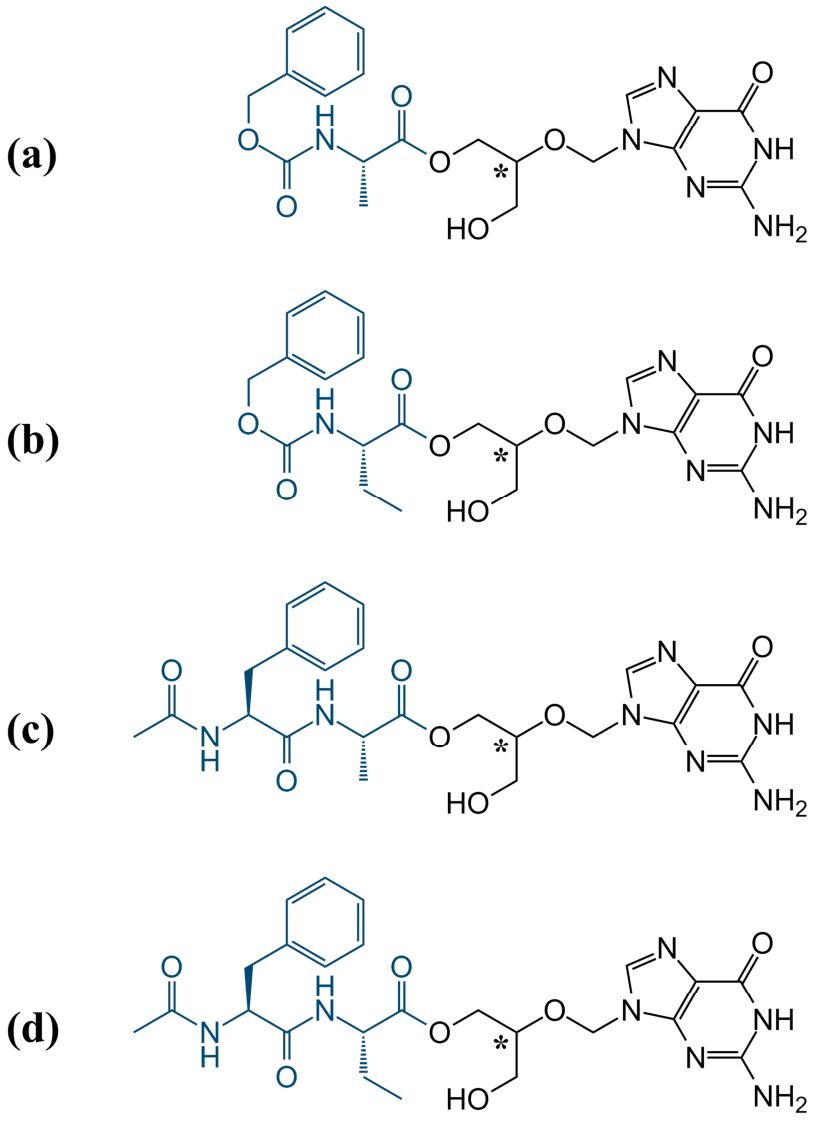

Figure 3.5. Chemical structures of monoester prodrugs of ganciclovir. (a) *N*-benzyloxycarbonyl-(L)-alanine-ganciclovir (**CbzAlaGCV**); (b) *N*-benzyloxycarbonyl-(α,L)-aminobutyric acid-ganciclovir (**CbzAbuGCV**); (c) *N*-acetyl-(L)-phenylalanine-(L)-alanine-ganciclovir (**AcPheAlaGCV**) and (d) *N*-acetyl-(L)-phenylalanine-(α,L)-aminobutyric acid-ganciclovir (**AcPheAbuGCV**). The acquired chiral carbons within the ganciclovir structure of the four prodrugs are denoted with asterisks (*). All four prodrugs are trifluoroacetic acid (TFA) salts.

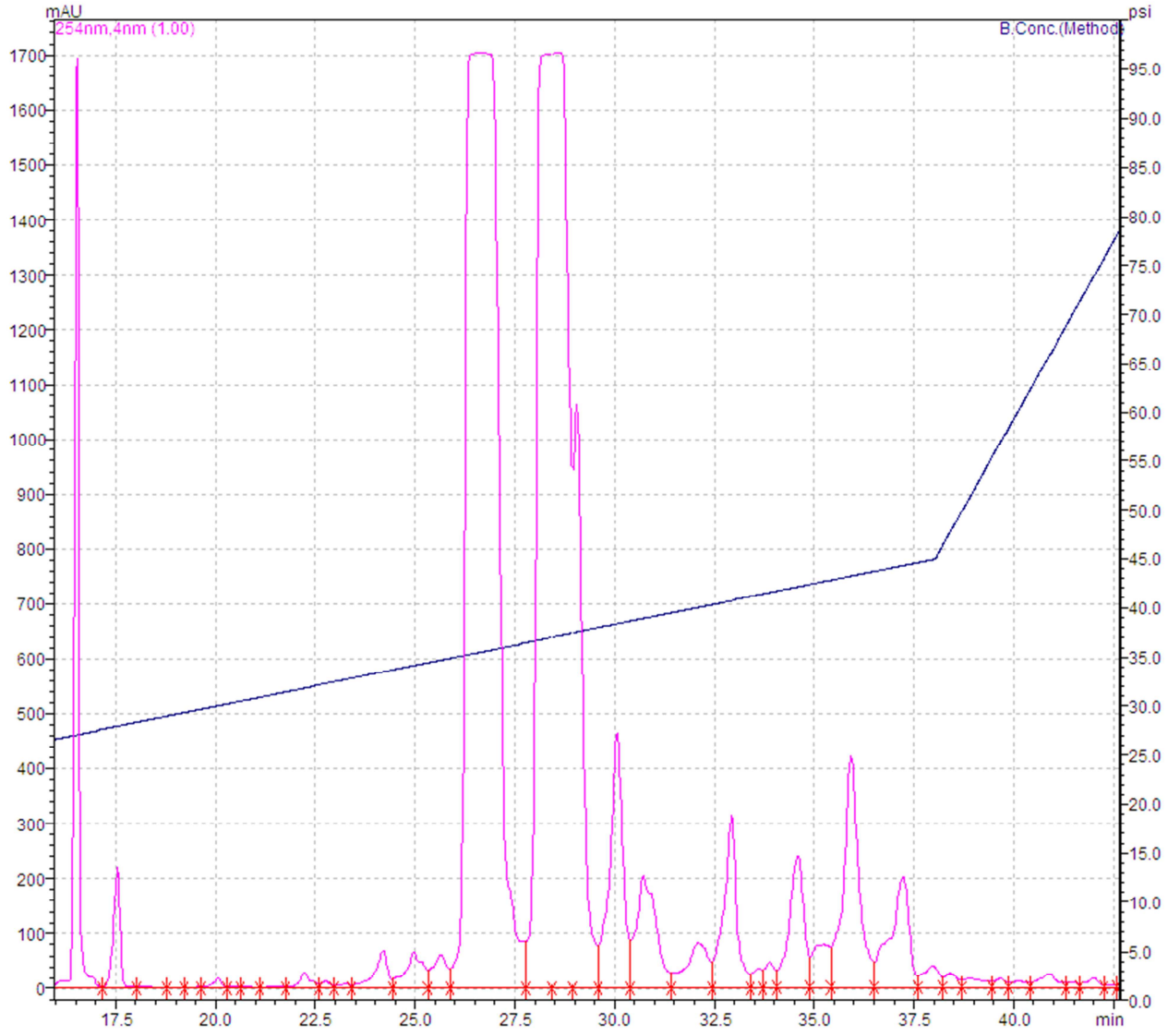

Figure 3.6. Partial chromatogram of the water content from water / ethyl acetate extraction of the AcPheAlaGCV reaction mixture, as monitored on the Shimadzu preparatory HPLC program during the purification run. The *x* axis shows time of run, left *y* axis the UV absorption at 254 nm in milli absorption units (mAU) and right *y* axis the percentage of mobile phase B (acetonitrile with 1‰ TFA). Fractions collected from 26.1 to 27.3 min were denoted **"A-4"** and from 27.7 min to 29.5 min marked as **"A-5"**, respectively.

Figure 3.7. Partial chromatogram of the water content from water / ethyl acetate extraction of the AcPheAbuGCV reaction mixture, as monitored on the Shimadzu preparatory HPLC program during the purification run. The *x* axis shows time of run, left *y* axis the UV absorption at 254 nm in milli absorption units (mAU) and right *y* axis the percentage of mobile phase B (acetonitrile with 1‰ TFA). Fractions collected from 28.0 to 29.4 min were denoted **"B-2"** and from 30.8 min to 32.2 min marked as **"B-3"**, respectively.

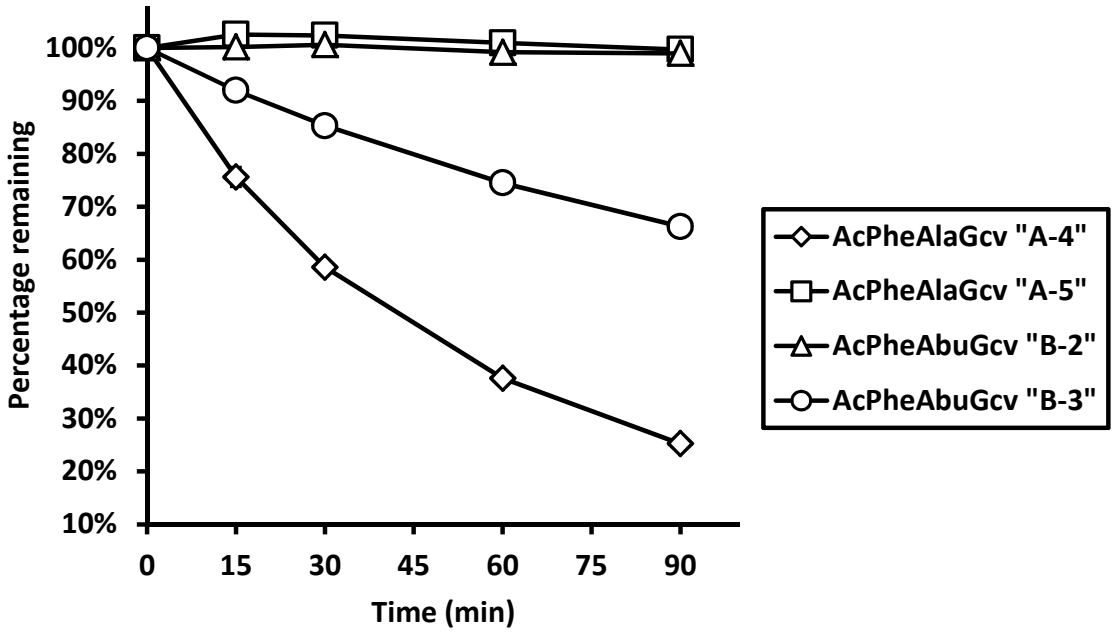

Figure 3.8. The time course of the hydrolysis of 200 µM diastereomers of acetylated dipeptide monoester prodrugs of ganciclovir (AcPheAlaGCV "A-4" and "A-5", AcPheAbuGCV "B-2" and "B-3") in reaction buffer (50 mM Tris HCl, pH 7.6 at 25°C, 0.5 M Na_2SO_4, 10% v/v glycerol) with 40 µg/mL hCMV protease A143S at 30°C. The *x* axis shows time elapsed since reactions were initiated and the *y* axis denotes the percentages of prodrugs remaining in their unchanged forms as compared to the zero-minute time point. n = 3 for all time points and error bars represent SEM.

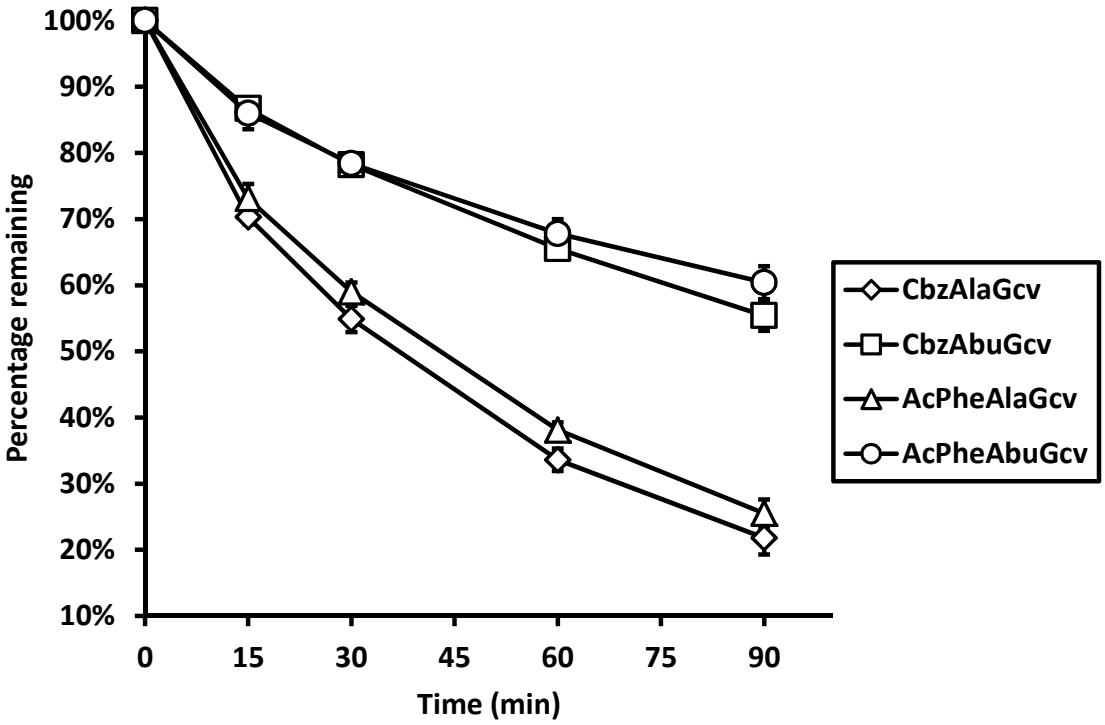

Figure 3.9. The time course of the hydrolysis of 200 µM monoester prodrugs of ganciclovir (CbzAlaGcv, CbzAbuGcv, AcPheAlaGCV "A-4" and AcPheAbuGCV "B-3") in reaction buffer (50 mM Tris HCl, pH 7.6 at 25°C, 0.5 M Na_2SO_4, 10% v/v glycerol) with 40 µg/mL hCMV protease A143S at 30°C. The *x* axis shows time elapsed since reactions were initiated and the *y* axis denotes the percentages of prodrugs remaining in their unchanged forms as compared to the zero-minute time point. At each time point, percentages remaining of the four prodrugs were compared to each other using one-way ANOVA with Tukey's multiple comparison tests. n = 3 for all time points and error bars represent SEM.

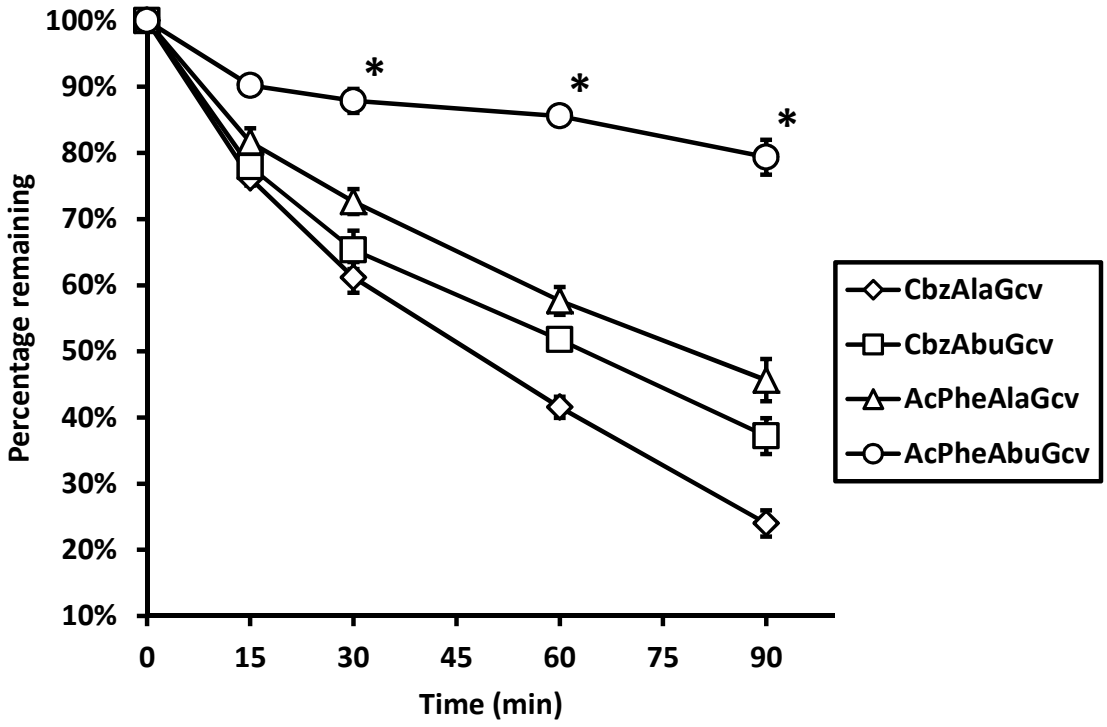

Figure 3.10. The time course of the hydrolysis of 200 μM monoester prodrugs of ganciclovir (CbzAlaGcv, CbzAbuGcv, AcPheAlaGCV "A-4" and AcPheAbuGCV "B-3") in 1 mg/mL Caco-2 homogenates at 37°C. The *x* axis shows time elapsed since reactions were initiated and the *y* axis denotes the percentages of prodrugs remaining in their unchanged forms as compared to the zero-minute time point. At each time point, percentages remaining of the four prodrugs were compared to each other using one-way ANOVA with Tukey's multiple comparisons. n = 3 for all time points and error bars represent SEM. Asterisks (*) denote percentage values different from those of all other prodrugs at that time point ($p < 0.05$).

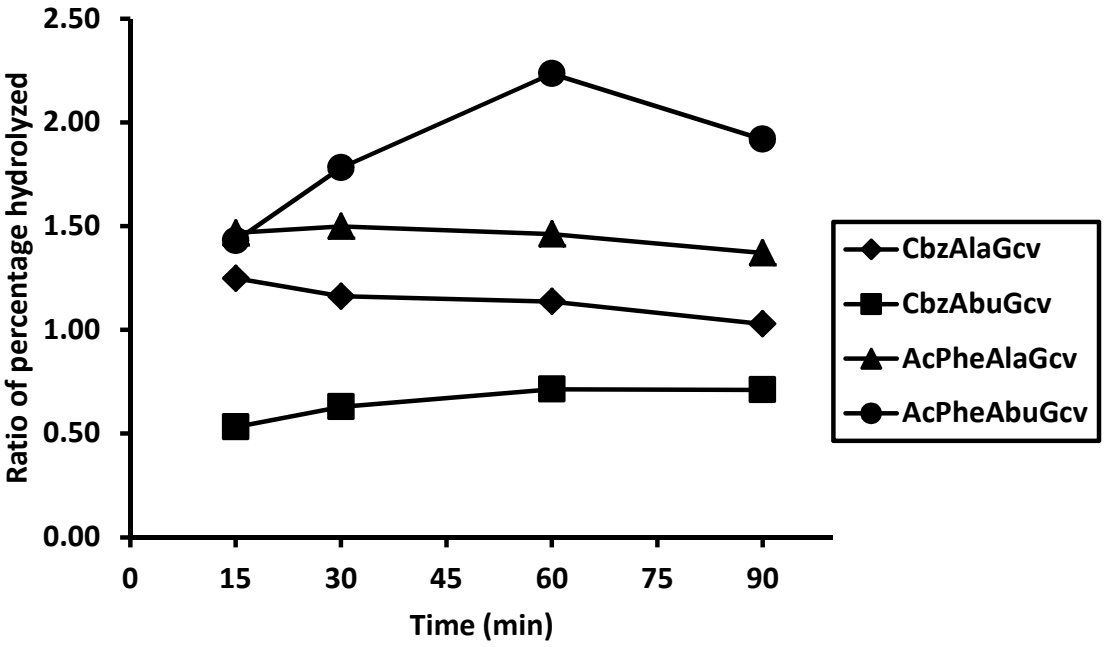

Figure 3.11. The time-course plot of the ratios of average percentages of 200 μM prodrugs hydrolyzed by 40 μg/mL hCMV protease A143S over those hydrolyzed by 1 mg/mL Caco-2 homogenates. Compiled using the data for all four prodrugs from Fig. 3.9 and 3.10. Percentages hydrolyzed are calculated from %Hydrolyzed = 100% – %Remaining.

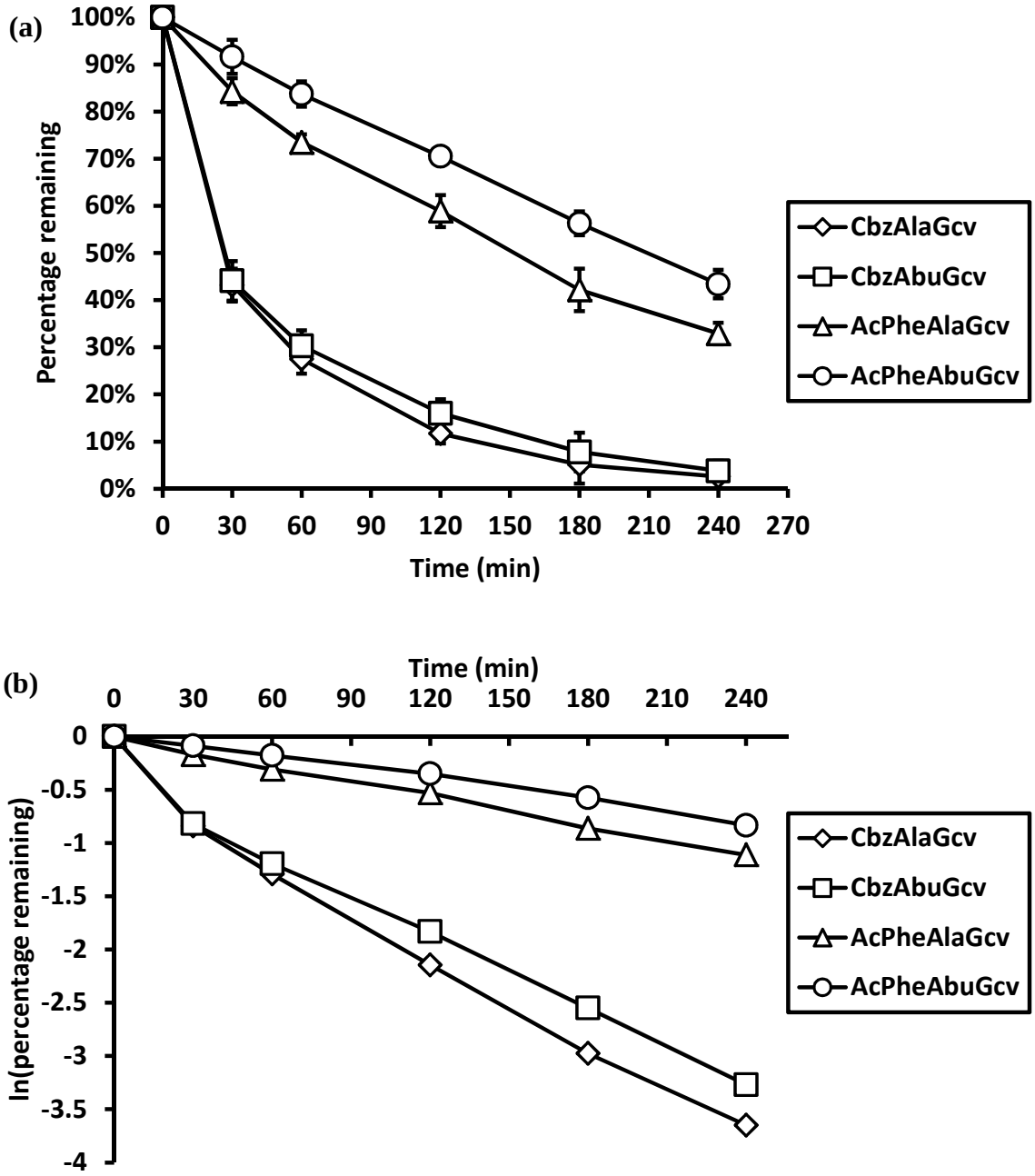

Figure 3.12. Stability of 80 μM ganciclovir monoester prodrugs (CbzAlaGcv, CbzAbuGcv, AcPheAlaGcv "A-4" and AcPheAbuGcv "B-3") in undiluted human plasma over the course of 240 min. The *y* axis, denoting percentages of the remaining unchanged prodrugs in plasma, is shown in **(a)** at normal scale and **(b)** at log scale. n = 3 for all time points and error bars represent SEM. The elimination constants (*k*) and half-lives ($t_{1/2}$) of the four prodrugs in plasma (**Table 3.1**) were calculated based on a first-order elimination model.

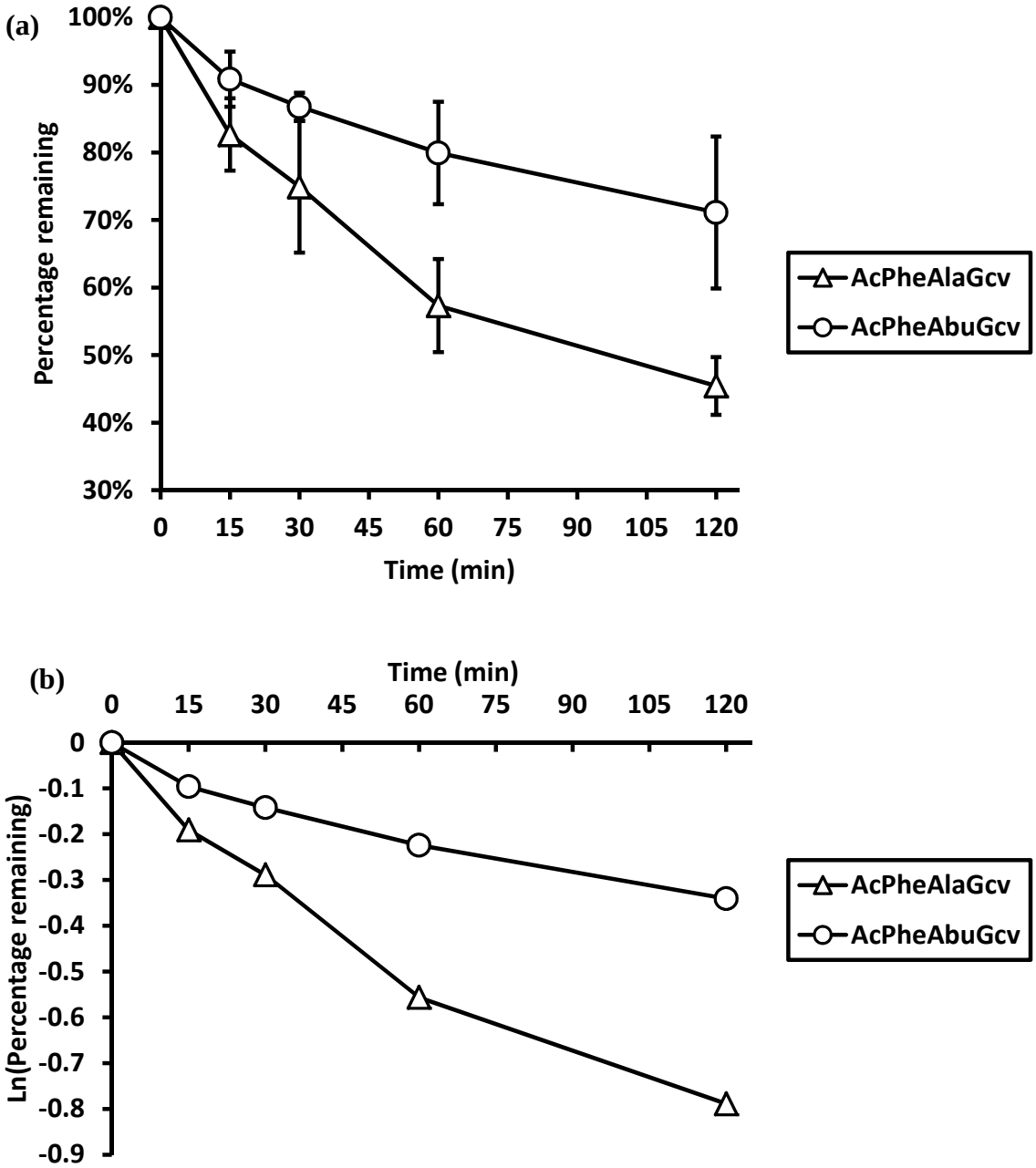

Figure 3.13. Stability of 2 µM acetylated dipeptide monoester prodrugs of ganciclovir (AcPheAlaGcv "A-4" and AcPheAbuGcv "B-3") in 1 mg/mL pooled human liver microsomes over the course of 120 min. The *y* axis, denoting percentages of the remaining unchanged prodrugs in liver microsomes, is shown in **(a)** at normal scale and **(b)** at log scale. n = 3 for all time points and error bars represent SEM. The elimination constants (*k*) and half-lives ($t_{1/2}$) of the two prodrugs in liver microsomes (**Table 3.2**) were calculated based on a first-order elimination model.

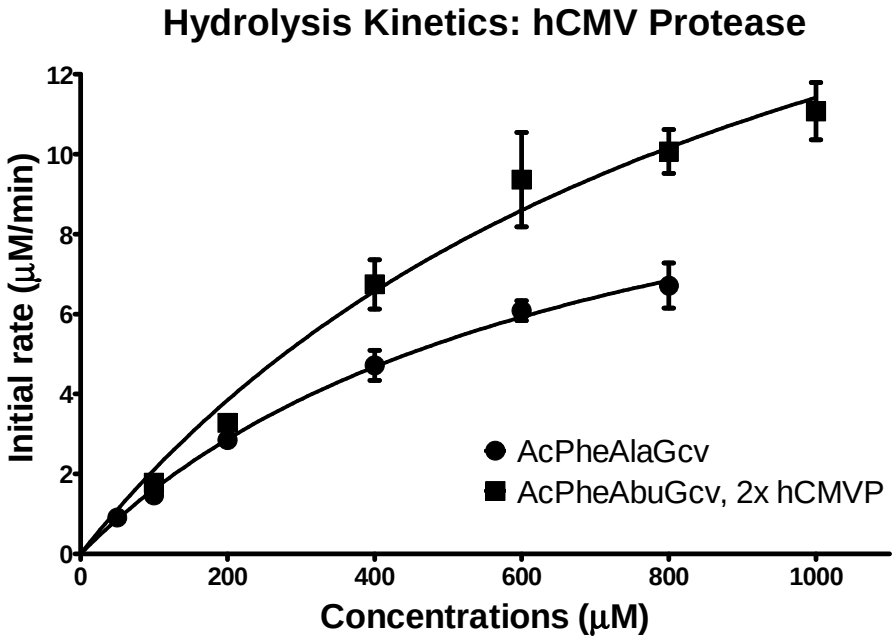

Figure 3.14. The initial rate (v_0, in μM/min) vs. concentrations ([S], in μM) plot for the hCMV protease A143S-catalyzed hydrolysis of AcPheAlaGCV "A-4" and AcPheAbuGCV "B-3" and curve-fitting to Michaelis-Menten models. For AcPheAlaGCV, the concentrations were 50, 100, 200, 400, 600 and 800 μM and 40 μg/mL hCMVP A143S was used. For AcPheAbuGCV, prodrug concentrations were 100, 200, 400, 600, 800 and 1000 μM and 80 μg/mL hCMVP A143S was used. n = 3 for each data point and error bars represent SEM. The data were fit to the Michaelis-Menten model using non-linear regressions with the least-square (ordinary) method. Kinetic parameters determined from the curve-fitting were shown in **Table 3.3**.

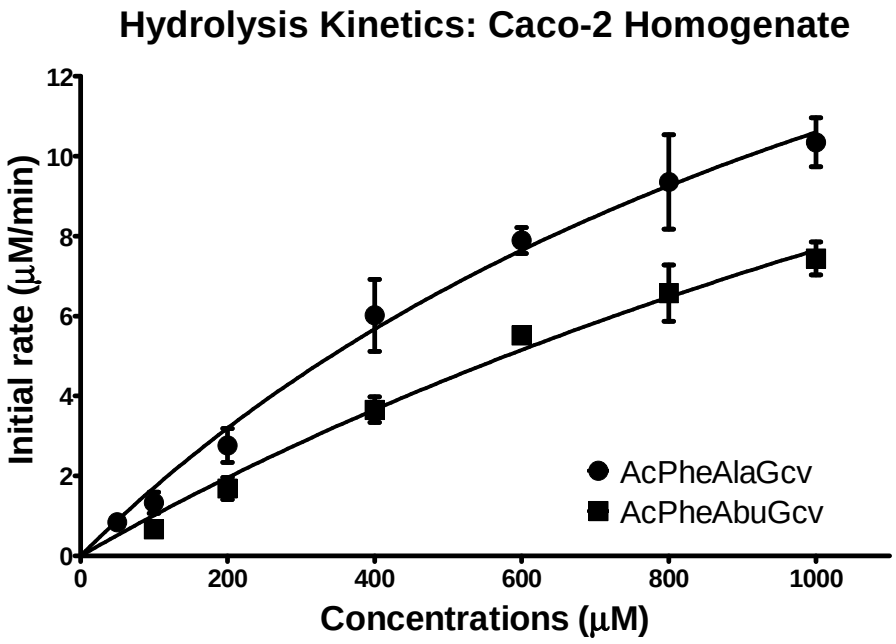

Figure 3.15. The initial rate (v_0, in μM/min) vs. concentrations ([S], in μM) plot for the Caco-2 homogenate-catalyzed hydrolysis of AcPheAlaGCV "A-4" and AcPheAbuGCV "B-3" and curve-fitting of these data to Michaelis-Menten models. For AcPheAlaGCV, the concentrations were 50, 100, 200, 400, 600, 800 and 1000 μM. For AcPheAbuGCV, prodrug concentrations were 100, 200, 400, 600, 800 and 1000 μM. 1 mg/mL Caco-2 homogenates were used for both prodrugs at all concentrations. n = 3 for each data point and error bars represent SEM. The data were fit to the Michaelis-Menten model using non-linear regressions with the least-square (ordinary) method. Kinetic parameters determined from the curve-fitting were shown in **Table 3.3**.

(a)

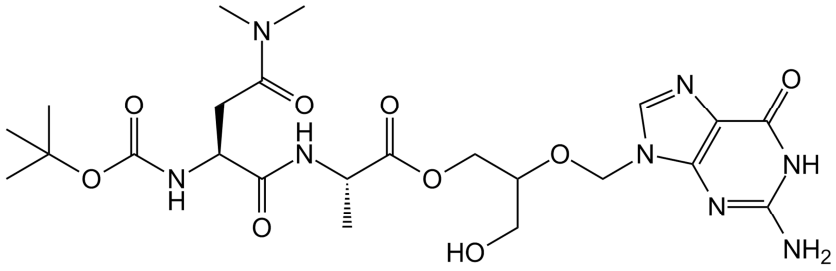

(b)

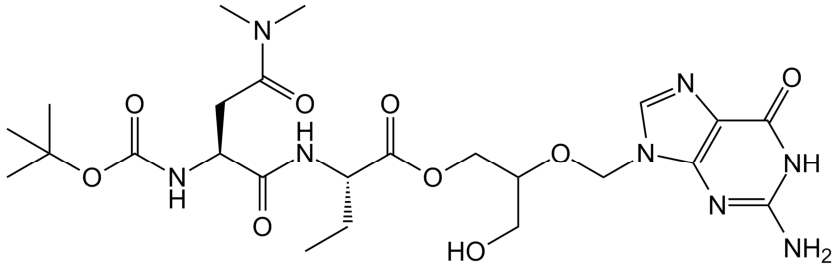

Figure 3.16. Chemical structures of two proposed monoester prodrugs of ganciclovir: (a) *N*-tert-butyloxycarbonyl-(*N*',*N*')-dimethyl-(L)-asparagine-(L)-alanine-ganciclovir (Boc-Asn(Me)$_2$-Ala-GCV) and (b) *N*-tert-butyloxycarbonyl-(*N*',*N*')-dimethyl-(L)-asparagine-(α,L)-aminobutyrate-ganciclovir (Boc-Asn(Me)$_2$-Abu-GCV).

TABLES

Prodrug	k (min^{-1})	$t_{1/2}$ (min)
CbzAlaGCV	0.0257	27
CbzAbuGCV	0.0248	28
AcPheAlaGCV	0.0047	148
AcPheAbuGCV	0.0033	210

Table 3.1. Elimination rate constants (k) and half-lives ($t_{1/2}$) of CbzAlaGCV, CbzAbuGCV, AcPheAlaGCV "A-4" and AcPheAbuGCV "B-3" in human plasma. Elimination rate constants (k) were derived from fitting the percentages remaining vs. time data to a first-order elimination equation ($C(t) / C_0 = e^{-kt}$). Half-lives were calculated as $t_{1/2} = 0.693 / k$.

Prodrug	k (min^{-1})	$t_{1/2}$ (min)
AcPheAlaGCV	0.0071	97
AcPheAbuGCV	0.0028	250

Table 3.2. Elimination rate constants (k) and half-lives ($t_{1/2}$) of AcPheAlaGCV "A-4" and AcPheAbuGCV "B-3" in pooled human liver microsomes. Elimination rate constants (k) were derived from fitting the percentages remaining vs. time data to a first-order elimination equation ($C(t) / C_0 = e^{-kt}$). Half-lives were calculated as $t_{1/2} = 0.693 / k$.

		AcPheAlaGCV	AcPheAbuGCV
hCMV protease A143S	k_{cat}	0.348 ± 0.043	0.308 ± 0.057
	K_m	685 ± 164	967 ± 337
	k_{cat} / K_m	5.08×10^{-4}	3.19×10^{-4}
Caco-2 homogenate	k_{cat}	0.0251 ± 0.0068	0.0281 ± 0.0121
	K_m	$1.37\times10^{3} \pm 0.56\times10^{3}$	$2.67\times10^{3} \pm 1.48\times10^{3}$
	k_{cat} / K_m	1.83×10^{-5}	1.05×10^{-5}

Table 3.3. Michaelis-Menten kinetic parameters for the hydrolysis of the two acetylated dipeptide prodrugs of ganciclovir by hCMV protease A143S or Caco-2 homogenates. The k_{cat} and K_m values were determined from Michaelis-Menten kinetic hydrolysis experiments (see Materials and Methods and Fig. 3.14 and 3.15) and expressed in mean ± SEM. k_{cat} has a unit of µM / (min·(µg/mL protein)),K_m is expressed in µM and k_{cat} / K_m has a unit of $(\text{min}\cdot(\mu\text{g/mL protein}))^{-1}$.

REFERENCES

1. *Cytovene (R) labels at Drugs@FDA.* [cited 2013 Jan. 29]; Available from: http://www.accessdata.fda.gov/drugsatfda_docs/label/2006/019661s030lbl.pdf.
2. *Vitrasert (R) Package Insert. Bausch & Lomb.* . Available from: http://www.bausch.com.au/en_AU/downloads/ecp/pharma/vitrasert4_5.pdf.
3. *Valcyte (R) labels at Drugs@FDA.* [cited 2013 Feb. 22]; Available from: http://www.accessdata.fda.gov/drugsatfda_docs/label/2010/021304s008,022257s003lbl.pdf.
4. *Foscavir (R) labels at Drugs@FDA.* [cited 2013 Feb. 21]; Available from: http://www.accessdata.fda.gov/drugsatfda_docs/label/2012/020068s018lbl.pdf.
5. *Vistide (R) labels at Drugs@FDA.* [cited 2013 Feb. 22]; Available from: http://www.accessdata.fda.gov/drugsatfda_docs/label/1999/020638s003lbl.pdf.
6. *Vitravene (R) label information at Drugs@FDA.* [cited 2013 Feb. 23]; Available from: http://www.accessdata.fda.gov/drugsatfda_docs/label/1998/20961lbl.pdf.
7. *CytoGam (R) package insert (US FDA).* [cited 2013 Feb. 22]; Available from: http://www.fda.gov/downloads/BiologicsBloodVaccines/BloodBloodProducts/ApprovedProducts/LicensedProductsBLAs/FractionatedPlasmaProducts/UCM197962.pdf.
8. *Approval History Retrieved from Searching "Cytovene" at Drugs@FDA.*; Available from: http://www.accessdata.fda.gov/scripts/cder/drugsatfda/index.cfm.
9. Biron, K.K., *Antiviral drugs for cytomegalovirus diseases.* Antiviral Res, 2006. **71**(2-3): p. 154-63.
10. Goodrich, J.M., et al., *Ganciclovir prophylaxis to prevent cytomegalovirus disease after allogeneic marrow transplant.* Ann Intern Med, 1993. **118**(3): p. 173-8.
11. Winston, D.J., et al., *Ganciclovir prophylaxis of cytomegalovirus infection and disease in allogeneic bone marrow transplant recipients. Results of a placebo-controlled, double-blind trial.* Ann Intern Med, 1993. **118**(3): p. 179-84.
12. McGavin, J.K. and K.L. Goa, *Ganciclovir: an update of its use in the prevention of cytomegalovirus infection and disease in transplant recipients.* Drugs, 2001. **61**(8): p. 1153-83.
13. Dieterich, D.T., et al., *Ganciclovir treatment of gastrointestinal infections caused by cytomegalovirus in patients with AIDS.* Rev Infect Dis, 1988. **10 Suppl 3**: p. S532-7.
14. Dieterich, D.T., et al., *Ganciclovir treatment of cytomegalovirus colitis in AIDS: a randomized, double-blind, placebo-controlled multicenter study.* J Infect Dis, 1993. **167**(2): p. 278-82.
15. Oshima, Y., et al., *Successful treatment of cytomegalovirus colitis with ganciclovir in a patient with adult T cell leukemia lymphoma: case report.* J Chemother, 1999. **11**(3): p. 215-9.
16. Emanuel, D., et al., *Cytomegalovirus pneumonia after bone marrow transplantation successfully treated with the combination of ganciclovir and high-dose intravenous immune globulin.* Ann Intern Med, 1988. **109**(10): p. 777-82.
17. Reed, E.C., et al., *Treatment of cytomegalovirus pneumonia with ganciclovir and intravenous cytomegalovirus immunoglobulin in patients with bone marrow transplants.* Ann Intern Med, 1988. **109**(10): p. 783-8.
18. Vancikova, Z., et al., *Perinatal cytomegalovirus hepatitis: to treat or not to treat with ganciclovir.* J Paediatr Child Health, 2004. **40**(8): p. 444-8.

19. Majumdar, S., et al., *Mechanism of ganciclovir uptake by rabbit retina and human retinal pigmented epithelium cell line ARPE-19.* Curr Eye Res, 2004. **29**(2-3): p. 127-36.
20. Sullivan, V., et al., *A protein kinase homologue controls phosphorylation of ganciclovir in human cytomegalovirus-infected cells.* Nature, 1992. **358**(6382): p. 162-4.
21. Littler, E., A.D. Stuart, and M.S. Chee, *Human cytomegalovirus UL97 open reading frame encodes a protein that phosphorylates the antiviral nucleoside analogue ganciclovir.* Nature, 1992. **358**(6382): p. 160-2.
22. Freitas, V.R., et al., *Activity of 9-(1,3-dihydroxy-2-propoxymethyl)guanine compared with that of acyclovir against human, monkey, and rodent cytomegaloviruses.* Antimicrob Agents Chemother, 1985. **28**(2): p. 240-5.
23. Matthews, T. and R. Boehme, *Antiviral activity and mechanism of action of ganciclovir.* Rev Infect Dis, 1988. **10 Suppl 3**: p. S490-4.
24. Lurain, N.S. and S. Chou, *Antiviral drug resistance of human cytomegalovirus.* Clin Microbiol Rev, 2010. **23**(4): p. 689-712.
25. Gilbert, C. and G. Boivin, *Human cytomegalovirus resistance to antiviral drugs.* Antimicrob Agents Chemother, 2005. **49**(3): p. 873-83.
26. Perrottet, N., et al., *Valganciclovir in adult solid organ transplant recipients: pharmacokinetic and pharmacodynamic characteristics and clinical interpretation of plasma concentration measurements.* Clin Pharmacokinet, 2009. **48**(6): p. 399-418.
27. Janoly-Dumenil, A., et al., *A pharmacodynamic model of ganciclovir antiviral effect and toxicity for lymphoblastoid cells suggests a new dosing regimen to treat cytomegalovirus infection.* Antimicrob Agents Chemother, 2012. **56**(7): p. 3732-8.
28. *Morbidity and toxic effects associated with ganciclovir or foscarnet therapy in a randomized cytomegalovirus retinitis trial. Studies of ocular complications of AIDS Research Group, in collaboration with the AIDS Clinical Trials Group.* Arch Intern Med, 1995. **155**(1): p. 65-74.
29. Sommadossi, J.P. and R. Carlisle, *Toxicity of 3'-azido-3'-deoxythymidine and 9-(1,3-dihydroxy-2-propoxymethyl)guanine for normal human hematopoietic progenitor cells in vitro.* Antimicrob Agents Chemother, 1987. **31**(3): p. 452-4.
30. Biron, K.K., et al., *Metabolic activation of the nucleoside analog 9-[(2-hydroxy-1-(hydroxymethyl)ethoxy]methyl)guanine in human diploid fibroblasts infected with human cytomegalovirus.* Proc Natl Acad Sci U S A, 1985. **82**(8): p. 2473-7.
31. Battiwalla, M., et al., *Ganciclovir inhibits lymphocyte proliferation by impairing DNA synthesis.* Biol Blood Marrow Transplant, 2007. **13**(7): p. 765-70.
32. De Clercq, E. and H.J. Field, *Antiviral prodrugs - the development of successful prodrug strategies for antiviral chemotherapy.* Br J Pharmacol, 2006. **147**(1): p. 1-11.
33. *Approval History Retrieved from Searching "Vitravene" at Drugs@FDA.*; Available from: http://www.accessdata.fda.gov/scripts/cder/drugsatfda/index.cfm.
34. Spada, S. and G. Walsh, *Directory of approved biopharmaceutical products*. 2005, Boca Raton: CRC Press. 317 p.
35. Snydman, D.R., et al., *A pilot trial of a novel cytomegalovirus immune globulin in renal transplant recipients.* Transplantation, 1984. **38**(5): p. 553-7.

36. Sokos, D.R., M. Berger, and H.M. Lazarus, *Intravenous immunoglobulin: appropriate indications and uses in hematopoietic stem cell transplantation.* Biol Blood Marrow Transplant, 2002. **8**(3): p. 117-30.
37. James, S.H., et al., *Cyclopropavir inhibits the normal function of the human cytomegalovirus UL97 kinase.* Antimicrob Agents Chemother, 2011. **55**(10): p. 4682-91.
38. Kern, E.R., et al., *Oral activity of a methylenecyclopropane analog, cyclopropavir, in animal models for cytomegalovirus infections.* Antimicrob Agents Chemother, 2004. **48**(12): p. 4745-53.
39. Kern, E.R., et al., *In vitro activity and mechanism of action of methylenecyclopropane analogs of nucleosides against herpesvirus replication.* Antimicrob Agents Chemother, 2005. **49**(3): p. 1039-45.
40. Evers, D.L., et al., *Inhibition of human cytomegalovirus replication by benzimidazole nucleosides involves three distinct mechanisms.* Antimicrob Agents Chemother, 2004. **48**(10): p. 3918-27.
41. Biron, K.K., et al., *Potent and selective inhibition of human cytomegalovirus replication by 1263W94, a benzimidazole L-riboside with a unique mode of action.* Antimicrob Agents Chemother, 2002. **46**(8): p. 2365-72.
42. Avery, R.K., et al., *Oral maribavir for treatment of refractory or resistant cytomegalovirus infections in transplant recipients.* Transpl Infect Dis, 2010. **12**(6): p. 489-96.
43. Marty, F.M. and M. Boeckh, *Maribavir and human cytomegalovirus-what happened in the clinical trials and why might the drug have failed?* Curr Opin Virol, 2011. **1**(6): p. 555-62.
44. *ViroPharma press release. ViroPharma Announces Initiation of Clinical Studies to Evaluate Maribavir for Treatment of Cytomegalovirus (CMV) Infection.* 2012 [cited 2013 Feb. 20]; Available from: http://ir.viropharma.com/releasedetail.cfm?releaseid=679480.
45. Avery, R.K., et al., *Utility of leflunomide in the treatment of complex cytomegalovirus syndromes.* Transplantation, 2010. **90**(4): p. 419-26.
46. Waldman, W.J., et al., *Novel mechanism of inhibition of cytomegalovirus by the experimental immunosuppressive agent leflunomide.* Transplantation, 1999. **68**(6): p. 814-25.
47. Goldner, T., et al., *The novel anticytomegalovirus compound AIC246 (Letermovir) inhibits human cytomegalovirus replication through a specific antiviral mechanism that involves the viral terminase.* J Virol, 2011. **85**(20): p. 10884-93.
48. Kaul, D.R., et al., *First report of successful treatment of multidrug-resistant cytomegalovirus disease with the novel anti-CMV compound AIC246.* Am J Transplant, 2011. **11**(5): p. 1079-84.
49. Crumpacker, C.S., *Ganciclovir.* N Engl J Med, 1996. **335**(10): p. 721-9.
50. Lowance, D., et al., *Valacyclovir for the prevention of cytomegalovirus disease after renal transplantation. International Valacyclovir Cytomegalovirus Prophylaxis Transplantation Study Group.* N Engl J Med, 1999. **340**(19): p. 1462-70.
51. *Foscarnet information at DrugBank.* [cited 2013 Feb. 23]; Available from: http://www.drugbank.ca/drugs/DB00529.

52. Saleh, S. and G. Hempel, *Quantification of ganciclovir in human plasma using capillary electrophoresis.* Electrophoresis, 2006. **27**(12): p. 2439-43.
53. Armstrong, M.D. and F. Binkley, *A metabolic study of alpha-aminobutyric acid.* J Biol Chem, 1949. **180**(3): p. 1059-63.
54. Chiarla, C., I. Giovannini, and J.H. Siegel, *Characterization of alpha-amino-n-butyric acid correlations in sepsis.* Transl Res, 2011. **158**(6): p. 328-33.
55. Ano, R., et al., *Relationship between structure and permeability of dipeptide derivatives containing tryptophan and related compounds across human intestinal epithelial (Caco-2) cells.* Bioorg Med Chem, 2004. **12**(1): p. 249-55.
56. Allenmark, S. and J. Gawronski, *Determination of absolute configuration--an overview related to this special issue.* Chirality, 2008. **20**(5): p. 606-8.
57. Landowski, C.P., et al., *Nucleoside ester prodrug substrate specificity of liver carboxylesterase.* J Pharmacol Exp Ther, 2006. **316**(2): p. 572-80.
58. Imai, T., et al., *Identification of esterases expressed in Caco-2 cells and effects of their hydrolyzing activity in predicting human intestinal absorption.* Drug Metab Dispos, 2005. **33**(8): p. 1185-90.
59. Vahlquist, B., *On the esterase activity of human blood plasma.* Skandinavisches Archiv Für Physiologie, 1935. **72**: p. 133-160.
60. Taketani, M., et al., *Carboxylesterase in the liver and small intestine of experimental animals and human.* Life Sci, 2007. **81**(11): p. 924-32.
61. Morgan, M.Y., et al., *Plasma amino-acid patterns in liver disease.* Gut, 1982. **23**(5): p. 362-70.
62. Hogan, D.L., K.L. Kraemer, and J.I. Isenberg, *The use of high-performance liquid chromatography for quantitation of plasma amino acids in man.* Anal Biochem, 1982. **127**(1): p. 17-24.
63. Matsuo, Y. and D.M. Greenberg, *Metabolic formation of homoserine and alpha-aminobutyric acid from methionine.* J Biol Chem, 1955. **215**(2): p. 547-54.
64. Orlowski, M. and S. Wilk, *Synthesis of ophthalmic acid in liver and kidney in vivo.* Biochem J, 1978. **170**(2): p. 415-9.
65. Soga, T., et al., *Differential metabolomics reveals ophthalmic acid as an oxidative stress biomarker indicating hepatic glutathione consumption.* J Biol Chem, 2006. **281**(24): p. 16768-76.
66. Tong, L., et al., *Conserved mode of peptidomimetic inhibition and substrate recognition of human cytomegalovirus protease.* Nat Struct Biol, 1998. **5**(9): p. 819-26.

CHAPTER IV

CHARACTERIZATION OF THE BIOPHARMACEUTICAL PROFILES OF THE MONOESTER PRODRUGS OF GANCICLOVIR

SUMMARY

The main locale where the hCMV protease performs its functions is inside the host cell nucleus, which is also where ganciclovir exerts its inhibitory effects on viral DNA synthesis. Therefore, it is important that the prodrugs of ganciclovir for targeted activation by the hCMV protease are efficiently taken up by the host cells in order to be activated in intracellular space. A Caco-2 cell system was used to determine the cellular uptake of AcPheAlaGCV and AcPheAbuGCV in comparison to those of ganciclovir and valganciclovir. I demonstrated that at the 1-h time point, the Caco-2 uptake of AcPheAbuGCV was significantly higher than ganciclovir and sufficient amounts of AcPheAbuGCV remained intact and thus available for potential hydrolytic activation by the hCMV protease. In addition to cellular uptake properties, I also characterized the permeability of AcPheAlaGCV and AcPheAbuGCV across the Caco-2 monolayer because it is important to explore whether the two prodrugs could potentially be delivered by oral administration, which is the preferred route for patients. It was shown that while the apparent permeability of intact AcPheAlaGCV and AcPheAbuGCV were potentially similar to that of ganciclovir, the oral route is likely suboptimal for the delivery of the two prodrugs because of metabolic reactions inside the gastrointestinal lumen and liver. The intravenous route is, therefore, a better option for delivery of the ganciclovir prodrugs in *in vivo* study settings.

BACKGROUND

Human Peptide Transporter 1 (PEPT1)

The peptide transporter 1 (PEPT1) is a member of the proton-coupled oligopeptide transporter (POT) superfamily which has been identified in a broad range of prokaryotic and eukaryotic species [1]. The amino acid sequences of PEPT1 are highly conserved, especially in mammals, as an amino acid sequence identity of 83% is observed between human and mouse PEPT1 [2]. The human PEPT1 (hPEPT1) is a 78.8-kD protein with 708 amino acids [3]. Also known as solute carrier 15A1 (SLC15A1), hPEPT1 is one of the four members of the human SLC15A family, which also includes peptide transporter 2 (PEPT2, SLC15A2), peptide histidine transporter 1 (PHT1, SLC15A4) and peptide histidine transporter 2 (PHT2, SLC15A3).

In human, PEPT1 is most abundantly expressed at the apical side of the intestinal brush border membrane, especially in the duodenum, jejunum and ileum, although it has also been found in various other tissues such as pancreas, bile duct, adrenal glands and nasal epithelium [1, 4, 5]. In the small intestine, the function of PEPT1, a proton/substrate symporter, is dependent on the inward proton gradient generated from the acidic environment in the gastrointestinal lumen (pH 5.9-6.8) [6] toward the neutral cytoplasm (pH around 7.4). With this proton gradient as the driving force, substrates such as di- and tripeptides from dietary digestion are transported by PEPT1 into the enterocytes. These nutrients are then further hydrolyzed by intracellular hydrolases and the resulting products are transported through basolateral transporters [7] out of the enterocytes and into the systemic circulation.

The roles of PEPT1 in the facilitated transport of xenobiotics have been extensively studied. Many drugs such as β-lactams [8] and bestatin [9] as well as valacyclovir and valganciclovir, the (L)-valyl esters of acyclovir [10, 11] and ganciclovir [12], were discovered to be substrates of PEPT1. The empirical substrate specificity and preference of hPEPT1 have also been well characterized. A peptide bond within the compound has been deemed not necessarily a requirement for its transport by PEPT1 [12-14], as observed in the cases of valacyclovir, valganciclovir and δ-aminolevulinic acid (5-ALA). For terminal moieties, PEPT1 prefers free amino and carboxyl groups at their respective termini. Modifications on

these groups could decrease affinity of the substrates to PEPT1; a free N-terminal amino group seems especially important [15, 16]. For stereochemical configurations, (L)-amino acid derivatives, (L)-(L)-dipeptides and derivatives and (L)-(L)-(L)-tripeptides are preferred over their counterparts with (D)-amino acid residues [15]. These properties have been utilized to tentatively predict a potential substrate's affinity for PEPT1 [17].

Valganciclovir

Valganciclovir (trade name Valcyte®, valganciclovir hydrochloride [18]) is the (L)-valyl ester prodrug of ganciclovir (**Figure 3.3a**). It was developed with the specific purpose to overcome the poor oral bioavailability of ganciclovir. Indeed, clinical studies demonstrated that while ganciclovir capsules only had an oral bioavailability of 6.2% – 8.5%, Valcyte tablets at comparable dosages showed an average of 60% or more oral bioavailability [12, 18]. Not only was the 0-24 h area-under-the-curve ($AUC_{0\text{-}24h}$) for ganciclovir from 900 mg once daily administration of Valcyte found to be comparable to that of once-daily intravenous injection of 5 mg/kg ganciclovir, but also significantly higher than the AUC of 3 times daily oral dosing of 1 g ganciclovir. Therefore, valganciclovir is currently the preferred form for the oral delivery of ganciclovir; it has the same indication and usage as well as similar systemic toxicities to those of IV-administered ganciclovir [18, 19].

Valganciclovir has been shown to be a substrate for both PEPT1 and PEPT2 transporters, as demonstrated by its inhibitory effects on glycylsarcosine uptake in cell models expressing the two transporters as well as its capability to induce inward currents in PEPT1-expressing *Xenopus laevis* oocytes [12]. In the human small intestine, the absorption of valganciclovir is primarily facilitated by PEPT1 which is predominantly and abundantly expressed in the duodenum, jejunum and ileum. Valganciclovir is rapidly hydrolyzed to ganciclovir through catalysis by the esterase valacylovirase (VACVase), which is expressed in the enterocytes, liver, kidneys as well as other tissues and organs [20, 21]. As an evidence of the first-pass metabolism of valganciclovir after its oral dosing, the maximum plasma concentration (c_{max}) of ganciclovir converted from valganciclovir was found to be more than 30 times that of unchanged valganciclovir [22]. Therefore, orally administered valganciclovir

possesses the same disposition, excretion and pharmacological properties as those of ganciclovir.

The Caco-2 Cell System: Usefulness and Limitations

Caco-2 is an adherent epithelial cell line that is derived from human colorectal adenocarcinoma [23]. In *in vitro* culture, once confluence is reached, Caco-2 cells undergo spontaneous differentiation toward a monolayer with many unique features of a functional intestinal epithelium, and the differentiation is usually complete within 3 weeks [24]. The differentiated monolayer has tight junction formations between the cells as well as develops a brush border on the apical surface. It also expresses enzymes and transporter proteins that are typically present in the microvilli [24, 25]. Due to its similarity to the intestinal epithelia, ease-of-use as a cell culture model and relatively low cost, the Caco-2 monolayer has been considered a gold standard for *in vitro* prediction of *in vivo* permeability and absorption of drugs [25, 26]. Notably, to date no false positive results have been produced in permeability studies using Caco-2 systems, indicating its strength as well as stringency [27].

Despite its widespread use, the Caco-2 cell system also has well-documented limitations that need to be considered when it is used to characterize the biopharmaceutical properties of certain types of compounds. The expression levels of many transporters and drug-metabolizing enzymes in Caco-2 cells are known to be significantly different from those in the human intestine. For example, PEPT1 is expressed on the apical membranes of Caco-2 cells and many studies have utilized Caco-2 to determine whether the compounds of interest were potential PEPT1 substrates. However, the level of PEPT1 expression in Caco-2 cells could be several-fold lower than in human small intestines, as shown by comparison of both mRNA and protein levels [28, 29]. Therefore, drugs that are transported by PEPT1 often display lower permeability when measured in the Caco-2 system than in actual perfusion studies with human intestinal segments [28]. Caco-2 cells also express fewer types and lower amounts of phase I and phase II metabolic enzymes than human duodenum does [28], making it a less reliable tool to predict and characterize the related metabolisms of certain compounds during their transport across the actual brush border. The relative levels of a number of esterases were also found to be different between Caco-2 cells and human duodenum or

jejunum, as demonstrated by studies comparing functional activities [30] and mRNA levels [28] of those esterases in the two models. Due to these disparities, caution is thus warranted when using Caco-2 cells to characterize the uptake and permeability of compounds that are potential substrates for carrier-mediated transport and / or intestinal metabolic enzymes.

Biopharmaceutical Profiles of Targetable Prodrugs of Ganciclovir

As introduced in Chapter III, ganciclovir exerts its pharmacological effects by inhibition of viral DNA synthesis, which takes place inside the host cell nucleus. The human cytomegalovirus (hCMV) protease is responsible for the degradation of the internal scaffolding proteins of the viral procapsid in order to create space for incorporation of newly synthesized viral DNA [31-33]. This proteolytic process also occurs inside the nuclei of hCMV-infected cells [31]. Therefore, it is critical that the targetable ganciclovir prodrugs are effectively taken up or absorbed by the host cells, after which process they could be activated by the hCMV protease and then execute their antiviral effects. In addition, it is also desirable that the intracellular concentration of the unchanged prodrug is similar to that of ganciclovir when the latter is dosed separately as a control, so that the pharmacological effects of the prodrug, after its hydrolytic activation, could be equivalent to the original treatment strategy with ganciclovir.

Oral pharmaceutical products are usually preferred by patients over other dosage forms (for example, parenteral and inhalational) due to its convenience and non-invasiveness. As shown in Chapter III, out of the four prodrug candidates, AcPheAlaGCV and AcPheAbuGCV are likely to be more stable than the other two in tissue matrices and, therefore, they are the better compounds for further development, including a possible oral dosing strategy. Their dipeptide promoieties make them potential substrates for PEPT1-mediated transports. Nevertheless, in oral dosing they would also be exposed to the first-pass enzymatic degradations. Therefore, if a sufficient amount of AcPheXaaGCV survives the first-pass metabolism and enters the systemic circulation in its unchanged form, it could potentially have a similar bioavailability to that of the orally delivered ganciclovir while ideally still retaining its selective activation capability. To determine whether the two acetylated dipeptide prodrugs of ganciclovir possess such a quality, the intact prodrugs'

apparent permeability across Caco-2 cell monolayers would be compared to that of ganciclovir. Valganciclovir would be used to verify the PEPT1-mediated transport in Caco-2 and metoprolol serves as the standard for highly permeable compounds.

MATERIALS AND METHODS

Materials

All the chemicals, cell lines and dispensable tissue culture hardware that have been mentioned in Chapters II and III were acquired from the same sources. In addition, 2-(*N*-morpholino)ethanesulfonic acid (MES) and dextrose ((D)-glucose) were purchased from Fisher Scientific (Fair Lawn, NJ). 6-well Transwell® inserts (membrane thickness 10 μm, pore size 0.4 μm) were purchased from Corning Inc. (Corning, NY).

Cell Culture

Caco-2 cells (passage 22 – 36) were routinely maintained in the same conditions detailed in Chapter III. For direct uptake studies, Caco-2 cells were seeded at a density of 3×10^5 cells per well into a 6-well plate and allowed to grow until 11-13 days post-confluence. The culture media were renewed every other day. For permeability studies, Caco-2 cells were seeded at 2×10^5 cells per Transwell insert into a 6-well Transwell plate (growth area 4.67 cm^2). The cells were cultured until 18-20 days post-confluence and the culture media in both apical and basolateral chambers were replaced on alternate days. Transepithelial electrical resistance (TEER) was regularly measured for each Transwell and only wells with TEER values larger than 1,400 $\Omega\cdot cm^2$ were used for permeability experiments.

Direct Uptake of *N*-acetylated Dipeptide Prodrugs of Ganciclovir by Caco-2 Cells

Post-confluent Caco-2 cells were washed with warm pH 6.0 uptake buffer (145 mM NaCl, 0.5 mM $MgCl_2$, 1 mM NaH_2PO_4, 1 mM $CaCl_2$, 3 mM KCl, 5 mM (D)-glucose, 5 mM MES). Ganciclovir, valganciclovir (ValGCV), AcPheAlaGCV and AcPheAbuGCV were diluted in the uptake buffer at concentrations of 200 μM and added into the respective wells in the 6-well plate. The plate was incubated at 37°C, 5% CO_2 for 60 min. Cells were then repeatedly washed with cold pH 6.0 uptake buffer and then collected in 1:1-mixed water / acetonitrile with 250 nM (S)-(-)-propranolol as internal standard for LC-MS. After centrifugation at 15,000 ×g at 4°C for 15 min, the contents of compounds in the organic supernatants were analyzed by LC-MS. The remaining pellets were dissolved in 0.5 M NaOH and the respective protein concentrations were quantified with bicinchoninic acid (BCA)

assays. The amounts of cellular proteins were used to normalize the amounts of compounds taken up by the cells in the corresponding wells.

Apical-to-basolateral Permeability of *N*-acetylated Dipeptide Prodrugs of Ganciclovir across Caco-2 Monolayers

Post-confluent Caco-2 cell monolayers were washed with the aforementioned pH 6.0 uptake buffer (apical chamber) and Dulbecco's phosphate buffered saline (DPBS, pH 7.4; basolateral chamber). 1.5 mL drug solutions in the pH 6.0 uptake buffer (metoprolol and ganciclovir at 1 mM, valganciclovir at 0.5 mM, AcPheAlaGCV or AcPheAbuGCV at 0.2 mM) were then added to their respective apical chambers and 2.5 mL DPBS to basolateral compartments. The cells were incubated at 37°C on an orbital shaker with 50 rpm rotation speed. Samples were retrieved from the basolateral chamber every 15 min until 120 or 135 min after dosing and equal volumes of fresh DPBS were replenished to maintain sink conditions. Quenching was performed with either 0.5% TFA and 20 μM caffeine (for HPLC analysis) or acetonitrile with 250 nM (S)-(-)-propranolol (for LC-MS analysis). The collected samples were frozen at -80°C until HPLC or LC-MS analyses.

HPLC Analysis

Using the same method and equipment employed in Chapter III, HPLC analyses were applied to samples from the receiving chambers of Transwells dosed with ganciclovir, valganciclovir and metoprolol in the Caco-2 permeability study. Caffeine, ganciclovir and valganciclovir were detected at UV 254 nm and metoprolol at 220 nm. The accuracy of the assays was 90% – 110%.

LC-MS Analysis

The same LC-MS equipment and methodology employed in Chapter III were applied to the analyses of all samples of Caco-2 direct uptake studies and, for the Caco-2 permeability study, samples from the receiving chambers of Transwells dosed with AcPheAlaGCV and AcPheAbuGCV. Mass-to-charge ratios (m/z's): ganciclovir $[M+H]^+$ 256.1, valganciclovir $[M+H]^+$ 355.1, AcPheAlaGCV 516.1, AcPheAbuGCV 530.1, (S)-(-)-propranolol $[M+H]^+$ 260.1. The accuracy of the assays was 75% – 125%.

Data Analysis

To determine the compounds' apparent permeability coefficient across Caco-2 monolayers, concentration vs. time curves were plotted for each sample well of every compound. The apparent permeability coefficient, P_{app}, is determined by Equation 4.1:

$$P_{\text{app}} = \frac{V_{\text{R}}}{A \times C_0} \times \frac{dC_{\text{R}}}{dt} \qquad \text{(Equation 4.1)}$$

Where V_R is the volume of the receiving chamber (2.5 cm^3), A is the area of cell growth (4.67 cm^2), C_0 is the initial concentration of the compound in the donor compartment (in µM), C_R is the concentration of the compound in the receiving compartment at a given time point (also in µM) and t is the collection time point since the initiation of dosing in the apical chamber (in seconds). For valganciclovir, C_R at each time point is the sum of C_R(ValGCV) and C_R(GCV), the latter generated from hydrolysis of ValGCV. For AcPheAlaGCV and AcPheAbuGCV, only the unchanged forms were used as their respective C_R's. dC_R / dt was calculated by linear regression of the C_R vs. t plots for each compound.

Statistical Analysis

All experiments had sample sizes of n = 3 – 6. Results are presented as the mean ± SEM. Statistical comparisons were performed with GraphPad Prism 5.0 using one-way ANOVA with *post-hoc* Tukey's multiple comparison tests. *P* values less than 0.05 were deemed significant.

RESULTS

Direct Uptake of Ganciclovir and Prodrugs by Caco-2 Cells

The total uptake for each prodrug was determined as the sum of the amount of the unchanged form and that of the ganciclovir that was generated from intracellular hydrolysis of the prodrug. As shown in **Figure 4.1(a)**, valganciclovir had the highest total uptake of all four compounds and a large part of that (~77%) was already bioconverted to ganciclovir. This result suggested that the PEPT1-mediated transport was likely active in the cultured Caco-2 cells. AcPheAbuGCV had the second highest total amount taken up by the cells, which was significantly higher than both AcPheAlaGCV and ganciclovir. The total uptake of AcPheAlaGCV was not found to be significantly different from that of ganciclovir. These results demonstrated the potential for enhanced cellular uptake of AcPheAbuGCV compared to the parent compound, ganciclovir, although AcPheAbuGCV clearly could not match the superiority of valganciclovir. In addition to total uptake, the amounts of unchanged prodrug remaining at 60 min in cells dosed with prodrug were also compared to the amount of ganciclovir in cells treated with ganciclovir (**Figure 4.1(b)**). The amount of intact AcPheAbuGCV was found to be comparable to that of ganciclovir when the latter was dosed separately. This suggests that, for AcPheAbuGCV, the membrane barrier and non-specific hydrolysis by the live Caco-2 cells did not significantly affect the targetability of the prodrug, since sufficient amounts of the unchanged AcPheAbuGCV remain available for selective activation by the hCMV protease expressed in infected cells. In contrast to AcPheAbuGCV, significantly less unchanged AcPheAlaGCV remains at 60 min in cells treated with the prodrug (**Fig. 4.1(b)**), indicating a diminished targeting ability for this prodrug. Finally, the percentages hydrolyzed of the three ganciclovir prodrugs are compared in **Figure 4.1(c)**. Almost 80% of valganciclovir taken up by the cells has been hydrolyzed to ganciclovir, a percentage that is much higher than with both dipeptide prodrugs. AcPheAbuGCV has a lower hydrolysis percentage than AcPheAlaGCV, again displaying a better stability profile and corroborating the related findings in Chapter III.

Apical-to-basolateral (A to B) Permeability across Caco-2 Monolayer

The apparent A to B permeability coefficients (P_{app}'s) of tested compounds were compared in **Figure 4.2**. Metoprolol, the drug often used as a high-permeability standard, showed the highest A to B permeability among all five; it was more than two times more permeable across the cell monolayer than the second most permeable compound, valganciclovir. The latter is significantly more permeable than ganciclovir, most likely due to the transport mediated by PEPT1 expressed on the apical membrane of Caco-2 cells. Permeability coefficients of the unchanged forms of AcPheAlaGCV and AcPheAbuGCV were both lower than that of valganciclovir and neither of them were found to be significantly different from the P_{app} of ganciclovir. In addition, the apparent permeability coefficients of AcPheAlaGCV and AcPheAbuGCV were not statistically different from each other. These results suggested that, for AcPheAlaGCV and AcPheAbuGCV, their effective permeability values (P_{eff}) in human intestines and oral bioavailability are unlikely to be significantly higher than those of ganciclovir, especially when probable degradation by digestive enzymes in the gut lumen is taken into consideration. Furthermore, as shown in Chapter III, hydrolytic degradation inside the liver will also eliminate a portion of the intact prodrugs. As a result, when these two prodrugs are administered at equivalent doses to oral ganciclovir dosages, they are unlikely to have similar oral bioavailability to that of ganciclovir when only the unchanged form of the prodrugs are considered.

DISCUSSION

In this chapter, I first compared the cellular uptake of the two acetylated dipeptide prodrugs of ganciclovir, AcPheAlaGCV and AcPheAbuGCV, to that of ganciclovir and valganciclovir. I found that AcPheAbuGCV had significantly higher total uptake than ganciclovir and also sufficient amounts of it remained unchanged for the sake of selective activation. I also characterized the permeability of the two targetable prodrugs across the Caco-2 monolayer and determined that oral dosing of these prodrug candidates would be unlikely to yield a desirable oral bioavailability for the intact prodrugs. Therefore, at this moment, intravenous injection seems to be the preferred route of administration for these prodrugs.

In the cellular uptake studies, the Caco-2 cells were used as a convenient surrogate for the target tissues / cells for the ganciclovir prodrugs. As detailed in Chapter II, cytomegalovirus infects many tissues and organs such as retina, lung, liver and gastrointestinal tract. In the case of targeting CMV retinitis, while human corneal and retinal epithelium cell lines are the more physiological representations of the ocular tissues, Caco-2 does share a common feature with those cell lines in the expression of peptide transporters. Previous functional studies by Mitra *et al*. have demonstrated the uptake of dipeptides, amino acid ester prodrugs and dipeptide prodrugs from circulation into the vitreous humor, indicating the presence of facilitated transport across the blood-ocular barrier and cornea by oligopeptide transporters [34-36]. Another study by Smith *et al*. also detected the mRNAs of several proton-coupled oligopeptide transporters in bovine and human retinal pigment epithelial (RPE) cell lines as well as retinas [37]. Therefore, in future studies such cell lines could be utilized to specifically characterize the prodrugs' uptake into ocular tissues.

In both uptake and permeability studies, valganciclovir was used as the standard compound for the verification of PEPT1-mediated transport. Indeed, for valganciclovir, its Caco-2 uptake and apparent permeability across the Caco-2 monolayer were both much higher than those of ganciclovir (Fig. 4.1 and 4.2), indicating PEPT1 was likely expressed and functional at the times of experiments. The total cellular uptake for AcPheAlaGCV and AcPheAbuGCV were both found to be significantly lower than that of valganciclovir (Fig.

4.1a). This phenomenon was likely due to the lower affinity of AcPheAlaGCV and AcPheAbuGCV to PEPT1. The N-acetyl group in the two dipeptide prodrugs could have contributed to this decreased affinity because a free N-terminal amino group has been shown to be important for the substrate's affinity to PEPT1 [1, 15]. Indeed, studies have demonstrated that once the N-terminal acetyl group was removed from a peptide derivative, the compound exhibited a 10- to 100-fold increase in permeability across the Caco-2 monolayer; however, it would be significantly less stable as well [38]. Since in our study the intact promoieties were critical for the prodrugs' targeting capabilities, the stability of the prodrugs was thus placed at a higher priority and the acetyl group, despite its probable negative impact on the compounds' permeability, was retained rather than removed in the prodrug design.

The oral delivery of tissue-targeting prodrugs is, without doubt, an ambitious goal. In order for an intact prodrug to have a similar oral bioavailability to that of the parent compound, a sufficient amount of the prodrug needs to survive metabolism in the gastrointestinal lumen, followed by degradation in the gut wall and then in the liver. The Caco-2 permeability study (Fig. 4.2) represented the step of translocation of prodrugs across the GI epithelia. In the LC-MS experiments, I did not observe peaks of ganciclovir in the chromatograms of basolateral chamber samples from AcPheAlaGCV and AcPheAbuGCV dosing. These data did not suggest that no ganciclovir was generated; rather, it was likely because sample concentrations of ganciclovir in the receiving compartment were below the lower limit of quantitation (LLOQ) for ganciclovir in LC-MS detection, which was actually much higher than the LLOQs of AcPheAlaGCV and AcPheAbuGCV. Nevertheless, the similar apparent permeability coefficients (P_{app}) of ganciclovir, AcPheAlaGCV and AcPheAbuGCV, the latter two in their unchanged forms, demonstrated that the two prodrug compounds could potentially have oral bioavailability values similar to ganciclovir, if metabolism in the gut lumen or liver were not considered. However, as shown in Chapter III, the two prodrugs could indeed be hydrolyzed by enzymes expressed in the liver microsomes, and they are also unlikely to be stable against the myriad digestive enzymes secreted within the GI tract. Therefore, I predict that the oral route would not be optimal for the two current

prodrug candidates. Further optimizations in medicinal chemistry and formulation strategies should be exploited to enhance the stability of tissue-targeting prodrugs for oral delivery.

CONCLUSIONS

Two potential prodrug candidates for targeted activation by human cytomegalovirus (hCMV) protease, *N*-acetyl-(L)-phenylalanine-(L)-alanine-ganciclovir (AcPheAlaGCV) and *N*-acetyl-(L)-phenylalanine-(α,L)-aminobutyric acid-ganciclovir (AcPheAbuGCV), displayed different biopharmaceutical properties when compared to ganciclovir and valganciclovir. Specifically, AcPheAbuGCV was potentially superior to AcPheAlaGCV in cellular uptake properties. The Caco-2 uptake of AcPheAbuGCV was significantly higher than ganciclovir and AcPheAlaGCV but less than valganciclovir. Moreover, sufficient amounts of AcPheAbuGCV remained intact and available for potential hydrolytic activations by the hCMV protease, an advantage not observed for AcPheAlaGCV.

In Caco-2 permeability studies, values of the apical-to-basolateral permeability for AcPheAlaGCV and AcPheAbuGCV in their unchanged forms were similar to that of ganciclovir and significantly less than that of valganciclovir. Considering probable metabolism of the prodrugs in the gastrointestinal tract lumen as well as degradations inside the liver, the oral route is thus suboptimal for the delivery of the two prodrugs for the purpose of targeted activation after the absorption processes. In *in vivo* studies, the intravenous route seems to be a better option for maximizing the bioavailability of the ganciclovir prodrugs for hydrolytic activations by the hCMV protease expressed at the infected tissues.

FIGURES

(a) **Total Uptake of Compounds**

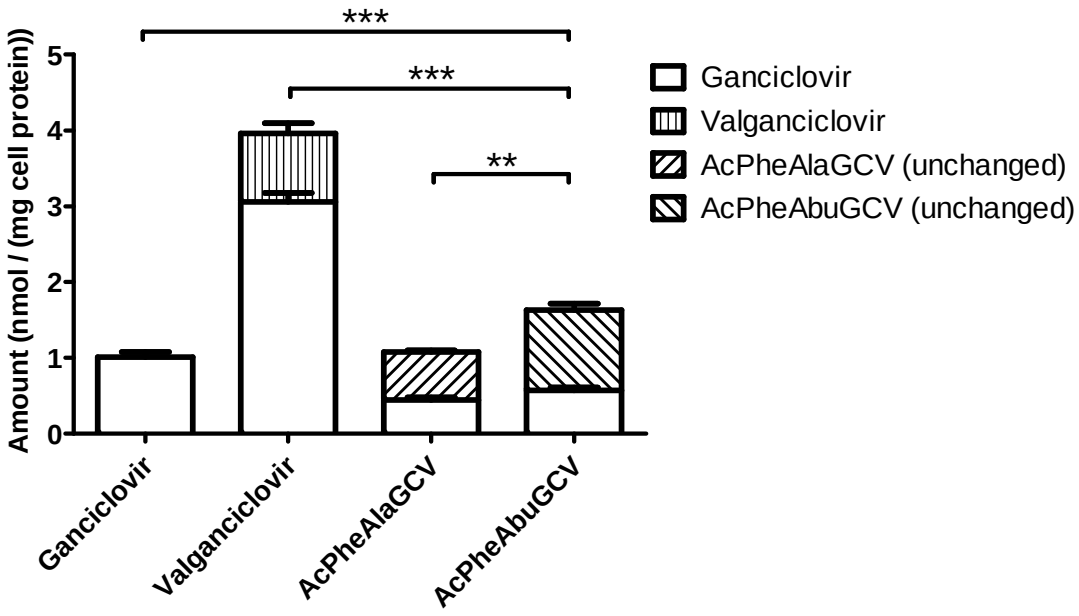

(b) **Uptake of Prodrugs (Unchanged)**

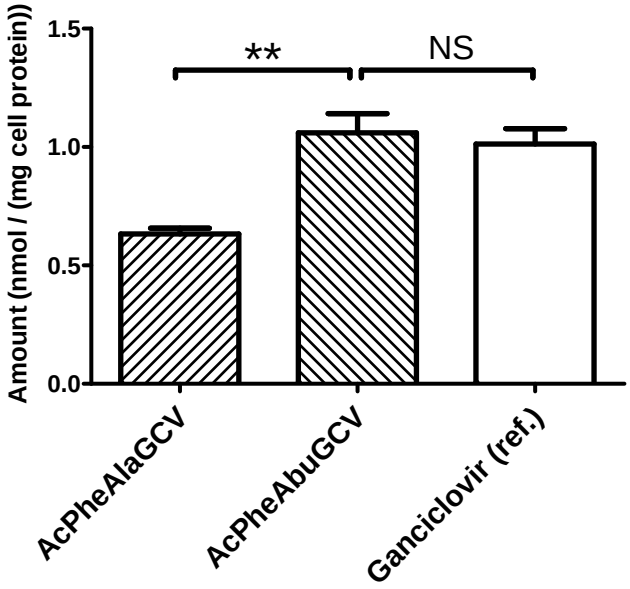

(c)

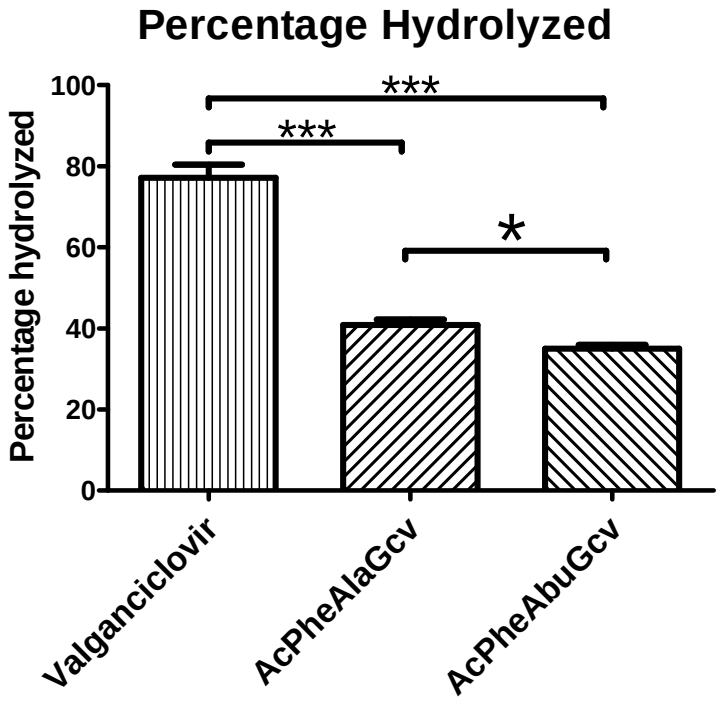

Figure 4.1. Direct uptake of ganciclovir and prodrugs of ganciclovir by Caco-2 cells measured at 60 min. **(a)** Amounts of total uptake as measured by nmol compounds per mg of cellular proteins. For each compound dosed, the amount of its unchanged form and amount of ganciclovir converted from the prodrug were separated in the same column. **(b)** The amounts of unchanged acetylated dipeptide prodrugs in Caco-2 cells at 60 min, with the amount of ganciclovir as a reference. **(c)** The percentages of prodrugs that have been hydrolyzed at 60 min. In all graphs, n = 5 for ganciclovir, 3 for valganciclovir, 6 for AcPheAlaGCV and AcPheAbuGCV. Error bars denote SEM. NS, not significant; *, $p < 0.05$; **, $p < 0.01$; ***, $p < 0.001$.

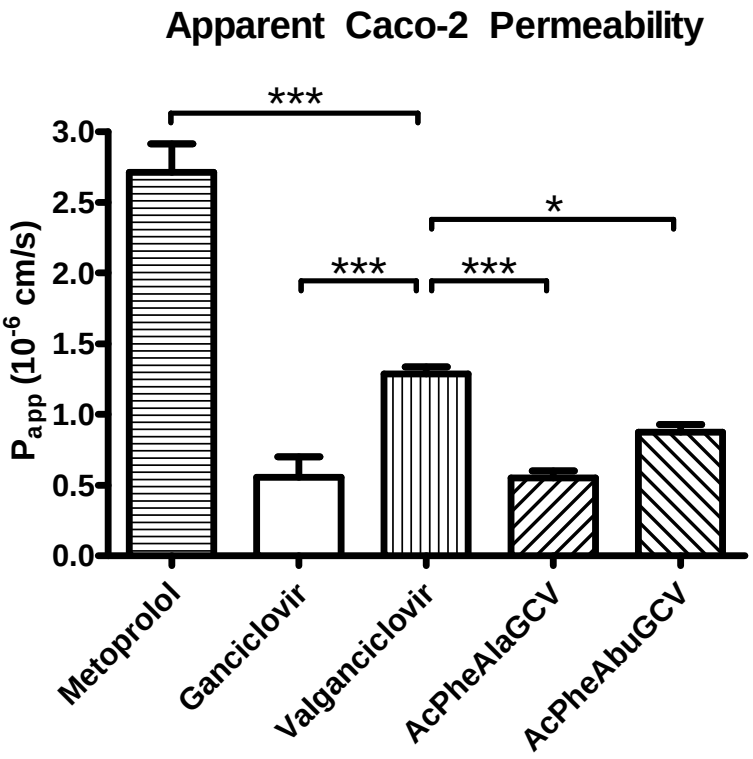

Figure 4.2. Apparent apical-to-basolateral (A to B) permeability coefficients (P_{app}) of compounds across the Caco-2 cell monolayer. The P_{app}'s were calculated according to Equation 4.1 and presented in 10^{-6} cm/s. For wells dosed with valganciclovir, the concentration in the receiving chamber (C_R) at each time point was the sum of that of valganciclovir and the ganciclovir generated from hydrolysis of valganciclovir; for AcPheAlaGCV and AcPheAbuGCV, only the concentrations of (unchanged) prodrugs themselves were used for calculations of dC_R / dt. n = 4 for all compounds except AcPheAbuGCV, for which n = 3. Error bars represent SEM. *, $p < 0.05$; **, $p < 0.01$; ***, $p < 0.001$.

REFERENCES

1. Brandsch, M., I. Knutter, and E. Bosse-Doenecke, *Pharmaceutical and pharmacological importance of peptide transporters.* J Pharm Pharmacol, 2008. **60**(5): p. 543-85.
2. Fei, Y.J., et al., *cDNA structure, genomic organization, and promoter analysis of the mouse intestinal peptide transporter PEPT1.* Biochim Biophys Acta, 2000. **1492**(1): p. 145-54.
3. *Solute carrier family 15 member 1 [Homo sapiens], NCBI Reference Sequence: NP_005064.1.* [cited 2013 Feb. 28]; Available from: http://www.ncbi.nlm.nih.gov/protein/NP_005064.1.
4. Adibi, S.A., *The oligopeptide transporter (Pept-1) in human intestine: biology and function.* Gastroenterology, 1997. **113**(1): p. 332-40.
5. Agu, R., et al., *Proton-coupled oligopeptide transporter (POT) family expression in human nasal epithelium and their drug transport potential.* Mol Pharm, 2011. **8**(3): p. 664-72.
6. Nugent, S.G., et al., *Intestinal luminal pH in inflammatory bowel disease: possible determinants and implications for therapy with aminosalicylates and other drugs.* Gut, 2001. **48**(4): p. 571-7.
7. Terada, T., et al., *Functional characteristics of basolateral peptide transporter in the human intestinal cell line Caco-2.* Am J Physiol, 1999. **276**(6 Pt 1): p. G1435-41.
8. Ganapathy, M.E., et al., *Differential recognition of beta -lactam antibiotics by intestinal and renal peptide transporters, PEPT 1 and PEPT 2.* J Biol Chem, 1995. **270**(43): p. 25672-7.
9. Tomita, Y., et al., *Transport mechanisms of bestatin in rabbit intestinal brush-border membranes: role of H+/dipeptide cotransport system.* J Pharmacol Exp Ther, 1990. **252**(2): p. 859-62.
10. Ganapathy, M.E., et al., *Valacyclovir: a substrate for the intestinal and renal peptide transporters PEPT1 and PEPT2.* Biochem Biophys Res Commun, 1998. **246**(2): p. 470-5.
11. Han, H.K., D.M. Oh, and G.L. Amidon, *Cellular uptake mechanism of amino acid ester prodrugs in Caco-2/hPEPT1 cells overexpressing a human peptide transporter.* Pharm Res, 1998. **15**(9): p. 1382-6.
12. Sugawara, M., et al., *Transport of valganciclovir, a ganciclovir prodrug, via peptide transporters PEPT1 and PEPT2.* J Pharm Sci, 2000. **89**(6): p. 781-9.
13. Enjoh, M., et al., *Inhibitory effect of arphamenine A on intestinal dipeptide transport.* Biosci Biotechnol Biochem, 1996. **60**(11): p. 1893-5.
14. Doring, F., et al., *Minimal molecular determinants of substrates for recognition by the intestinal peptide transporter.* J Biol Chem, 1998. **273**(36): p. 23211-8.
15. Brandsch, M., *Transport of drugs by proton-coupled peptide transporters: pearls and pitfalls.* Expert Opin Drug Metab Toxicol, 2009. **5**(8): p. 887-905.
16. Rubio-Aliaga, I. and H. Daniel, *Peptide transporters and their roles in physiological processes and drug disposition.* Xenobiotica, 2008. **38**(7-8): p. 1022-42.
17. Bailey, P.D., et al., *Affinity prediction for substrates of the peptide transporter PepT1.* Chem Commun (Camb), 2006(3): p. 323-5.

18. *Valcyte (R) labels at Drugs@FDA.* [cited 2013 Feb. 22]; Available from: http://www.accessdata.fda.gov/drugsatfda_docs/label/2010/021304s008,022257s003lbl.pdf.
19. *Cytovene (R) labels at Drugs@FDA.* [cited 2013 Jan. 29]; Available from: http://www.accessdata.fda.gov/drugsatfda_docs/label/2006/019661s030lbl.pdf.
20. Kim, I., et al., *Identification of a human valacyclovirase: biphenyl hydrolase-like protein as valacyclovir hydrolase.* J Biol Chem, 2003. **278**(28): p. 25348-56.
21. Lai, L., et al., *Molecular basis of prodrug activation by human valacyclovirase, an alpha-amino acid ester hydrolase.* J Biol Chem, 2008. **283**(14): p. 9318-27.
22. Perrottet, N., et al., *Valganciclovir in adult solid organ transplant recipients: pharmacokinetic and pharmacodynamic characteristics and clinical interpretation of plasma concentration measurements.* Clin Pharmacokinet, 2009. **48**(6): p. 399-418.
23. *Caco-2 (HTB-37) at ATCC.org.*; Available from: http://www.atcc.org/Products/All/HTB-37.aspx.
24. Meunier, V., et al., *The human intestinal epithelial cell line Caco-2; pharmacological and pharmacokinetic applications.* Cell Biol Toxicol, 1995. **11**(3-4): p. 187-94.
25. Hidalgo, I.J., T.J. Raub, and R.T. Borchardt, *Characterization of the human colon carcinoma cell line (Caco-2) as a model system for intestinal epithelial permeability.* Gastroenterology, 1989. **96**(3): p. 736-49.
26. Hubatsch, I., E.G. Ragnarsson, and P. Artursson, *Determination of drug permeability and prediction of drug absorption in Caco-2 monolayers.* Nat Protoc, 2007. **2**(9): p. 2111-9.
27. Dahan, A., H. Lennernas, and G.L. Amidon, *The fraction dose absorbed, in humans, and high jejunal human permeability relationship.* Mol Pharm, 2012. **9**(6): p. 1847-51.
28. Sun, D., et al., *Comparison of human duodenum and Caco-2 gene expression profiles for 12,000 gene sequences tags and correlation with permeability of 26 drugs.* Pharm Res, 2002. **19**(10): p. 1400-16.
29. Englund, G., et al., *Regional levels of drug transporters along the human intestinal tract: co-expression of ABC and SLC transporters and comparison with Caco-2 cells.* Eur J Pharm Sci, 2006. **29**(3-4): p. 269-77.
30. Prueksaritanont, T., et al., *Comparative studies of drug-metabolizing enzymes in dog, monkey, and human small intestines, and in Caco-2 cells.* Drug Metab Dispos, 1996. **24**(6): p. 634-42.
31. Loveland, A.N., et al., *The amino-conserved domain of human cytomegalovirus UL80a proteins is required for key interactions during early stages of capsid formation and virus production.* J Virol, 2007. **81**(2): p. 620-8.
32. Loveland, A.N., et al., *Cleavage of human cytomegalovirus protease pUL80a at internal and cryptic sites is not essential but enhances infectivity.* J Virol, 2005. **79**(20): p. 12961-8.
33. Brignole, E.J. and W. Gibson, *Enzymatic activities of human cytomegalovirus maturational protease assemblin and its precursor (pPR, pUL80a) are comparable: [corrected] maximal activity of pPR requires self-interaction through its scaffolding domain.* J Virol, 2007. **81**(8): p. 4091-103.

34. Dias, C., et al., *Ocular penetration of acyclovir and its peptide prodrugs valacyclovir and val-valacyclovir following systemic administration in rabbits: An evaluation using ocular microdialysis and LC-MS.* Curr Eye Res, 2002. **25**(4): p. 243-52.
35. Atluri, H., et al., *Mechanism of a model dipeptide transport across blood-ocular barriers following systemic administration.* Exp Eye Res, 2004. **78**(4): p. 815-22.
36. Anand, B.S. and A.K. Mitra, *Mechanism of corneal permeation of L-valyl ester of acyclovir: targeting the oligopeptide transporter on the rabbit cornea.* Pharm Res, 2002. **19**(8): p. 1194-202.
37. Ocheltree, S.M., et al., *Preliminary investigation into the expression of proton-coupled oligopeptide transporters in neural retina and retinal pigment epithelium (RPE): lack of functional activity in RPE plasma membranes.* Pharm Res, 2003. **20**(9): p. 1364-72.
38. Ano, R., et al., *Relationship between structure and permeability of dipeptide derivatives containing tryptophan and related compounds across human intestinal epithelial (Caco-2) cells.* Bioorg Med Chem, 2004. **12**(1): p. 249-55.

CHAPTER V

ENHANCED SOLUBILITY AND INTESTINAL PERMEABILITY OF AN AMIDE PRODRUG OF CIPROFLOXACIN

SUMMARY

Ciprofloxacin, a second-generation fluoroquinolone compound, is indicated for the treatment of a wide range of bacterial infections in human. It is classified as a Biopharmaceutics Classification System (BCS) class IV compound according to the fact that it has both low solubility at pH 1 – 7.5 and low intestinal permeability. These unfavorable biopharmaceutical properties of ciprofloxacin partially result from the inherent dissociation constants of the carboxyl group and the secondary amine within the compound, both of which determine the equilibria among the four solute species of the drug. The predominance of the zwitterionic form of ciprofloxacin at pH around its isoelectric point is a major cause for the drug's low solubility and intestinal permeability at neutral pH. A prodrug approach was employed to alter the equilibria among the solute species and to potentially enhance the compound's solubility and intestinal permeability. An amide prodrug, ciprofloxacyl-glycine-methyl ester (Cipro-Gly-OMe), was synthesized and its solubility and *in vitro* Caco-2 permeability were measured along with those of ciprofloxacin. When compared to the parent compound, Cipro-Gly-OMe was found to display potentially much higher solubility throughout the physiological pH range as well as a higher Caco-2 permeability at pH 7.4. However, Cipro-Gly-OMe could not be efficiently converted to ciprofloxacin in Caco-2

homogenates, plasma or liver microsomes. Our study thus presented a unique prodrug approach that could potentially transform a BCS class IV fluoroquinolone compound to a class I compound, although the promoiety of the prodrug does require further optimization to allow for efficient bioconversion to the parent compound.

BACKGROUND

Quinolones: History, Structures and Mechanisms of Action

Quinolones are a family of broad-spectrum antibiotics that share the common bicyclic backbone of 4-quinolone or 4-oxo-1,8-naphthyridine (4-naphthyridone) (**Figure 5.1(a,b)**). It is generally accepted that the first quinolone compound synthesized was nalidixic acid (**Fig. 5.1c**), which was discovered in 1962 as a byproduct of chloroquine synthesis [1]. In 1967, nalidixic acid was approved for treatment of urinary tract infections (UTI) caused by most Gram-negative bacteria, but its use was hampered by its low plasma concentrations, a high minimum inhibitory concentration (MIC), ineffectiveness against Gram-positive bacteria as well as systemic toxicities [2]. It was not until the late 1970s that research and development on quinolones started to flourish. Fluoroquinolones, the 6-fluorinated quinolones with various additional side groups at other positions on the bicyclic ring (Fig. 5.1a; also **Figure 5.2**), generally displayed improved potency against Gram-negative bacteria, efficacy against some Gram-positive species, better pharmacokinetic profiles and decreased toxicities [2]. To date, over 10,000 distinct quinolone compounds have been synthesized and tested and around 30 of them were approved by regulatory agencies around the world for clinical use [3]. These quinolones were generally categorized into four groups, or "generations", according to their spectra of activity [2, 3]. Currently, only II-, III- and IV-generation quinolones are available on the market. The international nonproprietary names (INNs) of fluoroquinolones all end with "-floxacin".

The general structure of fluoroquinolones is shown in **Fig. 5.2**. The hydrogen at position 2, carboxyl group at position 3, oxo at position 4 and fluoro at position 6 of the quinolone ring are all critical for antibacterial activity and are, therefore, generally left untouched during the structural modification for the design of new compounds [3]. Extensive research has been devoted to the functions and optimization of the R_1, R_5, R_7, and, to a lesser extent, the R_8 groups. The rationales for the structure-activity relationships (SAR) of these groups toward the antibiotic activities, pharmacokinetics and toxicities of the compounds are beyond the scope of this chapter; several studies have summarized the putative effects of

variations at those positions and provided general guidelines on the design of new fluoroquinolone compounds [3, 4].

Fluoroquinolones enter the bacterial cells by passive diffusion through their membrane porins [5, 6]. The compounds exert their bactericidal effects by inhibition of type II topoisomerases, which include DNA gyrase and topoisomerase IV, two critical enzymes involved in the bacterial DNA replication. During DNA replication, type II topoisomerases cleave and re-ligate the DNA ahead of the replication fork, thereby relaxing the stress caused by supercoiling of DNA [7]. Binding of fluoroquinolones to bacterial type II topoisomerases inhibit the enzymes' ligase functions and thus cause breaks in the DNA strands, leading to the fragmentation of DNA and cell death [3, 8, 9]. Indeed, mutations in bacterial porins and / or the binding domains for fluoroquinolones within type II topoisomerases have been found to confer clinical resistance to the drugs [6, 9, 10].

Ciprofloxacin: Indications and Dissociation Constants

Originally approved by the US FDA in 1987 [11], ciprofloxacin is a "second generation" fluoroquinolone compound [3]. It has demonstrated potent antibiotic activities against a wide range of Gram-negative bacteria as well as some Gram-positive species [12]. It was approved for clinical use against 13 types of infections caused by the aforementioned bacteria; some examples include urinary tract infections (UTI), lower respiratory tract infections, skin and skin structure infections and gonorrhea [12]. It is currently the most widely prescribed fluoroquinolone [2]. For oral administration, it is available in either tablets as a monohydrochloride salt form (ciprofloxacin·HCl), or oral suspensions which contains the non-salt form and several excipients [12].

Ciprofloxacin (structure shown in **Figure 5.3**) has a cyclopropyl group at the R_1 and a 1'-piperazinyl group at the R_7 positions of the generalized fluoroquinolone structure (Fig. 5.2). The carboxyl group on the quinolone ring and the secondary amine within the piperazinyl are both dissociable, with measured pK_a's at 6.09-6.18 and 8.73-8.76 at 25°C, respectively [13-16]. Therefore, four species of ciprofloxacin simultaneously exist in aqueous solutions at any given pH: the neutral form, the positively charged (i.e. protonated) form, the negatively charged (deprotonated) form and the zwitterionic form. Their equilibria in solution are shown

in **Figure 5.4**. The contents of the four species within a solution are controlled by the intrinsic micro-dissociation constants (k_{a1}, k_{a21}, k_{a12} and k_{a2}) and the solution pH. For the sake of simplicity, it is assumed that that $k_{a1} = k_{a12} = K_{a1}$, and $k_{a21} = k_{a2} = K_{a2}$, where K_{a1} and K_{a2} are the respective macro-dissociation constants for the carboxyl and secondary amine groups. The theoretical relationship between the percentages of each of the four species and the solution pH could thus be calculated using the Henderson-Hasselbalch equation (**Equation. 5.1**), where HA is the neutral form of an acid and A^- is the deprotonated ion (or "base"):

$$\log_{10}\left(\frac{[A^-]}{[HA]}\right) = pH - pK_a \qquad \text{(Equation. 5.1)}$$

The equilibria between the three ionic species of ciprofloxacin and the neutral form are shown in **Equations 5.2 – 5.4**:

Negatively charged (deprotonated) form:

$$\frac{[\text{Negative}]}{[\text{Neutral}]} = 10^{pH-pK_{a1}} \qquad \text{(Equation. 5.2)}$$

Positively charged (protonated) form:

$$\frac{[\text{Positive}]}{[\text{Neutral}]} = 10^{pK_{a2}-pH} \qquad \text{(Equation. 5.3)}$$

Zwitterionic form:

$$\frac{[\text{Zwitterion}]}{[\text{Neutral}]} = 10^{pK_{a2}-pK_{a1}} \qquad \text{(Equation. 5.4)}$$

Therefore, fractions of the four species of ciprofloxacin could be derived as **Equations 5.5 – 5.8**:

Neutral form:

$$\%(\text{Neutral}) = \frac{1}{1 + 10^{pH-pK_{a1}} + 10^{pK_{a2}-pH} + 10^{pK_{a2}-pK_{a1}}} \qquad \text{(Equation. 5.5)}$$

Negatively charged (deprotonated) form:

$$\%(\text{Negative}) = \frac{10^{pH-pK_{a1}}}{1 + 10^{pH-pK_{a1}} + 10^{pK_{a2}-pH} + 10^{pK_{a2}-pK_{a1}}} \quad \text{(Equation. 5.6)}$$

Positively charged (protonated) form:

$$\%(\text{Positive}) = \frac{10^{pK_{a2}-pH}}{1 + 10^{pH-pK_{a1}} + 10^{pK_{a2}-pH} + 10^{pK_{a2}-pK_{a1}}} \quad \text{(Equation. 5.7)}$$

Zwitterion:

$$\%(\text{Zwitterion}) = \frac{10^{pK_{a2}-pK_{a1}}}{1 + 10^{pH-pK_{a1}} + 10^{pK_{a2}-pH} + 10^{pK_{a2}-pK_{a1}}} \quad \text{(Equation. 5.8)}$$

And the isoelectric point, p*I*, is the midpoint of pK_{a1} and pK_{a2}:

$$pI = \frac{1}{2}(pK_{a1} + pK_{a2}) \quad \text{(Equation. 5.9)}$$

Figure 5.5(a,b) details the relationship between the fractions of the four species of ciprofloxacin and the pH of the solution. Particularly, at pH around the isoelectric point (around 7.5 at 25°C), the zwitterion is the predominant form. The fraction of the neutral form is very small (< 0.25% at isoelectric point).

Ciprofloxacin: A Low-Solubility Compound

Ciprofloxacin exhibits a "U"-shaped solubility vs. pH profile [15, 17]. It has relatively high solubility at both low (< 4) and high pH (> 10) but very poor solubility at pH around its isoelectric point, which also corresponds to the physiological pH range (6 – 8). Previous reports placed the solubility of ciprofloxacin·HCl at pH 6.8 – 7.5, 25°C at 0.070 to 0.088 mg/mL [18]. For oral dosage, the volumes of aqueous media required to solubilize a typical ciprofloxacin·HCl tablet (250 – 750 mg) at pH 5 – 7.5 are much larger than 250 mL [18], the volume recommended by an FDA guideline for classification of compound solubility [19]. Therefore, ciprofloxacin (along with its HCl salt) is considered a low-solubility compound.

The low solubility of ciprofloxacin at pH around its isoelectric point could also be explained by its ionization profiles. Generally speaking, in a saturated solution, the concentration of the uncharged, neutral form is constant. According to Eq. 5.4, the concentration of the zwitterion is also a constant and is often referred to as "intrinsic solubility" (S_0). Therefore, the solubility of ciprofloxacin (S), explained as the sum of the concentrations of the zwitterionic, the negatively charged and the positively charged forms, varies with the solution pH and follows the theoretical **Equations 5.10 and 5.11** [15].

$$S = S(\text{zwitterion}) + S(\text{negative}) + S(\text{positive}) \quad \text{(Equation. 5.10)}$$

$$S = S_0 \cdot (1 + 10^{pH - pK_{a2}} + 10^{pK_{a1} - pH}) \quad \text{(Equation. 5.11)}$$

The pH-dependent solubility of ciprofloxacin is shown in **Figure 5.6**. It is evident that at the intestinal luminal pH (6 – 8), the solubility of ciprofloxacin is very low, at only 1.2 to 2.5 times the intrinsic solubility; the lowest point of solubility theoretically occurs at the isoelectric point of ~7.5. The problem of the drug's low solubility is further complicated by quinolones having an unpleasant, extremely bitter taste; techniques such as film coating are frequently employed for tablet manufacturing [20]. The coating prevents the drug product from effectively dissolving in the relatively acidic gastric fluid (pH 1.5 – 3.5) and the majority of ciprofloxacin is left undissolved until it reaches the small intestine, where the luminal pH becomes unfavorable for its solubilization.

Ciprofloxacin: A Low-Permeability Compound

In human studies, the absolute oral bioavailability of ciprofloxacin was reported to be approximately 70%, with no significant loss from first-pass metabolism [12]. Therefore, orally dosed ciprofloxacin has a fraction of dose absorbed (F_a) of approximately 70%. This number is lower than the FDA-designated 90% boundary separating the high- and low-permeability compounds [19] and, therefore, ciprofloxacin has been classified as a low-permeability drug [18]. This was also confirmed in *in vitro* Caco-2 assays in which

ciprofloxacin was found to have a much lower apical-to-basolateral apparent permeability (P_{app}) at pH 6.8 compared to that of the high-permeability standard metoprolol [21].

Ciprofloxacin is absorbed in the gastrointestinal tract primarily through passive diffusion [22, 23]. It displays an inverted "U"-shape pH-dependent permeability profile with the highest *in vitro* apparent permeability occurring at pH around the isoelectric point of 7.5 [24]. This corresponds very well to its pH-distribution coefficient (log*D*) profile, which also peaks at a pH of ~7.5 [14]. These phenomena could be explained by the relationship between the pH and the fraction of the neutral form of ciprofloxacin (Fig. 5.5b). It is generally accepted that only the neutral, un-ionized form of an ionizable compound can enter the lipophilic environment of biological membranes or *n*-octanol [24]. For ciprofloxacin, the fraction of the neutral form is at its highest at the isoelectric point, hence the peak of its log*D* as well as membrane permeability. Nevertheless, with a theoretical value of 0.23%, the fraction of the neutral form at pH 7.5 is still relatively small, resulting in low absolute values of log*D* and passive diffusivity.

Ciprofloxacin is also a possible substrate for efflux transporters. The efflux ratio, defined as the ratio of the basolateral-to-apical permeability coefficient over that of the apical-to-basolateral direction, was found to be 4.6 for ciprofloxacin in the Caco-2 system [21]. Studies with Caco-2 and rats as model systems indicated that ciprofloxacin is not actively transported by P-glycoprotein (P-gp, also known as MDR1 or ABCB1) or multidrug resistance-associated protein 2 (MRP2 / ABCC2) [25, 26]. Later reports using cells and animal models showed that the breast cancer resistance protein (BCRP, also known as ABCG2) is likely the predominant efflux transporter for ciprofloxacin in the small intestine [27, 28]. Clearly, the efflux mechanism of ciprofloxacin is another contributing factor to its low intestinal permeability.

Pharmacokinetics of Ciprofloxacin

Oral dosages of ciprofloxacin at 250, 500 and 750 mg yield average maximum plasma concentrations (c_{max}) of 1.2, 2.4 and 4.3 µg/mL, respectively [12]. The plasma protein binding level for ciprofloxacin is 20% – 40% and is considered unlikely to cause interference of

protein binding for other drugs [12]. The drug is widely distributed throughout the body and the tissue concentrations are often higher than its plasma concentration.

A total of approximately 15% of ciprofloxacin absorbed after an oral dose is metabolized by phase I and phase II metabolic enzymes to four metabolites: desethyleneciprofloxacin (M1), sulfo-ciprofloxacin (M2), oxociprofloxacin (M3) and formylciprofloxacin (M4) (structures shown in **Figure 5.7**) [12, 29]. They all possess varying degrees of antibiotic activity, albeit all weaker than ciprofloxacin. The half-life of the drug is approximately 4 hours [12]. The majority of the dose after oral administration (55% to 65%) is excreted in the urine whereas 20% to 35% of the dose could be recovered in the feces several days after dosing, indicating biliary secretions for the drug [12].

Amide Prodrugs of Ciprofloxacin: Possible Enhancement of Both Solubility and Intestinal Permeability

Due to the low solubility *and* low permeability of ciprofloxacin, the drug is classified as a BCS class IV compound. Its oral absorption rate is thus limited by both the dissolution of the drug product and its permeability across the gastrointestinal epithelia. As detailed in the above sections, the low solubility and permeability are both related to the equilibria among the four species of ciprofloxacin in aqueous solutions. Therefore, if one or both of the ionizable groups could be masked by a promoiety (or promoieties), the equilibria will be greatly altered and result in potential changes to the compound's biopharmaceutical properties.

During the design process of the prodrug, a "double prodrug" with promoieties attached at both the secondary amine and carboxyl groups was not considered because of the complication concerning the two-step activation required to convert the prodrug back to ciprofloxacin. The option of an amide with acylation at the secondary amine was also eliminated because the prodrug would still be poorly soluble at low pH. Eventually, I decided to design a promoiety that masks the carboxyl group of ciprofloxacin. A ciprofloxacyl amide was chosen because the existence of a peptide bond could potentially make the prodrug a substrate for PEPT1-mediated transport. The methyl ester of glycine (Gly-OMe) was selected as the amide promoiety because glycine is the simplest amino acid and thus was a good starting point for the initial testing for this prodrug strategy. The prototypical prodrug,

ciprofloxacyl-glycine-methyl ester (Cipro-Gly-OMe, **Figure 5.8a**), could potentially possess both increased solubility as well as permeability over the physiological pH range.

First, for solubility it is generally accepted that the species with no net charge, i.e. the neutral form and zwitterion, are the least soluble [15]; their concentrations are often called the intrinsic solubility (S_0). Therefore, reducing the percentage of these species in the saturated solution will lead to increased total solubility of a compound because of an increase in the fractions of the species with net charges. The pH-dependent fractions of species with net charges follow **Equations 5.12 and 5.13**.

For ciprofloxacin, total fractions of positively and negatively charged species:

$$\%(\text{Species with Net Charges}) = \frac{10^{pH-pK_{a1}} + 10^{pK_{a2}-pH}}{1 + 10^{pH-pK_{a1}} + 10^{pK_{a2}-pH} + 10^{pK_{a2}-pK_{a1}}} \quad \text{(Equation. 5.12)}$$

For Cipro-Gly-OMe, the only charged species is the protonated form:

$$\%(\text{Species with Net Charges}) = \frac{10^{pK_{a2}-pH}}{1 + 10^{pK_{a2}-pH}} \quad \text{(Equation. 5.13)}$$

In **Figure 5.9a**, the theoretical fractions of the species with net charges are plotted against the pH. It is evident that Cipro-Gly-OMe could hypothetically possess higher fractions of species with net charges than ciprofloxacin throughout the physiological pH range. The total solubility of the two compounds, expressed in multiples of their intrinsic solubility (S_0), is predicted in **Fig. 5.9b** with respect to the varying pH. The solubility of ciprofloxacin follows Eq. 5.11 and Cipro-Gly-OMe's follow Equation. 5.14, where S_0 is the solubility of the neutral form:

$$S(\text{Cipro-Gly-OMe}) = S_0 \cdot (1 + 10^{pK_{a2}-pH}) \quad \text{(Equation. 5.14)}$$

The total solubility of Cipro-Gly-OMe within the physiological pH range is therefore potentially much higher than that of ciprofloxacin, assuming the two compounds have similar intrinsic solubility (S_0).

In addition to solubility, the prodrug Cipro-Gly-OMe may also have an enhanced intestinal permeability compared to ciprofloxacin because of the former's higher fractions of the un-ionized neutral form at the physiological pH range. The pH-dependent fractions of neutral form of ciprofloxacin follow Eq. 5.5 and that of Cipro-Gly-OMe **Equation. 5.15**:

For Cipro-Gly-OMe,

$$\%(\text{Neutral}) = \frac{1}{1 + 10^{pK_{a2} - pH}} \qquad \text{(Equation. 5.15)}$$

The theoretical relationship between the pH and fractions of neutral forms of compounds is depicted in **Figure 5.10**. At pH 6 – 8, Cipro-Gly-OMe has much higher fractions of neutral forms in solutions than ciprofloxacin does. Assuming that the two compounds' neutral forms have similar membrane permeability values, the one with a higher percentage of neutral form in solution at a given pH would thus be more permeable.

In this chapter, I synthesized the prodrug ciprofloxacyl-glycine-methyl ester (Cipro-Gly-OMe) as well as ciprofloxacyl-glycine (Cipro-Gly; structure shown in **Fig. 5.8b**), the latter a likely metabolite for Cipro-Gly-OMe. The pH-dependent solubility of ciprofloxacin was then measured and compared with that of Cipro-Gly-OMe. I also compared the apparent permeability of ciprofloxacin and Cipro-Gly-OMe across the Caco-2 monolayers at apical pH of 6.0 and 7.4. Lastly, I characterized the bioconversion of Cipro-Gly-OMe in tissue matrices, because the carboxyl group masked by the promoiety must be "freed" in order for the parent drug to exert antibacterial activities [3].

MATERIALS AND METHODS

Materials

All the reagents, cell lines, tissue matrices and dispensable tissue culture hardware that have been mentioned in Chapters II, III and IV were acquired from the same sources. In addition, ciprofloxacin and ciprofloxacin hydrochloride were purchased from AK Scientific (Palo Alto, CA). Glycine methyl ester hydrochloride (Gly-OMe·HCl) was purchased from Chem-Impex (Wood Dale, IL). Di-*tert*-butyl dicarbonate, *N*,*N*-diisopropylethylamine (DIPEA) and 1-[bis(dimethylamino)methylene]-1*H*-1,2,3-triazolo[4,5-*b*]pyridinium 3-oxid hexafluorophosphate (HATU) and all organic solvents were purchased from Sigma-Aldrich (St. Louis, MO). Citric acid, tricine, 4-(2-hydroxyethyl)-1-piperazineethanesulfonic acid (HEPES), 3-morpholinopropane-1-sulfonic acid (MOPS), 1,4-piperazinediethanesulfonic acid (PIPES) and 3-[[1,3-dihydroxy-2-(hydroxymethyl)propan-2-yl]amino]propane-1-sulfonic acid (TAPS) were purchased from Fisher Scientific (Pittsburgh, PA). Costar UV-transparent 96-well plates were purchased from Corning (Corning, NY).

Cell Culture

Caco-2 cells (passage 22 – 36) were routinely maintained in the same conditions detailed in Chapter III. For permeability studies, Caco-2 cells were seeded and processed using the same procedures as described in Chapter IV.

Chemical Synthesis

The strategy for the synthesis of the prodrugs is shown in **Figure 5.11**. ^{1}H-NMR and ESI MS were performed on the same equipment with the same respective solvents as detailed in Chapter III.

***Tert*-butyloxycarbonyl-ciprofloxacin (Boc-Cipro)**. 504 mg (1 molar equivalent) ciprofloxacin was dissolved in 12 mL tetrahydrofuran (THF) mixed with 6 mL 1 M NaOH in water. 450 µL (1.3 molar eq.) di-*tert*-butyl dicarbonate was diluted in 6 mL THF and added dropwise to the stirring ciprofloxacin / THF / NaOH mixture on ice. The reaction was kept on ice for 12 h. Dichloromethane (DCM) was added into the mixture and solvents were removed

in vacuo. The pellet, yellow in color, was washed with methanol for three times and each time the solvent was removed *in vacuo*. The precipitation was then re-dissolved in DCM. The reaction product was separated from others using silica gel chromatography with a mobile phase of 95% DCM, 5% methanol and 1‰ acetic acid. Fractions of the eluate containing the product were pooled and the solvent was removed *in vacuo*. Three washes with DCM were applied and solvent was removed *in vacuo*. ~600 mg powder form of the product was yielded. ESI-MS: $[M+H]^+$ 432.2.

***Tert*-butyloxycarbonyl-ciprofloxacyl-glycine-methyl ester (Boc-Cipro-Gly-OMe).** 300 mg Boc-Cipro (1 molar eq.), 430 mg glycine-methyl ester hydrochloride (5 eq.) and 3 mL DIPEA was dissolved in 25 mL DMF mixed with 10 mL DCM. 550 mg HATU (2 eq.) was then added to the stirring mixture and the reaction was carried out at room temperature for 2 h. Solvents were removed *in vacuo* and the pellet was dissolved in ethyl acetate and washed with 1‰ (v/v) HCl. The organic phase was then concentrated under vacuum and loaded onto a silica gel column. The product was eluted by 4% (v/v) methanol in ethyl acetate and solvents were removed *in vacuo*. ~150 mg powder of the product was obtained. ESI-MS: $[M+H]^+$ 503.2.

Ciprofloxacyl-glycine-methyl ester (Cipro-Gly-OMe). 56 mg Boc-Cipro-Gly-OMe was dissolved in a mixture of 5 mL 3 M HCl, 5 mL water and 5 mL ethanol and the mixture was stirred at room temperature for 15 min. Solvents were then removed *in vacuo*. The pellet was dissolved in 10 mL 1:1 (v/v) methanol: water and injected into preparatory HPLC with the same accessories as those used in Chapter III. Water (1‰ TFA) and acetonitrile (1‰ TFA) were used as mobile phases A and B, respectively. Percentage of phase B vs. time program: 0 min, 0.2%; 5 min, 20%; 35 min, 45%; 40 min, 85%. The chromatogram is monitored at UV 275 nm and all peak fractions with absorption greater than 500 mAU were collected. The compounds in all fractions were identified by ESI-MS. Solvents were first removed *in vacuo* and the residual water was removed by freeze-drying. ^{1}H-NMR (400 MHz, methanol-D_4): 1.21 (2H, s, cyclopropyl 2'-CH_2 and 3'-CH_2), 1.40 (2H, m, cyclopropyl 2'-CH_2 and 3'-CH_2), 3.50 (4H, d, piperazinyl 3'-CH_2 and 5'-CH_2, J = 8 Hz), 3.60 (4H, d, piperazinyl 2'-CH_2 and 6'-CH_2, J = 4 Hz), 3.70 (1H, s, cyclopropyl 1'-CH), 3.79 (3H, s, $COOCH_3$), 4.24 (2H, s, Gly

CH_2), 7.62 (1H, d, quinolone 8-CH, J = 8 Hz), 7.95 (1H, m, quinolone 5-CH), 8.80 (1H, s, quinolone 2-CH). ESI-MS: $[M+H]^+$ 403.1. Purity by HPLC: 97%.

Ciprofloxacyl-glycine (Cipro-Gly). 30 mg Cipro-Gly-OMe was dissolved in 2:1 (v:v) mixed methanol and water and 16 mg (10 eq.) LiOH was added to the stirring mixture. The reaction was stirred at room temperature for 4 h and terminated by addition of 1% HCl. The mixture was washed sequentially with DCM, hexane and ethyl acetate. The solvents were removed *in vacuo* and the pellet was dissolved in 10 mL 1:1 (v/v) methanol: water and injected into preparatory HPLC using the same method as Cipro-Gly-OMe. All peak fractions with absorption greater than 500 mAU were collected and compounds in all fractions were identified by ESI-MS. Solvents of the fraction containing the product were first removed *in vacuo* and the residual water was then removed by freeze-drying. ^{1}H-NMR (400 MHz, methanol-D_4): 1.17 (2H, s, cyclopropyl 2'-CH_2 and 3'-CH_2), 1.36 (2H, m, cyclopropyl 2'-CH_2 and 3'-CH_2), 3.46 (4H, d, piperazinyl 3'-CH_2 and 5'-CH_2, J = 8 Hz), 3.56 (4H, d, piperazinyl 2'-CH_2 and 6'-CH_2, J = 4 Hz), 3.69 (1H, s, cyclopropyl 1'-CH), 4.17 (2H, s, Gly CH_2), 7.59 (1H, d, quinolone 8-CH, J = 8 Hz), 7.93 (1H, d, quinolone 5-CH, J = 16 Hz), 8.78 (1H, s, quinolone 2-CH). ESI-MS: $[M+H]^+$ 389.1. Purity by HPLC: 99%.

Buffer Solutions

Table 5.1 lists the buffering agents and their concentrations used to make buffer solutions at different pHs.

The pH-Dependent Solubility in Buffers

Ciprofloxacin·HCl was weighed and added to the buffer solutions in Table 5.1 at concentrations above saturation at room temperature (25°C). For Cipro-Gly-OMe·TFA, it was added to 0.5 M TAPS (pH 8.78 at 25°C) for the measurement of its intrinsic solubility ($S_0 = S / 2$ at pK_{a2} = 8.75). The solutions were shaken at 60 rpm at room temperature (25°C) for 4 – 6 hours and the supernatants were filtered through 0.45 µm PVDF filter plates by centrifugation. The filtrates were assayed for concentrations by UV absorption analysis. The pH of saturated solutions of ciprofloxacin·HCl were measured and used as the real pH values in the analysis of pH-dependent solubility. Eq. 5.11 and S_0 = 0.0792 mg/mL [15] were used for the

prediction of pH-dependent solubility of ciprofloxacin; Eq. 5.14 for the prediction of that of Cipro-Gly-OMe.

Stability of Prodrugs in Buffer

1 – 1.2 mg Cipro-Gly-OMe·TFA powder was weighed and dissolved in PBS (pH 7.4; see Table 5.1) to 1 mg/mL solutions. The solutions were shaken at 60 rpm at room temperature (25°C) for 8 days. They were then diluted with water by 100× and assayed with HPLC as well as LC-MS.

Permeability across Caco-2 Monolayers

Experiments were carried out with apical chamber having a pH of either 6.0 or 7.4 and basolateral chamber at pH 7.4 After washing the post-confluent Caco-2 cell layer with the respective buffer solutions, 1.5 mL 0.5 mM ciprofloxacin, 0.5 mM Cipro-Gly-OMe or 1 mM metoprolol solutions in either 37°C pH 6.0 uptake buffer (145 mM NaCl, 0.5 mM $MgCl_2$, 1 mM NaH_2PO_4, 1 mM $CaCl_2$, 3 mM KCl, 5 mM (D)-glucose, 5 mM MES) or 37°C pH 7.4 uptake buffer (145 mM NaCl, 0.5 mM $MgCl_2$, 1 mM NaH_2PO_4, 1 mM $CaCl_2$, 3 mM KCl, 5 mM (D)-glucose, 5 mM HEPES) were then overlaid to the respective apical chambers and 2.5 mL pH 7.4 uptake buffer to basolateral chambers. The Caco-2 cells were incubated at 37°C on an orbital shaker rotating at a speed of 50 rpm. Samples were retrieved from the basolateral chamber every 15 min until 120 or 135 min after dosing and equal volumes of fresh pH 7.4 uptake buffer was replenished to maintain sink condition. Samples collected from ciprofloxacin and Cipro-Gly-OMe dosing were quenched with acetonitrile with 250 nM (S)-(-)-propranolol (internal standard for LC-MS analysis). Samples for metoprolol permeability were mixed with acetonitrile with 200 µM caffeine (internal standard for HPLC). All samples were kept on ice throughout the 120- or 135-min period and then frozen at -80°C until analyzed by LC-MS (for ciprofloxacin and Cipro-Gly-OMe) or HPLC (for metoprolol).

Bioconversion of Prodrug in Biological Matrices

For prodrug bioconversion in Caco-2 homogenates, a final concentration of 10 µM Cipro-Gly-OMe was added to 1 mg/mL Caco-2 homogenates and the reactions were incubated at 37°C. Samples were removed at 0, 1, 2, 3 and 4 h time points and quenched. For

metabolism of Cipro-Gly-OMe in pooled human liver microsomes, a final concentration of 2 µM Cipro-Gly-OMe was incubated with the activated liver microsome system (see Chapter III) at 37°C and samples were taken out at 0, 15, 30, 60 and 120 min and quenched. For bioconversion of Cipro-Gly-OMe in human plasma, a final concentration of 10 µM Cipro-Gly-OMe was added to undiluted human plasma and incubated at 37°C. Samples were collected at 0, 1, 2, 4, 8 and 24-h time points and quenched. All quenching solutions were acetonitrile with 250 nM (S)-(-)-propranolol. All quenched samples were centrifuged and the supernatant were analyzed with LC-MS for contents of Cipro-Gly-OMe, Cipro-Gly and ciprofloxacin.

UV Absorption Analysis

100 µL ciprofloxacin·HCl solutions diluted from saturated solutions were added to a UV-transparent 96-well plate. Absorptions at 280 nm were read in a Biotek Synergy HT plate reader with the interior sample chamber at room temperature. Standard curves containing at least 6 data points were used to calculate concentrations from A_{280} values. The accuracy of the assays was 95% – 105%.

HPLC Analysis

The HPLC instrument and mobile phases were identical to those that were used in Chapters III and IV. The mobile phase B (acetonitrile with 1‰ TFA) content versus time diagram was set up as follows: 0 min, 0.2%; 4 min, 30%; 13 min, 57%; 15.5 min, 80%. Ciprofloxacin, Cipro-Gly-OMe and Cipro-Gly were detected at UV 275 nm and metoprolol at 220 nm. Standard curves with at least five points were used to calculate concentrations from peak area values. The accuracy of the HPLC assay was 90% to 110%.

LC-MS Analysis

The LC-MS instrument and mobile phases were identical to those that were used in Chapters III and IV. The mobile phase B (acetonitrile with 1‰ formic acid) content versus time diagram was set up as follows: 0 min, 0.5%; 1 min, 0.5%; 6.5 min, 80%. Mass-to-charge ratios (m/z's) for chemical species: ciprofloxacin $[M+H]^+$ 332.1, Cipro-Gly-OMe $[M+H]^+$ 403.2, Cipro-Gly $[M+H]^+$ 389.1, (S)-(-)-propranolol $[M+H]^+$ 260.1. Standard curves

containing at least five points were utilized to calculate concentrations from peak areas. The accuracy of the LC-MS assay was 75% to 125%.

Data Analysis

The apparent permeability coefficient (P_{app}) of each compound was determined using Equation 4.1 (Chapter IV). For Cipro-Gly-OMe, the concentration in the receiving compartment (C_R) at each time point was the sum of C_R(Cipro-Gly-OMe) and C_R(Cipro-Gly), the latter generated from hydrolysis of Cipro-Gly-OMe.

Statistical Analysis

All experiments had sample numbers of n = 3 – 4. Results are presented as mean ± SEM. Statistical comparisons were performed in GraphPad Prism 5.0 using two-way ANOVA with *post-hoc* Bonferroni tests. *P* values less than 0.05 were deemed significant.

RESULTS

Stability of Cipro-Gly-OMe in Buffer

After 8 days in pH 7.4 buffer, 86.4% ± 1.2% (mean ± S.D.) Cipro-Gly-OMe remained in the system; the rest had been hydrolyzed to Cipro-Gly as confirmed by retention times in HPLC chromatographs as well as LC-MS chromatographs for the respective m/z's of Cipro-Gly and Cipro-Gly-OMe. No visible amount of ciprofloxacin was detected. Assuming zero-order chemical hydrolysis, the rate of Cipro-Gly-OMe's degradation in buffer was approximately 1.7% per day.

The pH-dependent Solubility of Ciprofloxacin and Cipro-Gly-OMe

For ciprofloxacin·HCl, the measured solubility values at different pHs are listed in **Table 5.2**. They are also plotted against the pH in **Figure 5.12a**. As observed from the measured values, it was evident that the solubility of ciprofloxacin generally decreases as the pH increases from 5 to ~7.8. For Cipro-Gly-OMe, it was extremely difficult to make a saturated solution even at its pK_a because of its high solubility and the small amount of available compound powder. The highest soluble concentration achieved was 17.3 mg/mL (2.6 mg Cipro-Gly-OMe·TFA dissolved in 150 µL 0.5 M TAPS buffer) or **0.0336 M**. Therefore, its intrinsic solubility is actually greater than 0.0336 M / 2 = 0.0168 M; as a convenience this number was taken as the S_0 for prediction of its pH-dependent solubility (**Fig. 5.12b**). Despite not being able to obtain an accurate measurement of the solubility of Cipro-Gly-OMe, it was obvious (as shown in Fig. 5.12b) that the prodrug possesses much higher solubility than ciprofloxacin at pH 6 – 8, with potentially increased solubility of over 17,500× at pH 6 to over 433× at pH 8.

The pH-dependent Permeability across Caco-2 Monolayers

The apical-to-basolateral (A-to-B) permeability coefficients for ciprofloxacin, Cipro-Gly-OMe and metoprolol are listed in **Table 5.3** and compared in **Figure 5.13**. At pH 6.0, the prodrug had a similar A-to-B permeability to that of the parent compound and both were lower than that of metoprolol. At pH 7.4, the P_{app} values of all three compounds were significantly higher than those at pH 6.0, although Cipro-Gly-OMe increased than

ciprofloxacin; as a result, at pH 7.4 Cipro-Gly-OMe was significantly more permeable than the parent drug. Both remained less permeable than metoprolol, however. Overall, the pH-dependent permeability profiles of ciprofloxacin and Cipro-Gly-OMe corresponded relatively well to the trends of fractions of neutral form at pH 6.0 and 7.4 (Fig. 5.10).

Bioconversion of Cipro-Gly-OMe

In all tissue matrices with Cipro-Gly-OMe added and incubated at 37°C, no ciprofloxacin was detected at the end of the experimental period (4 h for Caco-2 homogenates, 120 min for liver microsomes and 24 h for plasma). Almost all (> 95%) of the Cipro-Gly-OMe was converted to Cipro-Gly by 1 h in Caco-2 homogenates, 30 min in liver microsomes and 8 h in plasma, and in all three tissue matrices, the concentrations of Cipro-Gly remained relatively unchanged until the conclusion of experiments. These phenomena demonstrated the relatively high stability of Cipro-Gly in tissues where typical metabolism of xenobiotics takes place. Therefore, it is unlikely that Cipro-Gly-OMe could be rapidly transformed into ciprofloxacin when administered orally in future *in vivo* studies.

In conclusion, the prodrug Cipro-Gly-OMe possesses potentially much higher solubility at the physiological pH range than the parent compound ciprofloxacin does, as well as an improved Caco-2 permeability over that of the parent drug at neutral pH. However, the lack of an efficient biotransformation of the prodrug to ciprofloxacin may delay or even abolish the onset of its antibacterial pharmacological effects. Therefore, in future prodrug designs, other promoiety structures should be considered for masking the carboxyl group of ciprofloxacin.

DISCUSSION

In this chapter, I proposed and tested a prodrug strategy for improvements in the solubility as well as intestinal permeability of ciprofloxacin based on the physicochemical properties, in particular the dissociation constants, of the drug. The preliminary results demonstrated that the prodrug, ciprofloxacyl-glycine-methyl ester (Cipro-Gly-OMe), could potentially have a much enhanced solubility throughout the physiological pH range as well as an increased Caco-2 permeability around the neutral pH. Therefore, this prodrug strategy might convert a BCS class IV compound to a probable BCS class III or even a class I compound.

For the determination of the pH-dependent solubility of ciprofloxacin, a UV absorption assay was used for the calculation of concentrations based on an A_{280} vs. concentration standard curve. This methodology was more time- and resource-saving than other analytical methods such as HPLC and its accuracy, at 95% to 105%, was also acceptable. Combined with the buffer systems (Table 5.1), the measured pH-solubility relationship could reflect the theoretical curve relatively well (Fig. 5.12a). For Cipro-Gly-OMe, in theory it would be ideal to also generate a set of measured solubility values at different pHs. Nevertheless, even at its pK_a (~8.75), where its solubility $S = 2\ S_0$, saturation could not be reached after numerous attempts. Since I only synthesized barely enough Cipro-Gly-OMe (~ 25 mg), further attempts at generating saturated solutions were not carried out. The highest observed concentration at pH 8.75 was 0.0336 M or 17.3 mg/mL Cipro-Gly-OMe·TFA. Such a solubility value enables a (theoretical) highest dose of 1 g Cipro-Gly-OMe to completely dissolve in 250 mL water at pH 8.75. Since solubility of Cipro-Gly-OMe at lower pH would almost certainly be higher than at pH 8.75, it is reasonable to suggest that Cipro-Gly-OMe is highly soluble in aqueous media over the pH range of 1 – 7.5. Therefore, it fits the “high solubility” classification according to the FDA guideline on BCS [19].

In studies to characterize the compounds’ A-to-B permeability across the Caco-2 monolayer, the prodrug Cipro-Gly-OMe was found to have a similar permeability to the parent compound’s at an apical pH of 6.0 but a significantly higher one than that of ciprofloxacin at pH 7.4 (Fig. 5.13 and Table 5.3). The increase in permeability of both

compounds from pH 6.0 to 7.4 was predicted by the pH-dependent fractions of neutral forms (Fig. 5.10); Cipro-Gly-OMe would also have a higher fraction of neutral form than ciprofloxacin does at pH 7.4. Nevertheless, at pH 7.4, the apparent permeability of Cipro-Gly-OMe was still lower than that of metoprolol. This does not necessarily suggest that Cipro-Gly-OMe is a low-permeability compound, and the reasoning behind this statement is two-fold. First, ciprofloxacin has a fraction of dose absorbed (F_a) of greater than 70% (because its absolute bioavailability is 70% with no significant first-pass metabolism [12]). With an apparent permeability coefficient at more than two times that of ciprofloxacin at pH 7.4, Cipro-Gly-OMe could very possibly have a much higher F_a compared to ciprofloxacin's 70%; an F_a greater than 90% would be sufficient for a compound to be classified as highly permeable. Second, metoprolol has been considered a conservative high-permeability standard because it is almost 100% absorbed when administered orally [30]. It has been suggested that a compound with a lower F_a such as labetalol (F_a = 90%) be used as the threshold for high- and low- permeability classification [30]. Additional Caco-2 and / or intestinal perfusion studies should thus be performed to compare the permeability of Cipro-Gly-OMe to those of other reference compounds. In summary, the prodrug Cipro-Gly-OMe displayed enhanced apparent Caco-2 permeability at the apical pH of 7.4 compared to ciprofloxacin, and when solubility is also considered, it is possibly a BCS class I compound pending further verification.

Despite Cipro-Gly-OMe's advantages in its biopharmaceutical properties, a few issues have yet to be addressed. One concern is its bioconversion to the parent compound: the metabolite of Cipro-Gly-OMe, Cipro-Gly, was found to be very stable in tissue matrices and not readily converted to ciprofloxacin. A better promoiety to use may be (L)-proline because prolidase, a carboxypeptidase, is known to hydrolyze substrates with (L)-proline at the carboxyl terminus [31]. Previous studies have utilized prolidase as the activating enzyme for proline prodrugs [32-35]. Prolidase is ubiquitously expressed in the body [36] and could thus potentially hydrolyze the orally administered ciprofloxacyl-(L)-proline amide prodrugs (**Figure 5.14**) to yield the active parent compound. Another issue to address concerns the type of prodrug for the design. Initially, one reason for choosing the amide prodrugs of ciprofloxacin was that the existence of a peptide bond might make the prodrug a substrate for

PEPT1-mediated transport. However, as observed in permeability studies (Fig. 5.13), the P_{app} of Cipro-Gly-OMe at an apical pH of 7.4 was found to be much larger than that at pH 6.0. A pH of 6.0 was presumably a more favorable situation for transport by PEPT1 because of the pH gradient from the apical (6.0) to the basolateral (7.4, DPBS) chamber. Therefore, it is obvious that PEPT1 did not play a major role in the transport of Cipro-Gly-OMe and amide prodrugs of ciprofloxacin likely do not possess this presumed advantage. In light of this, other types of chemical linkages between ciprofloxacin and the promoiety, such as esters (**Figure 5.15**), should also be considered in future designs for the prodrug.

CONCLUSIONS

Ciprofloxacyl-glycine-methyl ester (Cipro-Gly-OMe), an amide prodrug of ciprofloxacin, possessed potentially much higher aqueous solubility throughout the physiological pH range when compared to the parent compound. Cipro-Gly-OMe also demonstrated a significantly higher Caco-2 permeability at pH 7.4 compared to ciprofloxacin. Therefore, this study presented a unique prodrug approach that potentially transformed a BCS class IV compound into a class I compound. However, the inefficient bioconversion of Cipro-Gly-OMe to ciprofloxacin in tissue matrices may pose a potential problem for the compound's pharmacological activity, and further optimization of the promoiety is thus required to confer more rapid *in vitro* and *in vivo* biotransformation of the prodrug to the parent compound. Nevertheless, the prodrug approach presented in this chapter could potentially be applied to increase the solubility as well as intestinal permeability of other BCS class IV compounds that predominantly exist as zwitterions within the physiological pH range.

FIGURES

(a)

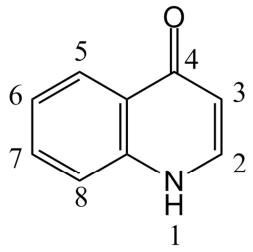

(b)

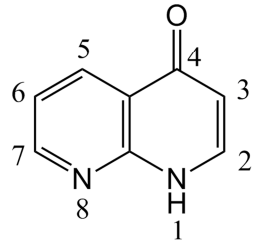

(c)

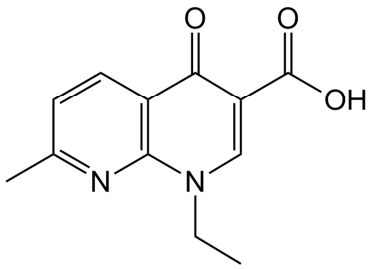

Figure 5.1. Chemical structures of **(a)** 4-quinolone, with position numbers on the bicyclic ring; **(b)** 4-oxo-1,8-naphthyridine (4-naphthyridone), with position numbers on the bicyclic ring; **(c)** nalidixic acid.

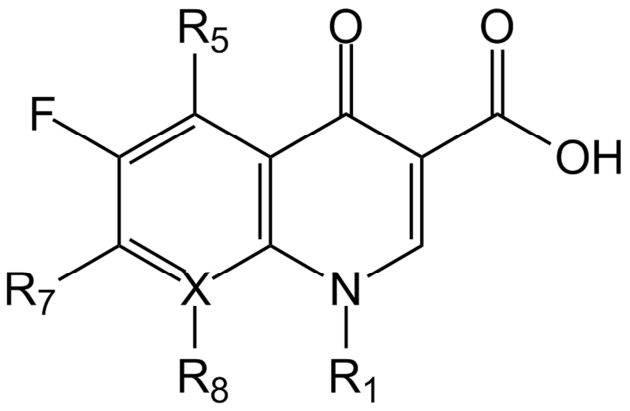

Figure 5.2. A general structure for the approved fluoroquinolone compounds. The carboxyl group at position 2 on the ring and fluorine at position 6 are fixed. At position 8, when X = N (nitrogen), R_8 could only be H (hydrogen); when X = C (carbon), R_8 could be any side group.

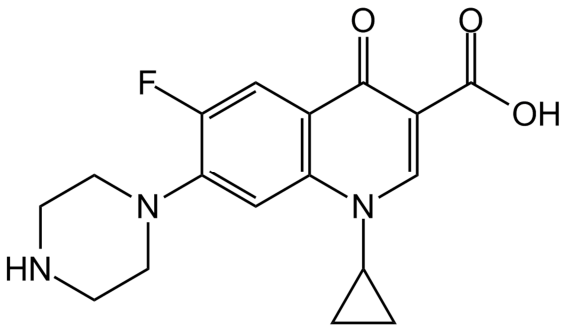

Figure 5.3. Chemical structure of ciprofloxacin. With respect to **Fig. 5.2**, R_1 = cyclopropyl and R_7 = 1'-piperazyl.

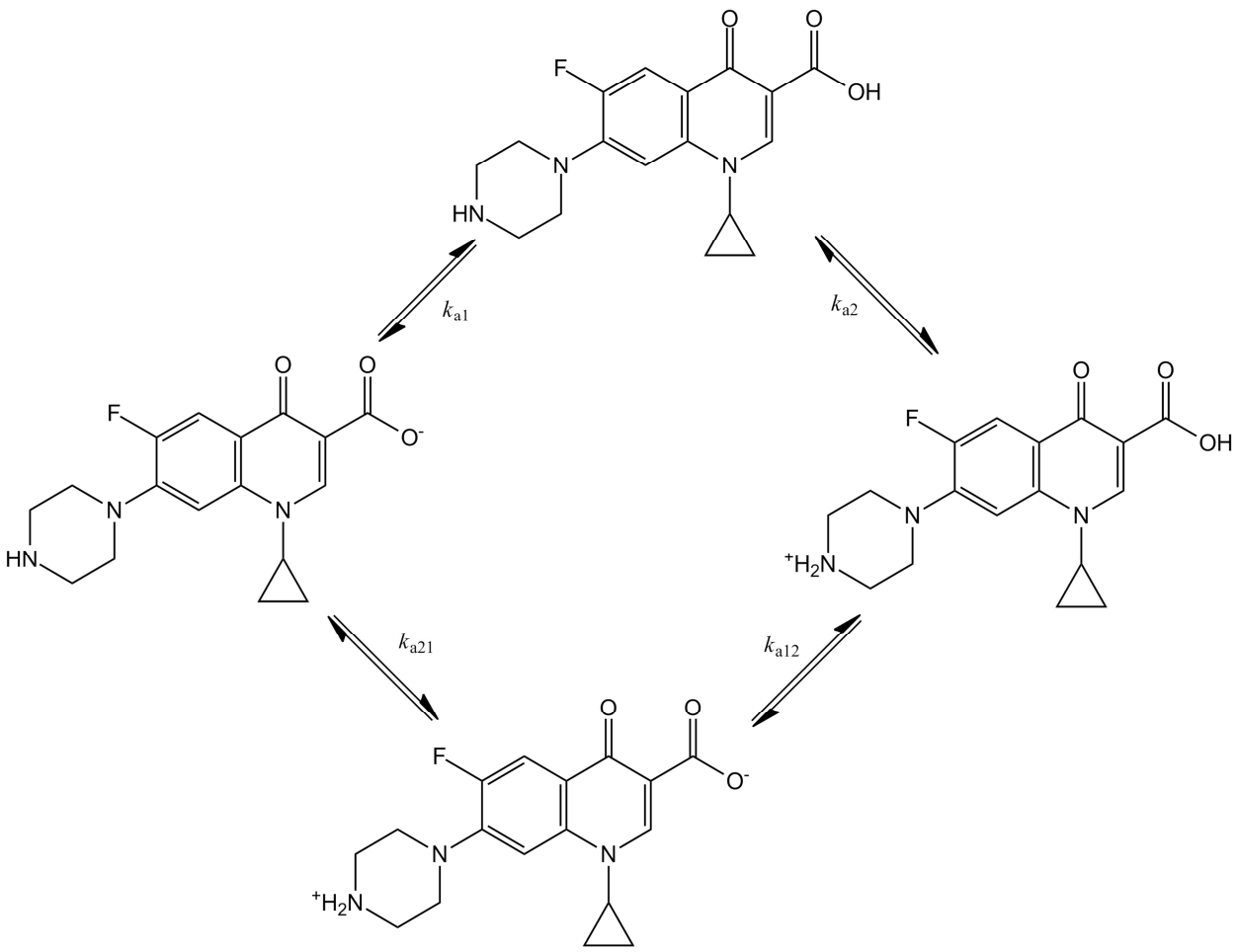

Figure 5.4. The equilibria between the four species of ciprofloxacin in aqueous solutions. The micro-dissociation constants are denoted as k_{a1}, k_{a21}, k_{a12} and k_{a2}. In this chapter, it was assumed that $k_{a1} = k_{a12} = K_{a1}$, and $k_{a21} = k_{a2} = K_{a2}$, where K_{a1} and K_{a2} are the respective macro-dissociation constants for the carboxyl and secondary amine groups.

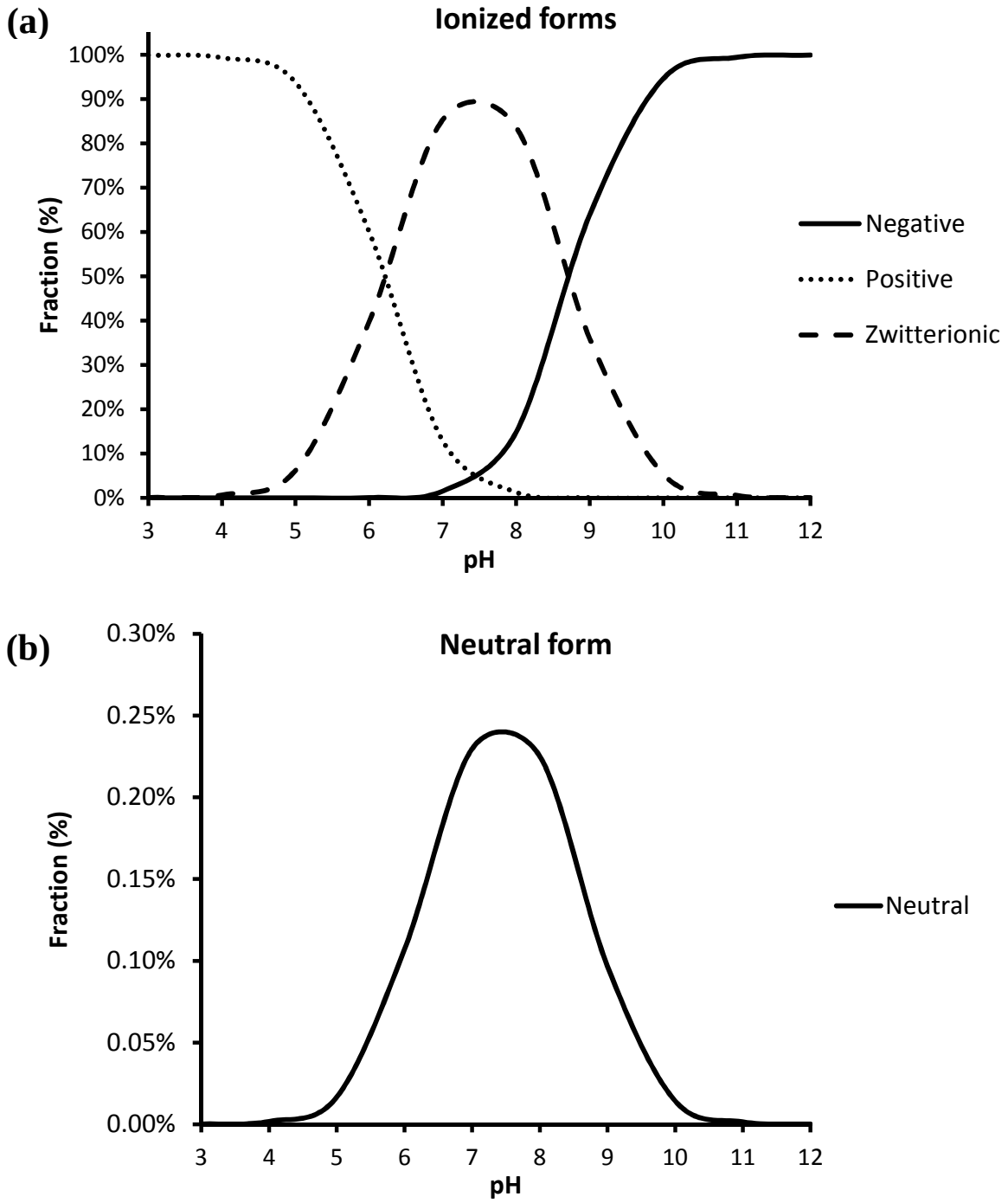

Figure 5.5. Theoretical relationship between the solution pH and the distribution of **(a)** the three ionized species and **(b)** the neutral form of ciprofloxacin. Parameters used to generate this graph: pK_{a1} = 6.18 and pK_{a2} = 8.75 at 25°C.

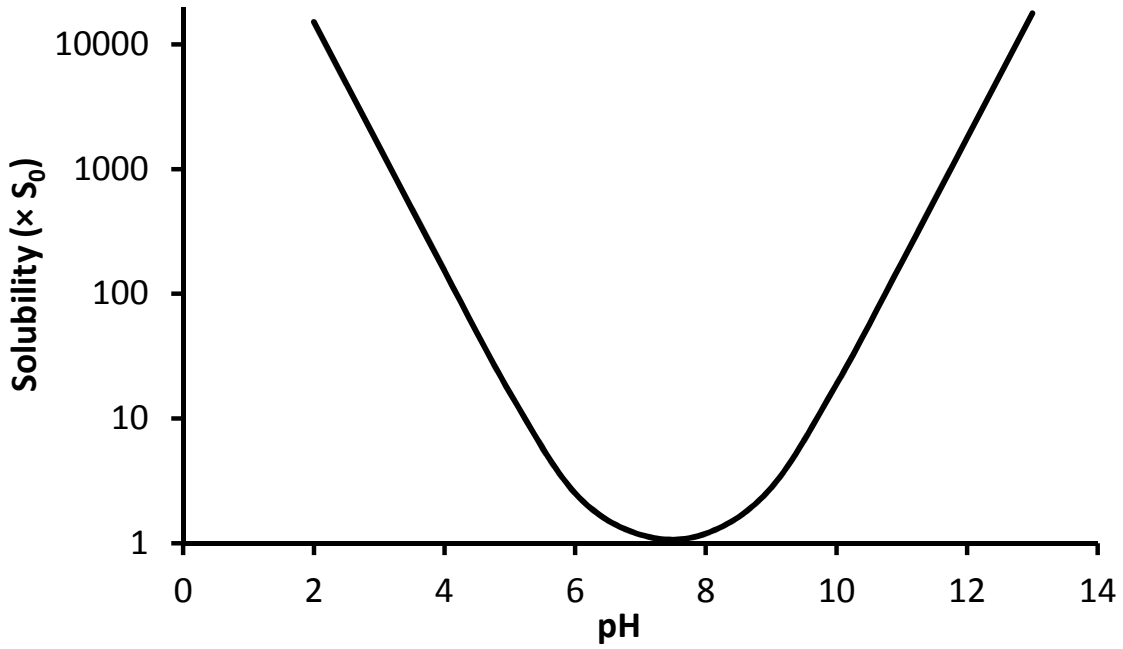

Figure 5.6. Theoretical relationship between the solution pH and the aqueous solubility of ciprofloxacin, expressed in multiples of intrinsic solubility (× S_0). The *y* axis is shown in $\log_{10}$ scale. Parameters used to generate this graph: pK_{a1} = 6.18 and pK_{a2} = 8.75 at 25°C.

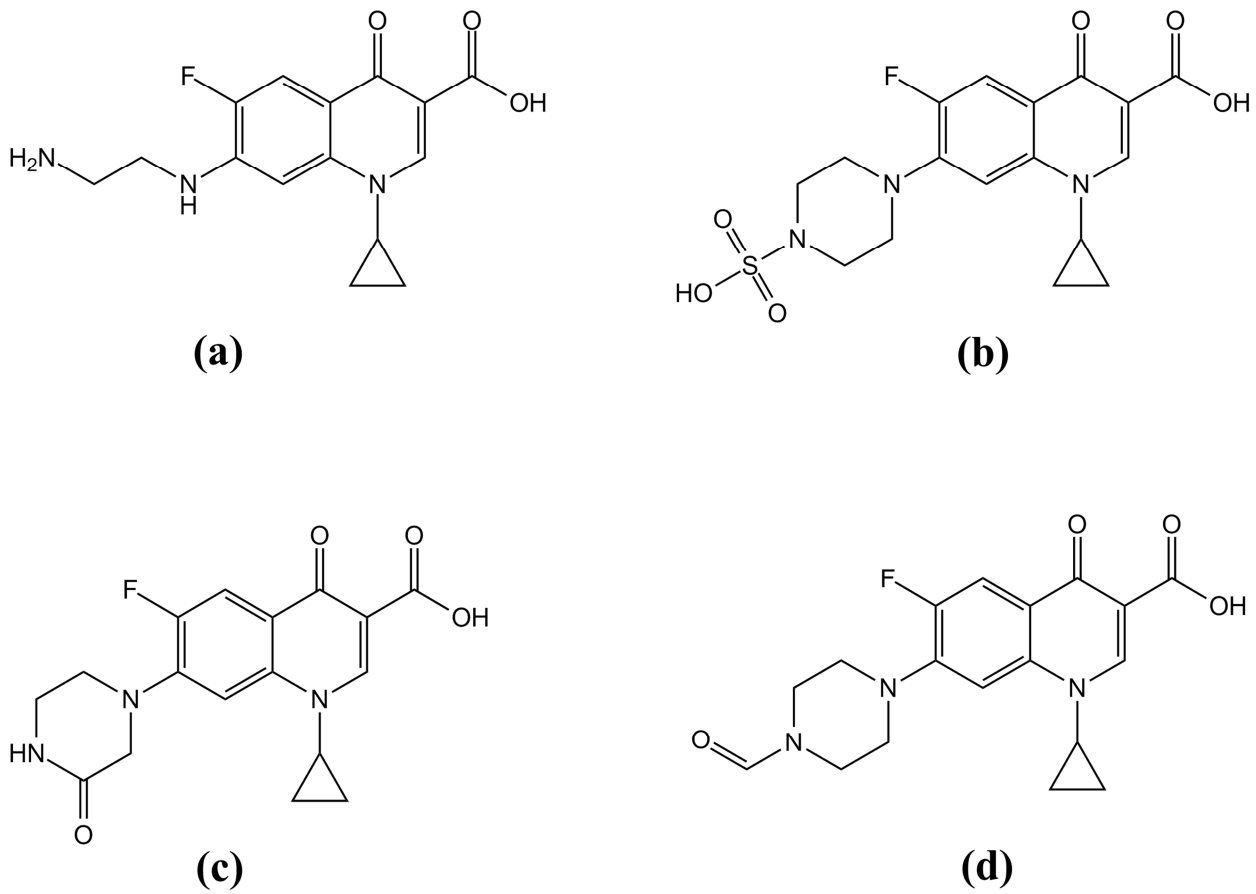

Figure 5.7. *In vivo* metabolites of ciprofloxacin: **(a)** desethyleneciprofloxacin (M1), molecular weight (MW) 305.3; **(b)** sulfo-ciprofloxacin (M2), MW 411.4; **(c)** oxociprofloxacin (M3), MW 345.3 and **(d)** formylciprofloxacin (M4), MW 359.3.

(a)

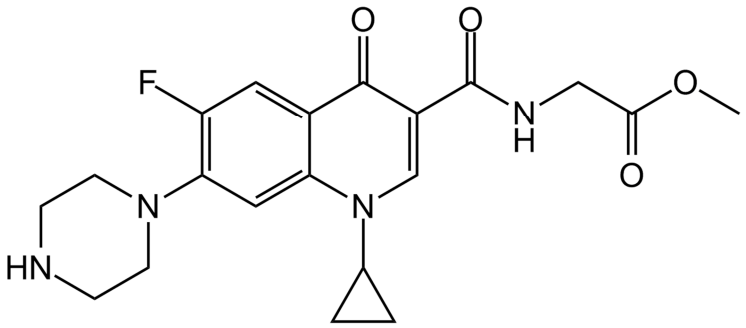

(b)

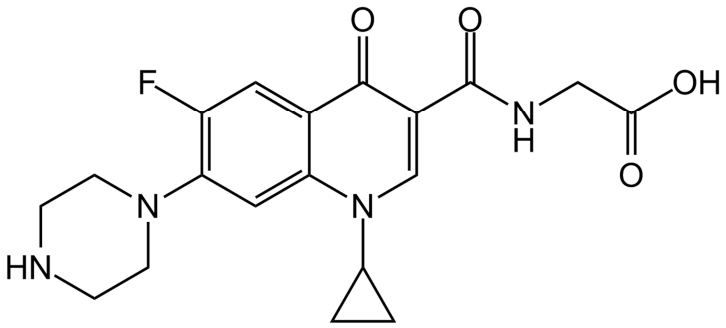

Figure 5.8. Amide prodrugs of ciprofloxacin: **(a)** Ciprofloxacyl-glycine-methyl ester (Cipro-Gly-OMe) and **(b)** Ciprofloxacyl-glycine (Cipro-Gly).

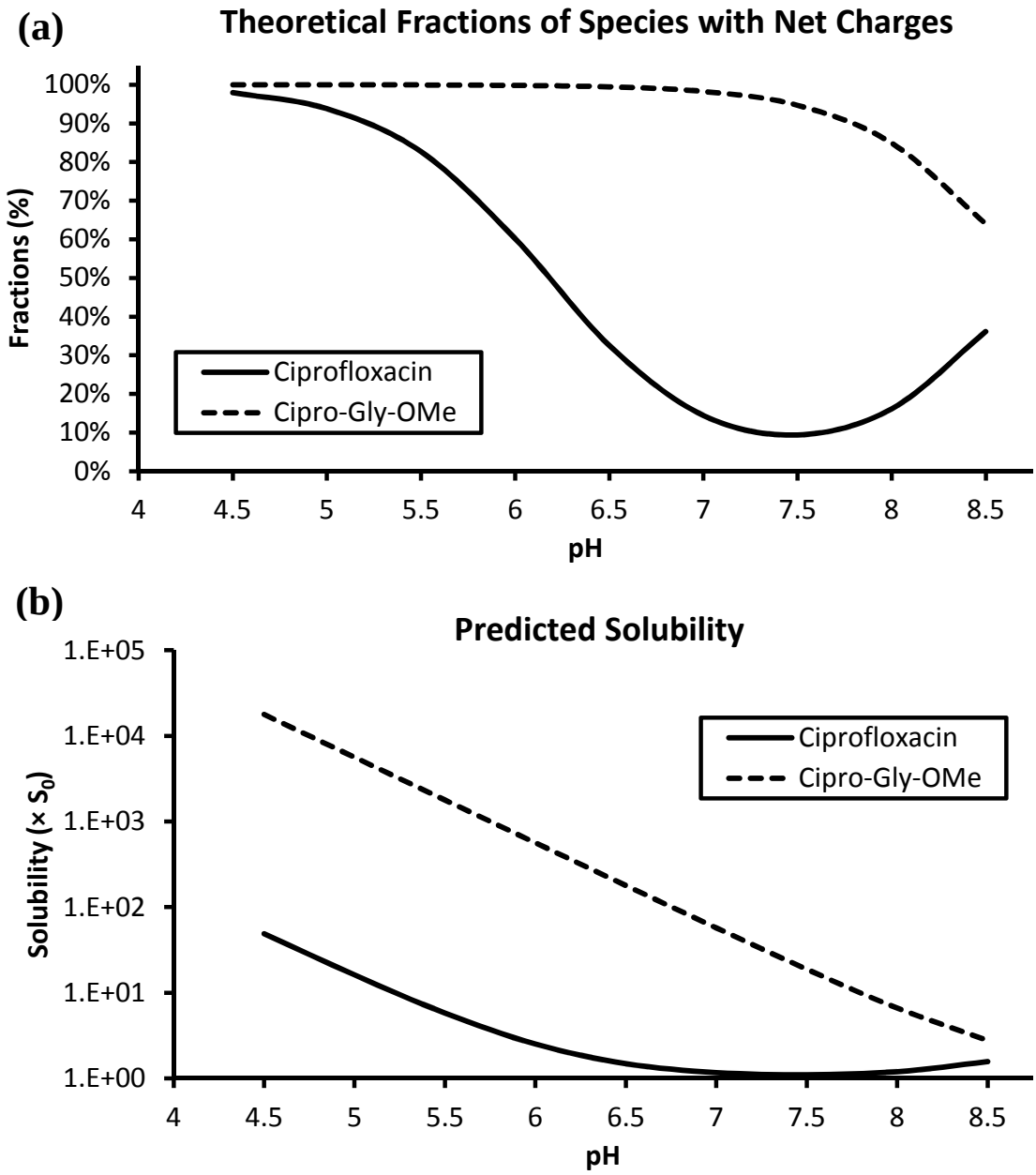

Figure 5.9. **(a)** The fractions of species with net charges (positively and negatively charged form of ciprofloxacin and positively charged form of Cipro-Gly-OMe) vs. pH. **(b)** Predicted pH-dependent solubility of ciprofloxacin and Cipro-Gly-OMe expressed in the multiples of their respective intrinsic solubility (S_0). The *y* axis is shown in $\log_{10}$ scale. Note that the S_0 of the two compounds are likely different from each other. The figures were generated based on pK_a values at 25°C: pK_{a1} = 6.18 and pK_{a2} = 8.75.

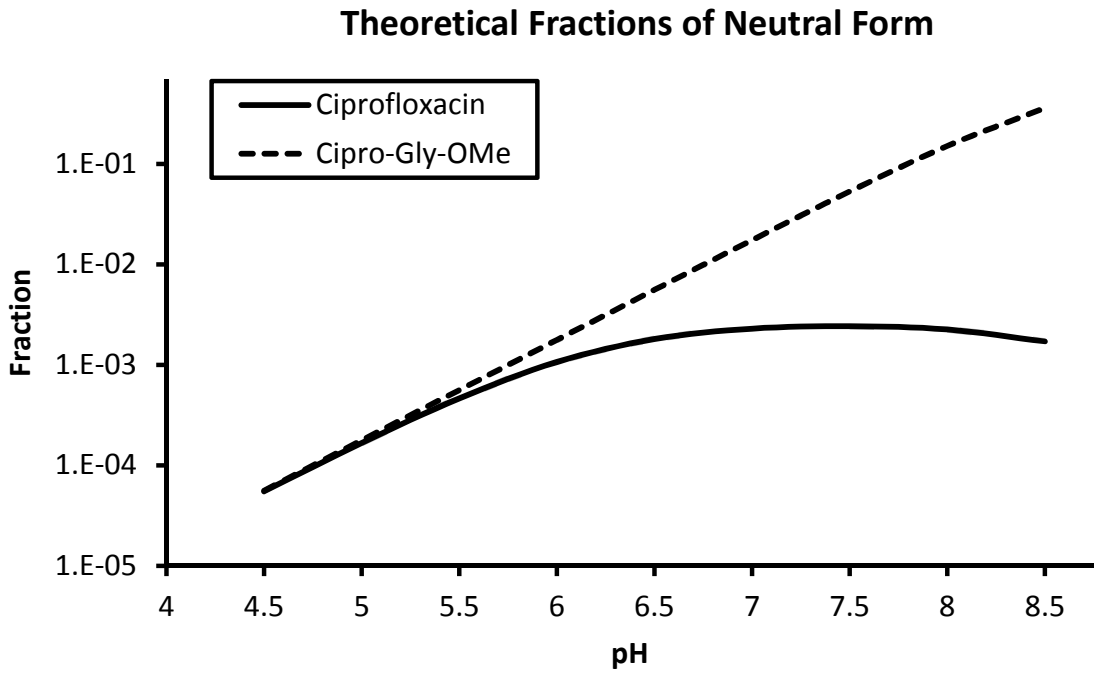

Figure 5.10. Theoretical relationship between the solution pH and the fractions of neutral forms of ciprofloxacin and Cipro-Gly-OMe. The *y* axis is presented in $\log_{10}$ scale. The figure was generated based on pK_a values at 25°C: pK_{a1} = 6.18 and pK_{a2} = 8.75.

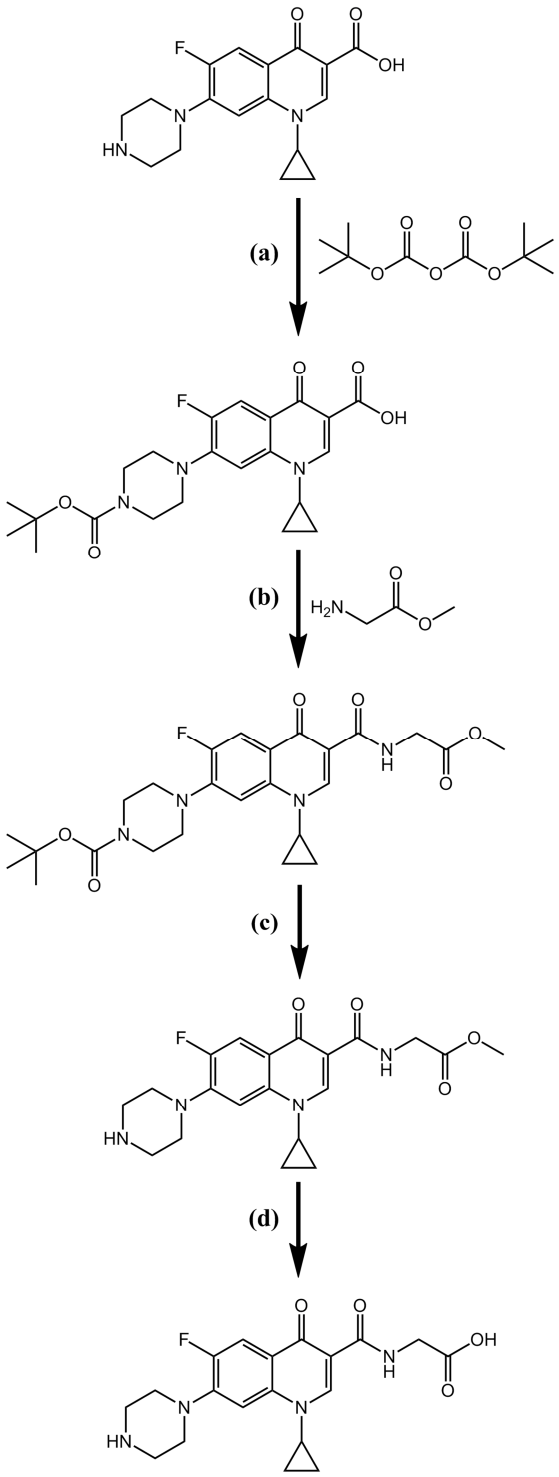

Figure 5.11. Steps for the synthesis of ciprofloxacyl-glycine-methyl ester (Cipro-Gly-OMe) and ciprofloxacyl-glycine (Cipro-Gly).

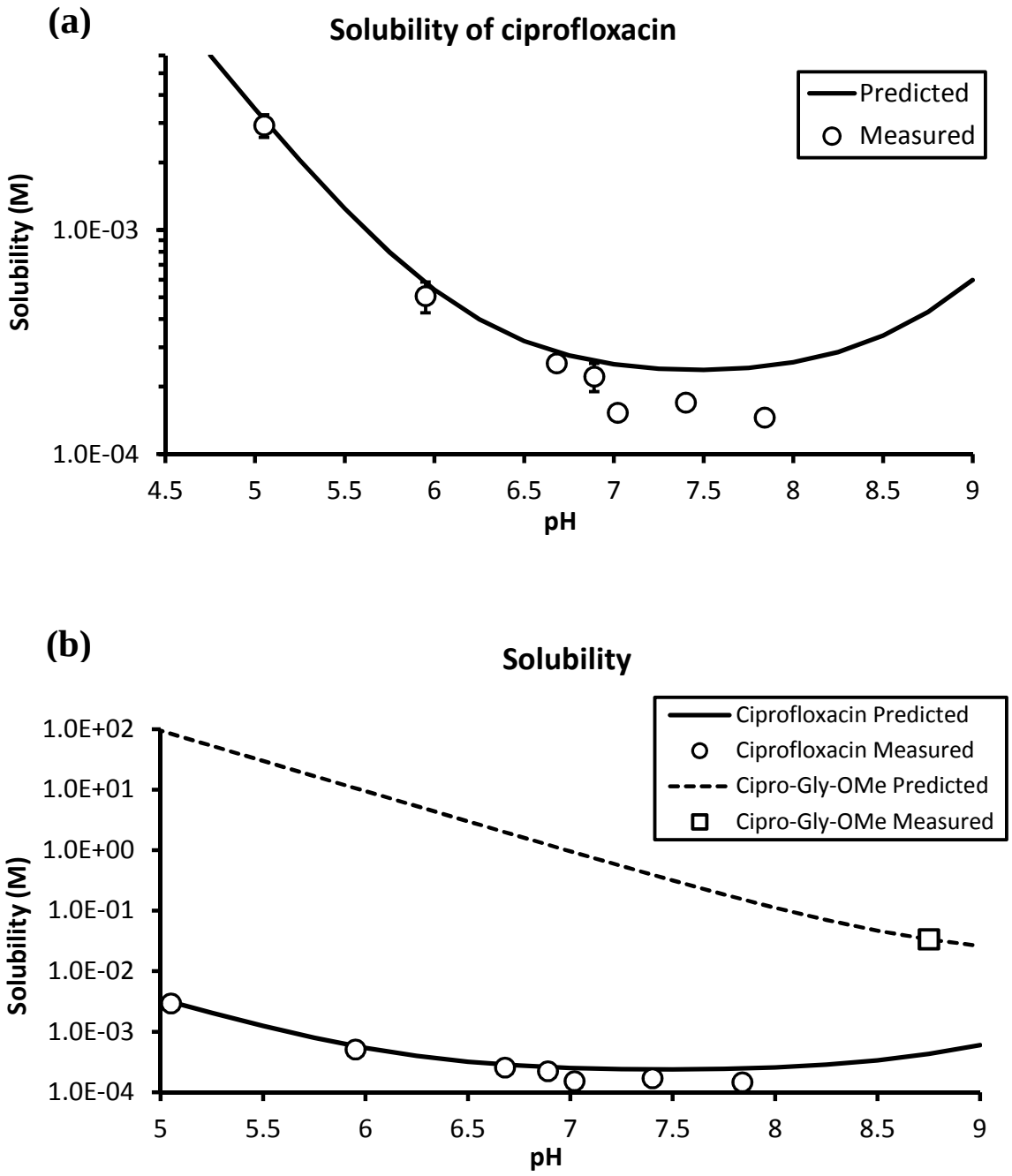

Figure 5.12. The pH-dependent solubility of ciprofloxacin and Cipro-Gly-OMe. **(a)** Solubility of ciprofloxacin (in M) measured at different pH along with the predicted solubility vs. pH curve. **(b)** Solubility of Cipro-Gly-OMe (measured and predicted) compared to that of ciprofloxacin. In both plots, the *y* axis was shown in $\log_{10}$ scale. n = 3 for all ciprofloxacin samples. Error bars represent SD.

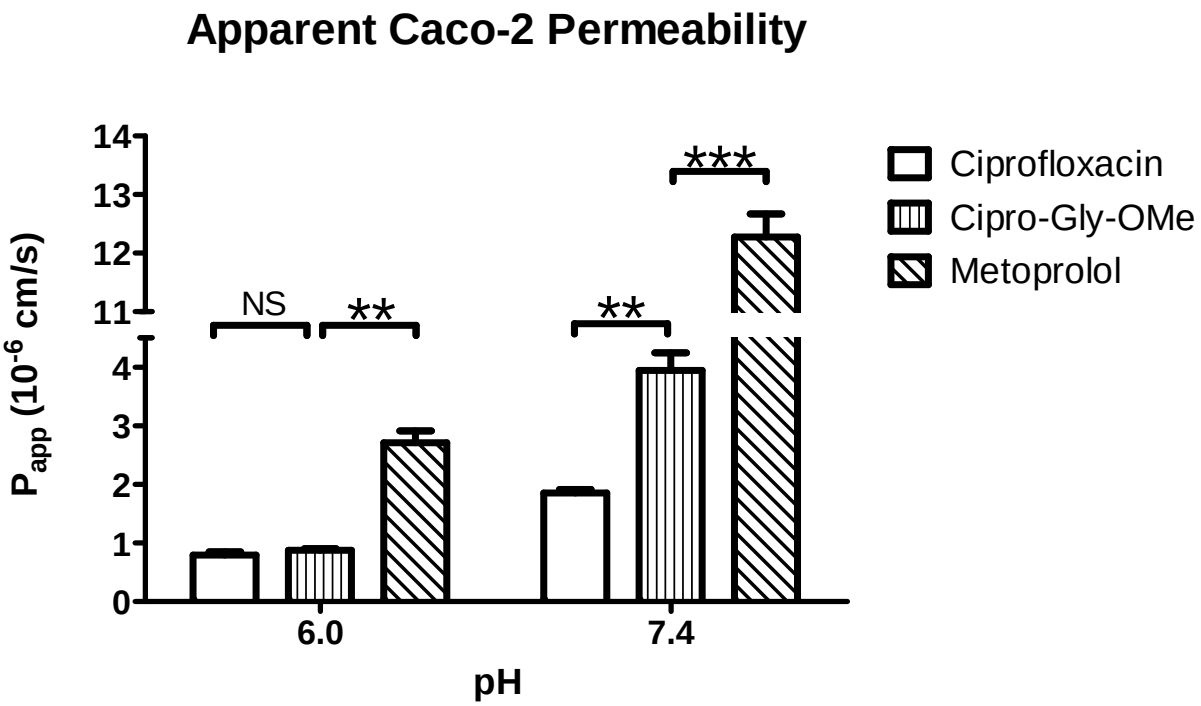

Figure 5.13. Apparent apical-to-basolateral (A to B) permeability coefficients (P_{app}) of compounds across the Caco-2 cell monolayer. The P_{app}'s were calculated according to Equation 4.1 and presented in 10^{-6} cm/s. n = 3 – 4 for all columns and error bars denote SEM. NS, not significant; **, $p < 0.01$; ***, $p < 0.001$. The P_{app} values were also presented in **Table 5.3**.

(a)

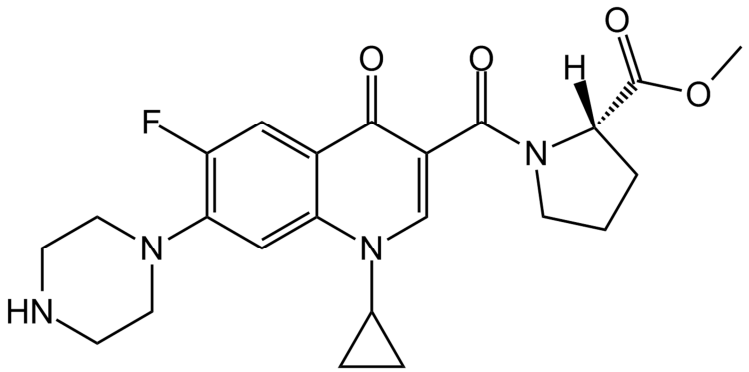

(b)

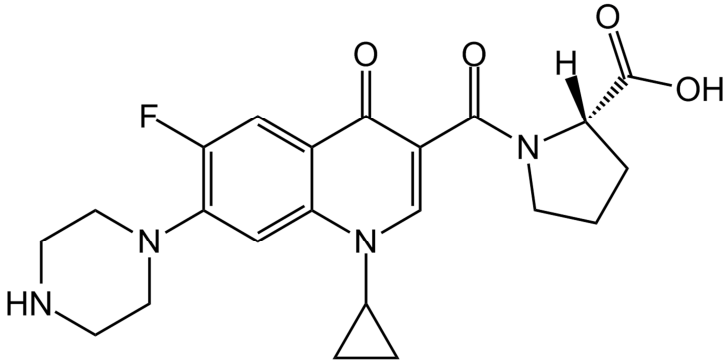

Figure 5.14. Proposed amide prodrugs of ciprofloxacin: **(a)** Ciprofloxacyl-(L)-proline-methyl ester (Cipro-Pro-OMe) and **(b)** ciprofloxacyl-(L)-proline (Cipro-Pro).

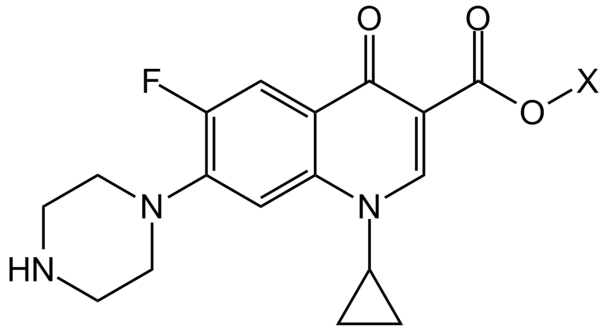

Figure 5.15. Proposed ester prodrug of ciprofloxacin (ciprofloxacyl ester) with X as the promoiety.

TABLES

pH	Buffer solution
5.00	100 mM Na_2HPO_4, 50 mM citric acid
6.05	25 mM MES
6.85	25 mM PIPES
7.22	25 mM MOPS
7.43	100 mM HEPES
7.45	PBS: 137 mM NaCl, 2.7 mM KCl, 8 mM Na_2HPO_4, 1.5 mM KH_2PO_4
7.81	100 mM tricine

Table 5.1. Buffer solutions used for making saturated solutions of ciprofloxacin·HCl. All pH values were measured at 25°C with a Corning pH meter 320.

Original buffer solution	Final pH	Solubility (M)
100 mM Na_2HPO_4, 50 mM citric acid	5.05	$2.93\times10^{-3} \pm 0.34\times10^{-3}$
25 mM MES	5.95	$5.07\times10^{-4} \pm 0.80\times10^{-4}$
25 mM PIPES	6.68	$2.55\times10^{-4} \pm 0.05\times10^{-4}$
PBS (see Table 5.1)	6.89	$2.22\times10^{-4} \pm 0.32\times10^{-4}$
25 mM MOPS	7.02	$1.53\times10^{-4} \pm 0.01\times10^{-4}$
100 mM HEPES	7.40	$1.70\times10^{-4} \pm 0.06\times10^{-4}$
100 mM tricine	7.80	$1.46\times10^{-4} \pm 0.02\times10^{-4}$

Table 5.2. Solubility of ciprofloxacin·HCl (in M) at different pHs. The pH values of the saturated solutions were measured again after the insolubles were precipitated by centrifugation. Each solubility is presented as mean ± SD; n = 3 for all groups.

Compound	Apparent Apical-to-Basolateral Permeability Coefficient (10^{-6} cm/s)	
	pH 6.0	pH 7.4
Ciprofloxacin	0.788 ± 0.058	1.85 ± 0.06
Cipro-Gly-OMe	0.875 ± 0.026	3.94 ± 0.31
Metoprolol	2.71 ± 0.20	12.3 ± 0.4

Table 5.3. The apparent apical-to-basolateral permeability coefficients (in 10^{-6} cm/s) across Caco-2 monolayers for ciprofloxacin, Cipro-Gly-OMe and metoprolol at pH 6.0 and 7.4. Data presented as mean ± SEM; n = 3 for ciprofloxacin and Cipro-Gly-OMe at pH 7.4 and 4 for all others.

REFERENCES

1. Lesher, G.Y., et al., *1,8-Naphthyridine Derivatives. A New Class of Chemotherapeutic Agents.* J Med Pharm Chem, 1962. **91**: p. 1063-5.
2. Emmerson, A.M. and A.M. Jones, *The quinolones: decades of development and use.* J Antimicrob Chemother, 2003. **51 Suppl 1**: p. 13-20.
3. Van Bambeke, F., et al., *Quinolones in 2005: an update.* Clin Microbiol Infect, 2005. **11**(4): p. 256-80.
4. Peterson, L.R., *Quinolone molecular structure-activity relationships: what we have learned about improving antimicrobial activity.* Clin Infect Dis, 2001. **33 Suppl 3**: p. S180-6.
5. Radu, B.M., et al., *Mechanisms of ceftazidime and ciprofloxacin transport through porins in multidrug-resistance developed by extended-spectrum beta-lactamase E.coli strains.* J Fluoresc, 2011. **21**(4): p. 1421-9.
6. Ceccarelli, M. and P. Ruggerone, *Physical insights into permeation of and resistance to antibiotics in bacteria.* Curr Drug Targets, 2008. **9**(9): p. 779-88.
7. Wigley, D.B., *Structure and mechanism of DNA topoisomerases.* Annu Rev Biophys Biomol Struct, 1995. **24**: p. 185-208.
8. Drlica, K. and X. Zhao, *DNA gyrase, topoisomerase IV, and the 4-quinolones.* Microbiol Mol Biol Rev, 1997. **61**(3): p. 377-92.
9. Laponogov, I., et al., *Structural insight into the quinolone-DNA cleavage complex of type IIA topoisomerases.* Nat Struct Mol Biol, 2009. **16**(6): p. 667-9.
10. Hooper, D.C., *Fluoroquinolone resistance among Gram-positive cocci.* Lancet Infect Dis, 2002. **2**(9): p. 530-8.
11. *Approval History: Cipro (tablet), (NDA) 019537, at Drugs@FDA.*; Available from: http://www.accessdata.fda.gov/scripts/cder/drugsatfda/.
12. *Cipro (R) label information at Drugs@FDA.* [cited 2013 Mar. 4]; Available from: http://www.accessdata.fda.gov/drugsatfda_docs/label/2013/019537s081,020780s039lbl.pdf.
13. Escribano, E., et al., *Structure-absorption relationships of a series of 6-fluoroquinolones.* Antimicrob Agents Chemother, 1997. **41**(9): p. 1996-2000.
14. Sun, J., et al., *Determination of lipophilicity of two quinolone antibacterials, ciprofloxacin and grepafloxacin, in the protonation equilibrium.* Eur J Pharm Biopharm, 2002. **54**(1): p. 51-8.
15. Ross, D.L. and C.M. Riley, *Aqueous Solubilities of Some Variously Substituted Quinolone Antimicrobials.* International Journal of Pharmaceutics, 1990. **63**(3): p. 237-250.
16. Vazquez, J.L., et al., *Determination by fluorimetric titration of the ionization constants of ciprofloxacin in solution and in the presence of liposomes.* Photochem Photobiol, 2001. **73**(1): p. 14-9.
17. Romanuk, C.B., et al., *Characterization of the solubility and solid-state properties of saccharin salts of fluoroquinolones.* J Pharm Sci, 2009. **98**(10): p. 3788-801.
18. Olivera, M.E., et al., *Biowaiver monographs for immediate release solid oral dosage forms: ciprofloxacin hydrochloride.* J Pharm Sci, 2011. **100**(1): p. 22-33.
19. *US FDA/CDER. Waiver of In Vivo Bioavailability and Bioequivalence Studies for Immediate-Release Solid Oral Dosage Forms Based on a Biopharmaceutics*

Classification System. URL: http://www.fda.gov/downloads/Drugs/GuidanceComplianceRegulatoryInformation/Guidances/UCM070246.pdf. 2000.
20. Sohi, H., Y. Sultana, and R.K. Khar, *Taste masking technologies in oral pharmaceuticals: recent developments and approaches.* Drug Dev Ind Pharm, 2004. **30**(5): p. 429-48.
21. Volpe, D.A., *Permeability classification of representative fluoroquinolones by a cell culture method.* AAPS J, 2004. **6**(2): p. 1-6.
22. Bermejo, M., et al., *Validation of a biophysical drug absorption model by the PATQSAR system.* J Pharm Sci, 1999. **88**(4): p. 398-405.
23. Merino, V., et al., *Biophysical models as an approach to study passive absorption in drug development: 6-fluoroquinolones.* J Pharm Sci, 1995. **84**(6): p. 777-82.
24. Bermejo, M., et al., *PAMPA--a drug absorption in vitro model 7. Comparing rat in situ, Caco-2, and PAMPA permeability of fluoroquinolones.* Eur J Pharm Sci, 2004. **21**(4): p. 429-41.
25. Dautrey, S., et al., *Active intestinal elimination of ciprofloxacin in rats: modulation by different substrates.* Br J Pharmacol, 1999. **127**(7): p. 1728-34.
26. Lowes, S. and N.L. Simmons, *Multiple pathways for fluoroquinolone secretion by human intestinal epithelial (Caco-2) cells.* Br J Pharmacol, 2002. **135**(5): p. 1263-75.
27. Merino, G., et al., *Breast cancer resistance protein (BCRP/ABCG2) transports fluoroquinolone antibiotics and affects their oral availability, pharmacokinetics, and milk secretion.* Drug Metab Dispos, 2006. **34**(4): p. 690-5.
28. Haslam, I.S., et al., *Intestinal ciprofloxacin efflux: the role of breast cancer resistance protein (ABCG2).* Drug Metab Dispos, 2011. **39**(12): p. 2321-8.
29. *Study 81-0037: An Open-Label, Single-Dose, Mass Balance and Pharmacokinetic Study of Proquin (TM) 500 mg Tablets in Healthy Adult Volunteers Under Fed Conditions.* [cited 2013 Mar. 6]; Available from: http://www.accessdata.fda.gov/drugsatfda_docs/nda/2005/021744s000_ClinPharmR_Part2.pdf.
30. Dahan, A., et al., *High-permeability criterion for BCS classification: segmental/pH dependent permeability considerations.* Mol Pharm, 2010. **7**(5): p. 1827-34.
31. Endo, F., et al., *Primary structure and gene localization of human prolidase.* J Biol Chem, 1989. **264**(8): p. 4476-81.
32. Mittal, S., et al., *Prolidase, a potential enzyme target for melanoma: design of proline-containing dipeptide-like prodrugs.* Mol Pharm, 2005. **2**(1): p. 37-46.
33. Mittal, S., et al., *Proline prodrug of melphalan targeted to prolidase, a prodrug activating enzyme overexpressed in melanoma.* Pharm Res, 2007. **24**(7): p. 1290-8.
34. Mittal, S., et al., *Proline prodrug of melphalan, prophalan-L, demonstrates high therapeutic index in a murine melanoma model.* Eur J Pharm Biopharm, 2007. **67**(3): p. 752-8.
35. Bielawski, K., et al., *Proline-linked nitrosoureas as prolidase-convertible prodrugs in human breast cancer cells.* Pharmacol Rep, 2008. **60**(2): p. 171-82.
36. Yang, L., et al., *Prolidase directly binds and activates epidermal growth factor receptor and stimulates downstream signaling.* J Biol Chem, 2013. **288**(4): p. 2365-75.

CHAPTER VI

CONCLUSIONS, SIGNIFICANCE AND FUTURE DIRECTIONS

The prodrug strategy has been considered an effective chemical approach for the improvement of certain inherent disadvantages of the parent drugs. In this dissertation, I have demonstrated the prodrug strategy's potentials for viral protease-targeted activation or enhancement of biopharmaceutical properties of the anti-infective compounds. The first research project concerns the utilization of human cytomegalovirus protease's esterase activity for potential selective activation of monoester prodrugs of ganciclovir. Four monoester prodrugs of ganciclovir, i.e. CbzAlaGCV, CbzAbuGCV, AcPheAlaGCV and AcPheAbuGCV, were designed and synthesized according to the order of preference of ester substrates by the hCMV protease. It was found that Ala-containing prodrugs had higher rates of hCMV protease-catalyzed activation than Abu-containing ones. In terms of tissue stability, *N*-acetylated dipeptide prodrugs were generally more stable than their Cbz-amino acid counterparts and the latter were thus not further pursued. Moreover, AcPheAbuGCV was shown to be the most stable among the four prodrugs in various tissue matrices. The kinetic selective activation factor (SAF) for AcPheAlaGCV and AcPheAbuGCV were found to be similar to each other. Nevertheless, when compared to AcPheAlaGCV, AcPheAbuGCV was more stable in plasma and liver microsomes and also displayed higher amounts of cellular uptake. Therefore, out of the four ganciclovir prodrug candidates, AcPheAbuGCV possesses the best overall potential to achieve the *in vivo* selective activation at hCMV infection sites.

For the second research project, Ciprofloxacyl-glycine-methyl ester (Cipro-Gly-OMe), a synthetic amide prodrug of ciprofloxacin, was demonstrated to possess both improved solubility as well as enhanced intestinal permeability (at neutral pH) over those of the parent

compound. Therefore, a BCS class IV fluoroquinolone compound could potentially be converted to a class I compound through a unique prodrug approach.

Altogether, I demonstrated that the prodrug strategy remains a versatile and promising method for improving the tissue targeting as well as biopharmaceutical properties of the existing drug compounds. The strategies derived from the projects of this dissertation could also serve as guidelines in future prodrug designs. For the targeted delivery of prodrugs, it is necessary that the design of promoieties facilitate both the activation of the prodrug at the target site(s) and stability of the prodrug throughout out the non-target tissues. As for the enhancement of the biopharmaceutical properties of zwitterionic BCS class IV compounds, it is paramount to locate the ionizable groups that are responsible for the compounds' poor solubility and / or intestinal permeability. Following rigorous model-based simulations, such groups may be masked by promoieties in order to alter the pH-dependent solubility and / or permeability profile(s) of the drug.

In future studies regarding the ganciclovir prodrugs, compounds with different promoieties should be explored for the sake of more rapid hydrolysis by the hCMV protease as well as better tissue stability compared to the current prodrug candidates. In addition, a validated cell system infected with live cytomegalovirus should be used to characterize the selective activation of ganciclovir prodrugs. If a significantly higher rate of prodrug hydrolysis is observed in infected cells compared to uninfected cells, the prodrug could potentially be a good candidate for testing in infected animal models.

For the ciprofloxacin prodrug project, more efforts need to be dedicated to the testing of more ciprofloxacyl amides with different amino acid promoieties or ciprofloxacyl ester prodrugs, so that one or more candidates could possess higher solubility, higher intestinal permeability along with rapid bioconversion to the parent drug after oral absorption. If such prodrugs could be successfully identified, their effective intestinal permeability (P_{eff}) as well as absolute oral bioavailability (F) will then be determined in animal models.

APPENDIX

EXPLORING THE PROTEOLYTIC ACTIVITIES OF THE INFLUENZA A PA PROTEIN

SUMMARY

Influenza remains a serious threat to the worldwide public health. Although the genome of the influenza A virus does not appear to encode a dedicated protease, the PA protein has been reported to exhibit *in vitro* proteolytic activities. Nevertheless, the protease-like functions of the influenza A PA protein remains poorly understood. In this chapter, we expressed and purified the full-length, N-terminally His_6-tagged PA protein from influenza strain A/WSN/33 with a *Spodoptera frugiperda* cell system using optimized experimental procedures and conditions. We then tested the hydrolysis of the only known putative peptide substrate for PA, Suc-Leu-Leu-Val-Tyr-AMC, in a PA-containing buffered system. We found that the substrate was unable to be hydrolyzed by the purified His_6-tagged PA protein. Therefore, we concluded that PA is likely not a *bona fide* protease and its previously reported proteolytic activities require further verification.

BACKGROUND

Influenza (flu) has been and remains one of the most widespread respiratory diseases around the world. The pandemic of "Spanish flu" between 1918 and 1919 was estimated to cause the deaths of 30 to 50 million people worldwide and two other major influenza outbreaks in 1957 and 1968 also inflicted significant morbidities and mortalities [1-3]. Currently, the seasonal epidemic of influenza is responsible for annual deaths of 250,000 to 500,000 [1, 4]. Most recently, the 2009 H1N1 influenza pandemic was estimated to have killed over 294,000 people globally [5]. Of all three types of influenza viruses (A, B and C), type A is the most virulent and also the most extensively researched [4].

The genome of influenza A virus consists of eight single-stranded negative-sense RNA molecules. A total of 11 proteins are encoded: hemagglutinin (HA), neuraminidase (NA), PA, PB1, PB1-F2, PB2, nucleoprotein (NP), M1, M2, NS1 and NS2 [6]. Among them HA and NA are large glycoproteins that play crucial roles in the entry of viral genome into the host cells and release of progeny virions from the infected cells, respectively [7, 8]. The adsorption of viral particles onto the host cells is mediated by the interaction of HA with surface receptors bearing N-acetylneuraminic acid (NANA), whereas NA cleaves NANA from the glycoprotein receptor at the host cell surface, enabling the "escape" and spread of the influenza virion. The nomenclature of serotypes of influenza A viruses, H*x*N*y*, are based on the antibody response to different subtypes of HA and NA proteins. The PA, PB1 and PB2 proteins form a large RNA-dependent RNA polymerase (RdRp) complex. The complex is responsible for the transcription and replication of the viral genome segments [9], with PB1 harboring the active polymerase site [10, 11] and PB2 involved in binding of 5'-cap of pre-mRNA [12].

The influenza PA protein ("PA": polymerase acidic) is of particular interest to us. It contains 716 amino acid residues and its sequence is highly conserved among different strains. Recombinant PA protein purified from *Spodoptera frugiperda* could be hydrolyzed by trypsin into two fragments: an N-terminal domain (PA(N), ~25 kDa) and a larger C-terminal domain (PA(C), ~55 kDa) [13, 14]. Crystal structures for separate C- and N- terminal domains have been published (PA(C): [15, 16]; PA(N): [17, 18]). However, the structure for the intact PA is

still unavailable, presumably due to difficulties in expressing the full-length protein at a large scale in a prokaryotic system [18].

Activities of influenza PA protein have been indicated in vRNA synthesis, virus assembly and proteolysis and these mechanisms all require further clarification [19]. Research on PA has been primarily focused on its roles in RNA transcription and replication [13, 17-23]. The function of the PA protein that we were interested in is its putative proteolytic activity, as it has been shown to induce the proteolysis of various proteins in *in vitro* and cell culture assays [24-27]. Currently, two conflicting theories attempt to explain this activity. In one series of studies by Nieto *et al.*, the proteolytic activity is attributed to the N-terminal segment of PA and the proteolysis induced by PA(N) could affect the replication of the virus [24, 26, 28, 29]. The authors further claim that PA induces the degradation of RNA polymerase II of the host cell and that threonine 157 is the most crucial amino acid residue for proteolysis [27]. This model has been challenged by functional studies that refutes the causal relationship between PA-induced proteolysis and viral replication [30] as well as structural insights into the environment of the T157 residue [18]. The other theory proposed by Toyoda *et al.* specifically states that PA is a serine protease with the active site at Ser 624, which resides within the C-terminal domain [25]. More studies imply that the protease activity is inhibited by binding of PA to influenza M1 protein [31] and that mutation at Ser 624 hampers viral growth [32]. The study has its limitation in the fact that only one tetrapeptide (*N*-succinyl-(L)-leucine-(L)-leucine-(L)-valine-(L)-tyrosine-(7-amino-4-methyl)-coumarin, Suc-Leu-Leu-Val-Tyr-AMC) was identified (of only five substrates tested) as a substrate for PA and no further results have been published to characterize the protease activity, even after the crystal structure of PA(C) has been published in 2008 [15, 16].

The contradictory reports on the function of PA as a protease clearly demonstrated the current limitations of our understanding on this important protein. Its function as a protease remained very much in doubt and its preferred substrate sequences poorly characterized. Nevertheless, like viral proteases from other virus species, PA does possess the unique advantage that it is only expressed in influenza-infected locales. If the proteolytic profile of

PA could be further characterized and more substrates for PA identified, it could potentially serve as a target protease for the activation of anti-influenza prodrugs.

Therefore, we intended to express and purify the full-length influenza PA protein using a *Spodoptera frugiperda* cell expression system [25, 31]. If the proteolytic activity of PA against the only known putative substrate, Suc-Leu-Leu-Val-Tyr-AMC, could be verified, substrate profiling of PA at the P1 position would be carried out using a library of fluorogenic compounds.

MATERIALS AND METHODS

Materials

The plasmid pcDNA-His_6-PA (A/WSN/33) was a generous gift from Tristram Parslow and Yuying Liang at Emory University (Atlanta, GA). Plasmid pFastBac1, competent *Escherichia coli* strains Mach 1 and DH10Bac, gentamicin, tetracycline hydrochloride, halogenated indolyl-β-galactoside (Bluo-Gal), insect cell line *Spodoptera frugiperda* 9 (Sf9), SF900-III SFM media, penicillin / streptomycin (tissue culture grade) and Cellfectin® II transfection reagent were purchased from Invitrogen (Grand Island, NY). DNA primers were synthesized by Integrated DNA Technologies (Coralville, IA). Restriction enzymes and T4 DNA ligase were purchased from New England Biolabs (Ipswich, MA). Gel purification kits for DNA and miniprep kits for plasmid DNA were purchased from Qiagen (Gaithersburg, MD). Anti-influenza PA polyclonal antibody was purchased from GenScript (Piscataway, NJ). *N*-succinyl-(L)-leucine-(L)-leucine-(L)-valine-(L)-tyrosine-(7-amino-4-methyl)coumarin (Suc-Leu-Leu-Val-Tyr-AMC) was purchased from Bachem (Torrance, CA). In addition, all other materials that have been mentioned in Chapters II through V were acquired from the same respective sources.

Cell Culture

The insect cell line *Spodoptera frugiperda* 9 (Sf9) (generation number 5-20) was regularly maintained as a suspension culture in SF900-III SFM media supplemented with 0.5% (v/v) penicillin / streptomycin. The culture is constantly shaken at 180 rpm at 25°C. A typical culture started at a density of $0.4 – 0.6 \times 10^6$ cells per milliliter (mL) and would be allowed to grow for approximately 3 days to $1.8 – 2.5 \times 10^6$ cells / mL with > 98% viability, at which point they would be diluted (i.e. “split”) into fresh SF900-III SFM media for a new generation.

Molecular Subcloning

The plasmid pcDNA-His_6-PA was digested with EcoRI / KpnI and the PA-containing DNA fragment was purified from agarose gels. It was ligated to the EcoRI / KpnI-digested pFastBac1 vector and the resulting pFastBac1-His_6-PA plasmid was confirmed by DNA sequencing. The *E. coli* DH10Bac strain was transformed with pFastBac1-His_6-PA and plated

on agar plates with 50 µg/mL kanamycin, 7 µg/mL gentamicin, 10 µg/mL tetracycline·HCl, 40 µg/mL IPTG and 100 µg/mL Bluo-Gal. The plate was incubated at 37°C for 48 h and the largest white colony was picked and re-streaked on a fresh plate containing the same antibiotics and reagents. The confirmed white colonies were then inoculated into a Terrific Broth miniculture. The recombinant bacmid containing the N-terminally His_6-tagged PA gene was purified from the miniculture using a Qiagen plasmid miniprep kit, with extra care being taken to avoid shearing the large bacmid DNA during the pipetting processes. The amounts of the prepared bacmid were quantified by A_{260} in a Biotek Synergy HT plate reader.

Generation of Recombinant Baculovirus

12 µL Bacmid prep containing the N-terminally His_6-tagged PA gene was mixed 1:1 (v:v) with Cellfectin II in SF900-III SFM and overlaid on Sf9 cells that had been seeded in 6-well tissue culture plates. The transfection mixture was incubated at 27°C for 5 h and then replaced with fresh SF900-III SFM. After 72 h, culture supernatants containing the first-generation (P1) recombinant baculovirus were collected. The P1 baculovirus was then used to infect Sf9 cells at an approximate multiplicity of infection (MOI) of 0.1, assuming the titer of the P1 baculovirus was approximately 8×10^6 PFU / mL. The second-generation (P2) recombinant baculovirus was acquired from the culture supernatant of Sf9 cells infected with P1 baculovirus and was assumed to have a titer of approximately 1×10^8 PFU / mL. This supernatant was then used to infect Sf9 cells at MOI = 0.1 for the generation of third-generation (P3) recombinant baculovirus contained in the SF900-III SFM media. P3 baculovirus generally would possess a large enough titer ($> 5\times10^8$ PFU / mL), and the volume of the supernatant containing the P3 baculovirus, at over 40 mL, would be large enough for use in subsequent infections of relatively large-scale Sf9 cultures for the production of recombinant PA protein. The supernatants containing the P1, P2 and P3 recombinant baculoviruses were stored at 4°C and kept for up to three months after their respective collections.

Expression and Purification of Recombinant PA Protein

One liter of Sf9 cells was grown to a density of ~$3x10^6$ cells / mL. Third-passage (P3) recombinant baculovirus containing the N-terminally His_6-tagged PA gene was added to the

culture at an approximate MOI of 1. After 72 hours, the cells were collected by centrifugation and immediately lysed by sonication in lysis buffer (0.1 M NaH_2PO_4, 10 mM imidazole, 0.1% Triton X-100, 1 mM freshly-added dithiothreitol (DTT); pH 7.6). After centrifugation at 10,000×g for 15 min at 4°C, the pellets were discarded and the cleared supernatants were removed and incubated with Ni^{2+}-NTA resins for binding of His_6-tagged proteins. Subsequent steps of purification, storage and detection of the PA protein were very similar to those used for the hCMV protease A143S in Chapter II.

Protease Activity Assays

The assay was carried out in a 96-well plate format. A final concentration of 100 μM Suc-Leu-Leu-Val-Tyr-AMC was added to either blank reaction buffer (50 mM HEPES, 10 mM $CaCl_2$, 1 mM DTT, pH 7.8) or reaction buffer containing PA protein at concentrations from 10 to 100 μg/mL. Reactions were incubated at 37°C and periodically shaken. The generation of free AMC compound was monitored on a Biotek Synergy HT plate reader with an excitation wavelength of 430 nm and emission 508 nm for a period of up to 4 hours.

RESULTS

Expression and Purification of PA Protein of Influenza Strain A/WSN/33

N-terminally His_6-tagged PA protein was purified from baculovirus-infected Sf9 lysates with an approximate yield of 0.5 mg per liter of culture. Such an amount was consistent with literature reports [25]. The recombinant PA protein was visualized in Western blots (**Fig. A1.1**) and SDS-PAGE gels (**Fig. A1.2**) at an apparent molecular weight of ~90 kD. Purity of the batch with the optimized procedures (03/25/2011 batch) was approximately 52%.

Proteolytic Activity of Influenza PA Protein against the Putative Substrate Suc-Leu-Leu-Val-Tyr-AMC

The tetrapeptide substrate was very stable in the blank reaction buffer. For the wells with blank buffer and the substrate, no significant increase in fluorescence was observed throughout the 4-hour period. Fluorescence readings of the wells supplemented with various concentrations of PA did not display significant differences compared to those with only buffer blanks, indicating a lack of PA-catalyzed hydrolysis of Suc-Leu-Leu-Val-Tyr-AMC in the previously published reaction conditions [25]. Therefore, it was obvious that the recombinant N-terminally His_6-tagged PA protein did not possess the proteolytic activity toward the only known putative substrate.

DISCUSSION

The ultimate goal of this project was to utilize the putative proteolytic activities of the influenza PA protein for the rational design of prodrugs that could be specifically activated by PA, thereby potentially targeting the prodrug to the influenza infection sites. Eventually, we were able to generate a few crudely purified batches of PA protein of influenza A/WSN/33 from lysates of Sf9 cells infected with recombinant baculovirus. Nevertheless, we failed to demonstrate PA's catalytic activity in the hydrolysis of the only published putative substrate, Suc-Leu-Leu-Val-Tyr-AMC, despite numerous attempts to enhance protein stability and assay conditions. Due to this result, we deemed that the batches of PA protein that we produced did not possess the inherent protease activity as reported [25] and did not proceed further with this project.

Significant efforts were devoted to protecting the integrity and the possible enzymatic activities of PA during its purification process because protease / esterase inhibitors were not allowed to be used in this case. For the final batch of purified PA, for which the procedures were considered optimized, the total time of purification was shortened to less than 5 hours and all steps were performed either on ice or at 4°C (cold room) in order to reduce the possibility of protein degradation. In addition, no precipitation or aggregation was observed throughout the process. The purity of the final "optimized batch", at approximately 52%, was lower than expected. This likely resulted from the low amount of His_6-tagged protein expression in the baculovirus-infected Sf9 system and high non-specific binding of the cellular proteins to the Ni^{2+}-NTA resin. No high-intensity band was detected in western blotting with either anti-His_6 monoclonal antibody or anti-PA polyclonal antibodies, showing that the recombinant PA protein was kept largely intact throughout the purification process. Despite our best efforts, the PA protein still did not display proteolytic activity toward the putative substrates. We suspect that two possible factors may be the culprit. First, it was possible that the N-terminal His_6 tag could inhibit the protein's activity; indeed, in the original article on PA's protease activity, no His_6 tag was attached onto the PA protein. Second, it was also possible that the PA protein underwent modifications within the Sf9 cells that forfeited

its proteolytic function. If this was the actual case, a different insect cell line such as Sf21 may be used as an alternative system for protein expression.

Nevertheless, it remains entirely plausible that the influenza PA protein is not a *bona fide* protease. First, the existence of the proteolytic activity of intact PA has only been claimed by one research group in two publications [25, 31]. No other independent study has since verified their findings, let alone further clarified the roles of PA's proteolytic activity in the viral life cycle or the substrate preference of PA. Therefore, the authenticity of the results from the initial studies could be in doubt. Second and perhaps as a more compelling case against PA being a protease, crystal structures of the C-terminal part of PA found no structure remotely resembling a catalytic triad around the claimed active site, Ser 624 [15], in contrast to statements in the original report on PA's protease function [25]. This finding casts serious doubt on the claimed mechanism of PA's catalytic activity on peptide hydrolysis and PA is thus unlikely a protease with Ser624 as the active residue. In summary, one possible explanation on why we were unable to characterize PA's proteolytic activities was that PA was not, in fact, a "real" protease. Therefore, in future studies utilizing a protease's activity for targeting purposes, it would be wise to select a protease with well-studied functions and substrate preferences in order to avoid potentially large amounts of time and resources spent on the characterization of the protease itself.

FIGURES

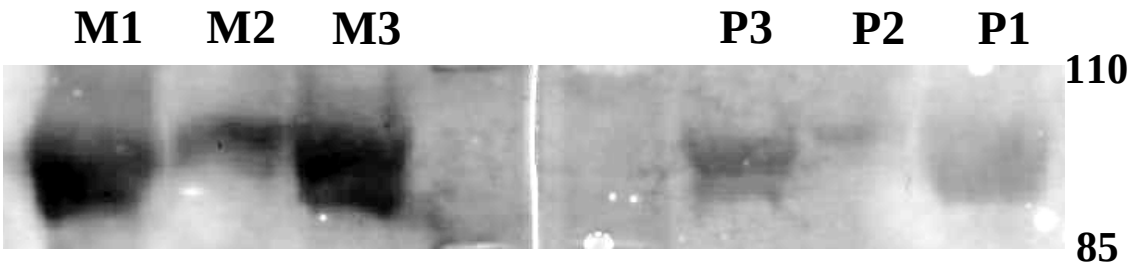

Figure A1.1. Western blotting of different batches of purified PA proteins. **M1-3**, blotting done with mouse anti-His_6 monoclonal antibody. M1, 12/19/2010 batch of purified PA; M2, 12/30/2010 batch; M3, 03/25/2011 batch. **P1-3**, blotting done with rabbit anti-PA polyclonal antibodies. P1, 12/19/2010 batch of purified PA; P2, 12/30/2010 batch; P3, 03/25/2011 batch. Numbers on the right denote the locations of the markers with the respective molecular weights. Only the 03/25/2011 batch of purified PA protein was used for subsequent substrate hydrolysis assays.

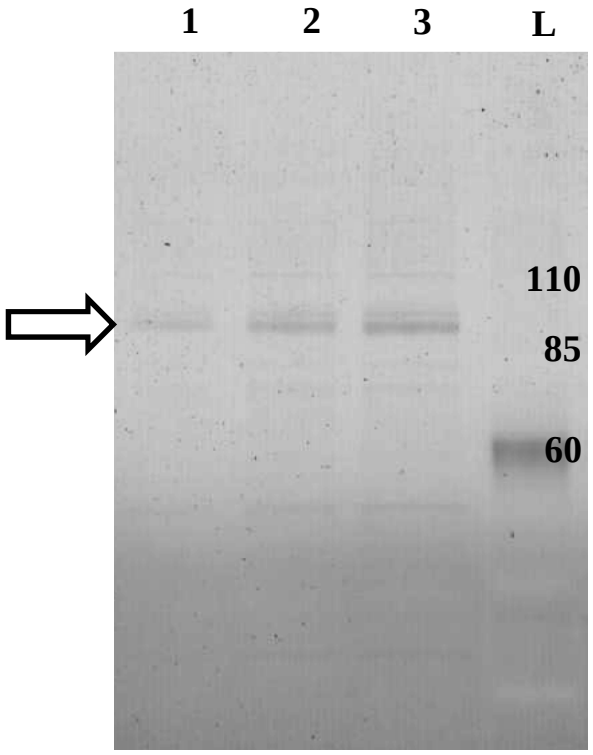

Figure A1.2. Krypton staining of an SDS-PAGE gel loaded with the 03/25/2011 batch of purified N-terminally His_6-tagged PA protein. Lanes 1, 2 and 3, total loading amount of 1 µg, 2 µg and 3 µg PA protein aliquots; lane L, Benchmark pre-stained protein ladder with molecular weights of protein ladder bands. Arrow shows the ~90-kD N-terminally His_6-tagged PA protein.

REFERENCES

1. *WHO Influenza Factsheet.*; Available from: http://www.who.int/mediacentre/factsheets/fs211/en/.
2. De Clercq, E., *Antiviral agents active against influenza A viruses.* Nat Rev Drug Discov, 2006. **5**(12): p. 1015-25.
3. Cox, N.J. and K. Subbarao, *Global epidemiology of influenza: past and present.* Annu Rev Med, 2000. **51**: p. 407-21.
4. Rambaut, A., et al., *The genomic and epidemiological dynamics of human influenza A virus.* Nature, 2008. **453**(7195): p. 615-9.
5. Dawood, F.S., et al., *Estimated global mortality associated with the first 12 months of 2009 pandemic influenza A H1N1 virus circulation: a modelling study.* Lancet Infect Dis, 2012. **12**(9): p. 687-95.
6. Ghedin, E., et al., *Large-scale sequencing of human influenza reveals the dynamic nature of viral genome evolution.* Nature, 2005. **437**(7062): p. 1162-6.
7. Nayak, D.P., E.K. Hui, and S. Barman, *Assembly and budding of influenza virus.* Virus Res, 2004. **106**(2): p. 147-65.
8. Cros, J.F. and P. Palese, *Trafficking of viral genomic RNA into and out of the nucleus: influenza, Thogoto and Borna disease viruses.* Virus Res, 2003. **95**(1-2): p. 3-12.
9. Neumann, G., et al., *Orthomyxovirus replication, transcription, and polyadenylation.* Curr Top Microbiol Immunol, 2004. **283**: p. 121-43.
10. Poch, O., et al., *Identification of four conserved motifs among the RNA-dependent polymerase encoding elements.* EMBO J, 1989. **8**(12): p. 3867-74.
11. Li, M.L., P. Rao, and R.M. Krug, *The active sites of the influenza cap-dependent endonuclease are on different polymerase subunits.* EMBO J, 2001. **20**(8): p. 2078-86.
12. Guilligay, D., et al., *The structural basis for cap binding by influenza virus polymerase subunit PB2.* Nat Struct Mol Biol, 2008. **15**(5): p. 500-6.
13. Hara, K., et al., *Amino acid residues in the N-terminal region of the PA subunit of influenza A virus RNA polymerase play a critical role in protein stability, endonuclease activity, cap binding, and virion RNA promoter binding.* J Virol, 2006. **80**(16): p. 7789-98.
14. Guu, T.S., et al., *Mapping the domain structure of the influenza A virus polymerase acidic protein (PA) and its interaction with the basic protein 1 (PB1) subunit.* Virology, 2008. **379**(1): p. 135-42.
15. He, X., et al., *Crystal structure of the polymerase PA(C)-PB1(N) complex from an avian influenza H5N1 virus.* Nature, 2008. **454**(7208): p. 1123-6.
16. Obayashi, E., et al., *The structural basis for an essential subunit interaction in influenza virus RNA polymerase.* Nature, 2008. **454**(7208): p. 1127-31.
17. Dias, A., et al., *The cap-snatching endonuclease of influenza virus polymerase resides in the PA subunit.* Nature, 2009. **458**(7240): p. 914-8.
18. Yuan, P., et al., *Crystal structure of an avian influenza polymerase PA(N) reveals an endonuclease active site.* Nature, 2009. **458**(7240): p. 909-13.
19. Maier, H.J., et al., *Differential role of the influenza A virus polymerase PA subunit for vRNA and cRNA promoter binding.* Virology, 2008. **370**(1): p. 194-204.

20. Fodor, E., et al., *A single amino acid mutation in the PA subunit of the influenza virus RNA polymerase inhibits endonucleolytic cleavage of capped RNAs.* J Virol, 2002. **76**(18): p. 8989-9001.
21. Fodor, E., et al., *A single amino acid mutation in the PA subunit of the influenza virus RNA polymerase promotes the generation of defective interfering RNAs.* J Virol, 2003. **77**(8): p. 5017-20.
22. Perez, D.R. and R.O. Donis, *Functional analysis of PA binding by influenza a virus PB1: effects on polymerase activity and viral infectivity.* J Virol, 2001. **75**(17): p. 8127-36.
23. Ghanem, A., et al., *Peptide-mediated interference with influenza A virus polymerase.* J Virol, 2007. **81**(14): p. 7801-4.
24. Sanz-Ezquerro, J.J., et al., *The amino-terminal one-third of the influenza virus PA protein is responsible for the induction of proteolysis.* J Virol, 1996. **70**(3): p. 1905-11.
25. Hara, K., et al., *Influenza virus RNA polymerase PA subunit is a novel serine protease with Ser624 at the active site.* Genes Cells, 2001. **6**(2): p. 87-97.
26. Perales, B., et al., *The replication activity of influenza virus polymerase is linked to the capacity of the PA subunit to induce proteolysis.* J Virol, 2000. **74**(3): p. 1307-12.
27. Rodriguez, A., A. Perez-Gonzalez, and A. Nieto, *Influenza virus infection causes specific degradation of the largest subunit of cellular RNA polymerase II.* J Virol, 2007. **81**(10): p. 5315-24.
28. Sanz-Ezquerro, J.J., et al., *Individual expression of influenza virus PA protein induces degradation of coexpressed proteins.* J Virol, 1995. **69**(4): p. 2420-6.
29. Bradel-Tretheway, B.G., et al., *The human H5N1 influenza A virus polymerase complex is active in vitro over a broad range of temperatures, in contrast to the WSN complex, and this property can be attributed to the PB2 subunit.* J Gen Virol, 2008. **89**(Pt 12): p. 2923-32.
30. Naffakh, N., P. Massin, and S. van der Werf, *The transcription/replication activity of the polymerase of influenza A viruses is not correlated with the level of proteolysis induced by the PA subunit.* Virology, 2001. **285**(2): p. 244-52.
31. Hara, K., et al., *Inhibition of the protease activity of influenza virus RNA polymerase PA subunit by viral matrix protein.* Microbiol Immunol, 2003. **47**(7): p. 521-6.
32. Toyoda, T., K. Hara, and Y. Imamura, *Ser624 of the PA subunit of influenza A virus is not essential for viral growth in cells and mice, but required for the maximal viral growth.* Arch Virol, 2003. **148**(9): p. 1687-96.